JPRS L/9180

3 July 1980

USSR Report

METEOROLOGY AND HYDROLOGY

No. 4, April 1980

FBIS FOREIGN BROADCAST INFORMATION SERVICE

APPROVED FOR RELEASE: 2007/02/08: CIA-RDP82-00850R000200100010-7

NOTE

JPRS publications contain information primarily from foreign newspapers, periodicals and books, but also from news agency transmissions and broadcasts. Materials from foreign-language sources are translated; those from English-language sources are transcribed or reprinted, with the original phrasing and other characteristics retained.

Headlines, editorial reports, and material enclosed in brackets [] are supplied by JPRS. Processing indicators such as [Text] or [Excerpt] in the first line of each item, or following the last line of a brief, indicate how the original information was processed. Where no processing indicator is given, the information was summarized or extracted.

Unfamiliar names rendered phonetically or transliterated are enclosed in parentheses. Words or names preceded by a question mark and enclosed in parentheses were not clear in the original but have been supplied as appropriate in context. Other unattributed parenthetical notes within the body of an item originate with the source. Times within items are as given by source.

The contents of this publication in no way represent the policies, views or attitudes of the U.S. Government.

For further information on report content call (703) 351-2938 (economic); 3468 (political, sociological, military); 2726 (life sciences); 2725 (physical sciences).

APPROVED FOR RELEASE: 2007/02/08: CIA-RDP82-00850R000200100010-7

JPRS L/9180

3 July 1980

USSR REPORT

METEOROLOGY AND HYDROLOGY

No. 4, April 1980

Selected articles from the Russian-language journal METEOROLOGIYA I GIDROLOGIYA, Moscow.

CONTENTS

PUBLICATION DATA

English title	:	METEOROLOGY AND HYDROLOGY
Russian title	:	METEOROLOGIYA I GIDROLOGIYA
Author (s)	:	
Editor (s)	:	Ye. I. Tolstikov
Publishing House	:	Gidrometeoizdat
Place of Publication	:	Moscow
Date of Publication	:	April 1980
Signed to press	:	21 Mar 80
Copies	:	3790
COPYRIGHT	:	"Meteorologiya i gidrologiya", 1980

UDC 551.(515.8+557.5)

VERTICAL CIRCULATIONS IN JET STREAMS AND FRONTOGENESIS

Moscow METEOROLOGIYA I GIDROLOGIYA in Russian No 4, Apr 80 pp 5-11

[Article by Candidate of Physical and Mathematical Sciences N. P. Shakina, USSR Hydrometeorological Scientific Research Center, submitted for publication 25 July 1979]

Abstract: The author gives a theoretical analysis of the dependence between the direction of vertical circulation in a jet stream and the nature of evolution of a high-altitude frontal zone. It is shown that with accentuation of the frontal zone the vertical circulation in this zone and in the jet stream is "thermally direct," whereas with blurring of the frontal zone the vertical circulation is "thermally inverse." In a quasigeostrophic approximation these movements are manifested as compensatory. In the approximation of full equations the descending branch of circulation in an accentuating frontal zone occupies a region of maximum frontogenesis as a result of ageostrophic effects. The subsidence of stratospheric air occurring in this region is manifested locally as a branch of "thermally inverse" circulation, acting as a regulator of the sharpness of fronts.

[Text] In jet streams in the upper troposphere, associated with high-altitude frontal zones, the trajectories of air particles are usually spiral, with ascent along one side of the jet stream axis and with descent on the other. The results of experimental investigations made by different authors (see review by V. A. Dzhordzhio [2]) show that the direction of circulation in the vertical plane normal to the axis of the jet stream can be both "thermally direct" (ascent on the side of the warm air) and "thermally inverse" (the colder air ascends, the warmer air subsides). The reasons for the complex mesoscale structure of the vertical movements

and wind fields in jet streams and, in particular, the reasons for the formation of any type of vertical circulation must be sought in the large-scale dynamics of high-altitude frontal zones.

Proceeding on the basis of analytical and numerical results of investigations of atmospheric frontogenesis [4-6], it is possible to formulate some regularities in the development of thermally direct and thermally inverse circulations in jet streams. At the same time it is possible to obtain a physical explanation of "indirect circulations" observed in intensive upper tropospheric frontal zones. Although the fact of existence of such circulations was established rather long ago and has been repeatedly confirmed by an analysis of frontogenesis on the basis of real data (for example, see [7]), a failure to understand the physical essence of this process until now has been leading some meteorologists to an incorrect interpretation of the observed phenomena.

We will begin with an analysis of frontogenesis in a quasigeostrophic approximation. Usually the intensity of frontogenesis (or frontolysis) is evaluated using a scalar frontogenetic function which in the case of a plane adiabatic movement is described in the form [1]

$$F = \frac{d}{dt}\left|\nabla\theta\right| = \frac{\partial\theta/\partial x}{|\nabla\theta|}\left[-\frac{\partial u}{\partial x}\frac{\partial\theta}{\partial x} - \frac{\partial v}{\partial x}\frac{\partial\theta}{\partial y}\right] + \frac{\partial\theta/\partial y}{|\nabla\theta|}\left[-\frac{\partial u}{\partial y}\frac{\partial\theta}{\partial x} - \frac{\partial v}{\partial y}\frac{\partial\theta}{\partial y}\right], \quad (1)$$

where $\nabla\theta$ is the horizontal gradient of potential temperature.

Now we will write an equation for the instantaneous distribution of vertical movements in a quasigeostrophic approximation (so-called omega equation) in the form proposed in [6]:

$$N^2\nabla_h^2 w + f^2\frac{\partial^2 w}{\partial z^2} = 2\nabla\cdot\vec{Q}_g. \quad (2)$$

Here

$$N^2 = \frac{g}{\theta_0}\frac{d\bar{\theta}}{dz}$$

is the square of the Brent-Väisälä frequency (θ_0 is the potential temperature at the earth's surface, $\bar{\theta}$ is the standard potential temperature at the level z), ∇_h^2 is the Laplace operator in the horizontal plane (z = h), f is the Coriolis parameter, assumed to be constant, $\vec{Q}_g$ is a vector, whose divergence or convergence determines the sign of the vertical movements and their value:

$$\vec{Q}_g = \left\{-\frac{g}{\theta_0}\frac{\partial\vec{V}_g}{\partial x}\cdot\nabla\theta, -\frac{g}{\theta_0}\frac{\partial\vec{V}_g}{\partial y}\cdot\nabla\theta\right\}, \quad (3)$$

$$-\frac{g}{\theta_0}\frac{\partial\vec{V}_g}{\partial x}\cdot\nabla\theta = Q_1,$$

$$-\frac{g}{\theta_0}\frac{\partial \vec{V}_g}{\partial y}\cdot\nabla\theta = Q_2 \tag{3}$$

($\vec{V}_g$ is the vector of the geostrophic wind with the components u_g, v_g).

It is easy to see that the $\vec{Q}_g$ vector is related to the scalar frontogenetic function F_g, computed from the field of the geostrophic wind, by the expression

$$F_g = \frac{\theta_0}{g|\nabla\theta|}\nabla\theta\cdot\vec{Q}_g. \tag{4}$$

On the other hand, $\vec{Q}_g$ can be regarded as a vector frontogenetic function in geostrophic movement. In actuality, if the ageostrophic components of the wind are absent, it is easy to confirm that

$$\vec{Q}_g = \frac{d_g}{dt}\frac{g}{\theta_0}\nabla\theta, \quad \frac{d_g}{dt} = \frac{\partial}{\partial t} + u_g\frac{\partial}{\partial x} + v_g\frac{\partial}{\partial y}. \tag{5}$$

Thus, we find that in a quasigeostrophic approximation the distribution of vertical movements is determined by the divergence or convergence of the frontogenetic vector function, in other words, by the distribution of frontogenetic effects horizontally. With sufficiently large scales of movements in the free atmosphere, when the wind can be considered close to geostrophic, equation (2) is useful not only for qualitative estimates, but also for many computations. We will limit ourselves to an evaluation of the direction of vertical movements in the sectors of the thermopressure field of interest to us, proceeding on the basis of (2) and (5).

Usually in such evaluations as a first approximation it is assumed that in the case

$$N^2\nabla_h^2 w + l^2\frac{\partial^2 w}{\partial z^2} > 0$$

there is a descent of the air, whereas with a negative left-hand side of (2) there is ascent. Now we will examine the conditions characteristic for the jet stream "entry" and "delta" (Fig. 1a). In the "entry" region the geostrophic movement should lead to frontogenesis, and in the "delta" region to frontolysis. The $\vec{Q}_g$ vectors in the "entry" region are oriented as indicated in the diagram and there is a divergence $\vec{Q}_g$ to the left of the flow and convergence at the right; these correspond to descending movements (and generation of anticyclonic vorticity in the lower-lying layers) under the left side of the "entry" region and ascending movements at the right (with the generation of cyclonic vorticity). We see that the vertical circulation is thermally direct. In the "delta" region, where the geostrophic movement tends to decrease the horizontal temperature gradient (here frontolysis occurs), to the right of the flow there will be convergence of the $\vec{Q}_g$ vector, and to the left -- divergence. Accordingly, the warm air will descend and the cold air will rise, and thus the circulation will be thermally inverse.

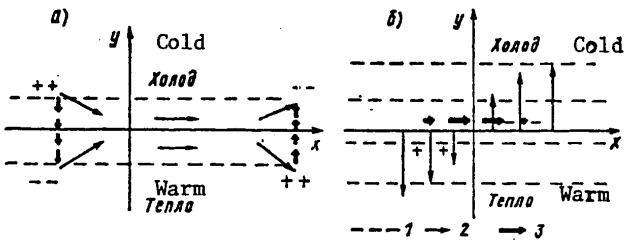

Fig. 1. Distribution of $\vec{Q}_g$ and $\nabla \cdot \vec{Q}_g$ in entry and delta of jet stream (a) and in flow with transverse shear (b). 1) isotherms, 2) wind velocity vectors, 3) $\vec{Q}_g$ vectors. The signs on $\nabla \cdot \vec{Q}_g$ are indicated.

We will direct the x-axis along the isotherm so that we will have $Q_1 = 0$. The forced vertical movements then will be determined by the value

$$\frac{\partial}{\partial y} Q_2 = \frac{\partial}{\partial y} \frac{d_g}{dt} \left(\frac{\partial \theta}{\partial y} \right).$$

If plane frontogenesis occurs (as in the entry region), then

$$\frac{d_g}{dt} \frac{\partial \theta}{\partial y} < 0$$

(since $\partial\theta / \partial y < 0$ and increases in value for each individual particle). If this frontogenesis is anywhere maximum (for example, at y = 0 in the figure), the derivative $\partial / \partial y \; Q_2$ changes sign at this point; on the side with the cold air ($y > 0$) it is positive, and on the side of the warm air ($y < 0$) it is negative. Accordingly, with $y > 0$ there is development of descending movements and with y 0 there are ascending movements: the circulation is thermally direct relative to the axis of greatest intensity of frontogenesis. In the delta region the picture is the opposite.

In another special case, when the geostrophic motion causes only a turning of the isotherms, not their squeezing together, it is also easy to show that the forced vertical circulation always has a thermally direct character relative to the axis of the maximum turning of the isotherms (ascent in the region of heat advection, descent in the region of cold advection). Such a situation is shown in Fig. 1b; it can be considered characteristic for a plane baroclinic wave. In order to determine the direction of circulation in this case we note that $\vec{V}_g = \{0, v_g\}$ and $Q_2 = 0$; everywhere $\partial v_g / \partial x > 0$, but the second derivative $\partial^2 v_g / \partial x^2$ is positive in the left part of the figure and negative in the right part. Therefore, when $(\partial T / \partial y) = \text{const} < 0$ we obtain $\nabla \cdot \vec{Q}_g > 0$ in the right part of the figure, that is, in the region of cold advection, and $\nabla \cdot \vec{Q}_g < 0$ in the region of heat advection, whereas at the point of bending of the $v_g(x)$ curve at x = 0 we will have $\nabla \cdot \vec{Q}_g = 0$, although Q_1, and this means, also $|\vec{Q}_g|$ have a maximum here. The straight line x = 0 in our case is in actuality the "line of zero advection," to use the terminology employed by Pogosyan and Taborovskiy [3].

We note that closed circulations (with a change in the sign of w) arise only in the presence of maxima or minima of the functions describing the squeezing together of the isotherms or their turning (that is, accordingly the functions Q_2 and Q_1, if the x-axis is directed along the isotherms).

Frontogenesis in the usual understanding of the word, evaluated using the scalar function F_g, at the time shown in Fig. 1b is equal to zero, as follows from (4). However, the horizontal shear mechanism, leading initially only to a turning of the isotherms, already at the next moment creates a non-zero component of the temperature gradient along the x-axis and with it, also non-zero F_g values; frontogenesis in the region of horizontal shear will be intensified, with a tendency to the formation of a zone of maximum $|\nabla\theta|$ -- a frontal zone -- along the line of maximum Q_1 (that is, with $x = 0$). This mechanism leads to frontogenesis in developing baroclinic disturbances.

Thus, vertical circulations, developing during quasigeostrophic movement, actually are thermally direct during frontogenesis ($F_g > 0$) and inverse in the case of frontolysis ($F_g < 0$); in addition, they are thermally direct in those cases when advection by the geostrophic wind leads to a turning of the isotherms (regardless of the direction of the latter).

Does this conclusion agree with the observed facts of subsidence of stratospheric potentially warmer air in high frontal zones -- a phenomenon observed in the case of intensive frontogenesis and perceived in the neighborhood of the jet stream as a branch of thermally indirect circulation?

As we have already seen, the subsidence of air on the cold side of a high frontal zone during accentuation of a front (like the ascent on the warm side) is a compensatory circulation which should develop even within the framework of a quasigeostrophic approximation. The fact that the descending branch of this circulation intensifies and acquires a special character, also taking in the zone of maximum frontogenesis, is a consequence of two factors: first, nongeostrophic effects, taken into account by the quasigeostrophic model only in part, and second, the presence of the tropopause as a layer of change of the vertical temperature gradient.

Figure 2 shows a characteristic section of a tropospheric frontal zone and a jet stream by a vertical plane normal to the axis of the latter. This picture corresponds both to observations [7] and to the results of hydrodynamic modeling of frontogenesis along the axis of compression of the horizontal deformation field [5]. As already mentioned, the tropopause level differs in that there is a break in the vertical temperature gradient here and together with it, Ertel potential vorticity

$$q = \frac{1}{\rho}(l\vec{k} + \nabla \cdot \vec{V}) \cdot \nabla\theta \qquad (6)$$

a conserved value in the system of so-called full (primitive) equations, which we, after some additional assumptions, will use for an analysis of the nongeostrophic effects playing an important role in forming the

vertical structure of atmospheric frontal zones and fronts. As is well known [4, 5], a changeover from quasigeostrophic to full equations makes it possible to obtain the most significant refinements precisely with respect to vertical structure, which for us is of the greatest interest in this case.

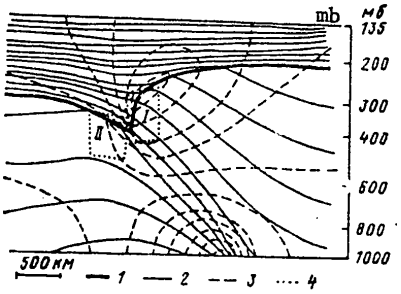

Fig. 2. Characteristic section of tropospheric frontal zone and jet stream during intensive frontogenesis. 1) tropopause, potential temperature isolines, 3) isotachs, 4) boundaries of regions I and II (see text).

The intensity of frontogenetic processes differs greatly in different layers of the atmosphere. It has been demonstrated theoretically [5] that sharp frontal discontinuities, where the vertical component of absolute vorticity ζ in the course of a finite time can attain (in a nonviscous examination) infinitely high values, can arise only near the underlying surface or near such levels where there are "discontinuities" of potential vorticity q or its first or second derivatives. In particular, such a level is the tropopause, which separates stratospheric air from tropospheric air, having substantially different potential vorticities. In the troposphere layer frontal zones cannot attain such a high intensity as near its boundaries. Accordingly, during frontogenesis vertical circulations are most clearly expressed either in the lower layers or under the tropopause.

Within the framework of a quasigeostrophic approximation the vertical movements change sign at the point of maximum frontogenesis. Accordingly, the vorticity field is also found to be symmetric relative to this point, which does not correspond to the really observed picture. However, within the framework of models with full equations or even with a more limited allowance for the ageostrophic components only in a direction transverse to the front [5] the maximum of positive vorticity is obtained, in accordance with observations, at the point of most intensive frontogenesis. The increase in positive vorticity during frontogenesis, maximum at the lower boundary or near the tropopause, is accompanied by a decrease in pressure or a lessening of the altitudes of the isobaric surfaces. At the ground this leads to the formation of a trough along the front. However, if such a process occurs near the tropopause -- a moving internal discontinuity q -- the pressure decrease in the region of the front leads to a "drawing" of the tropopause into this region, situated on the cyclonic side of the jet stream. The localization of the latter on the warm side of a high

frontal zone is also a result of the influence of essentially nongeostrophic factors [5].

Positive vorticity, maximum in the zone of greatest horizontal temperature contrasts, increases with time, and in addition, increases with altitude with approach to the tropopause from below (since the tropopause is the level of the discontinuity q), and also with transition through the tropopause. This leads to the appearance of the ageostrophic component u_{ag}, directed from the zone of maximum v at each level to the zone of increase in ζ (that is, in the direction of low pressure); u_{ag} will increase with altitude. As a result, a counterclockwise circulation develops in the jet stream and on the cyclonic side of the latter, that is, in the zone of maximum ζ, a descending branch of this circulation develops (Fig. 2).

Thus, the subsidence of air, and with it the "drawing in" of the tropopause, is a passive consequence of the distribution of vorticity and wind velocity arising in the frontogenesis process; from this point of view the "thermally indirect" circulation appears to be a result of dynamic, not thermal factors.

There is a close relationship between the generation of vorticity in the process of development of an upper tropospheric front and vertical circulation. We will write a vorticity equation corresponding to full equations in our two-dimensional model:

$$\frac{d\zeta}{dt} = \zeta \frac{\partial w}{\partial z} - \frac{\partial w}{\partial x}\frac{\partial v}{\partial z}. \qquad (7)$$

In Figure 2 it is possible to define two regions -- to the right and left of the center of the forming frontal zone. In region I $\partial w/\partial x > 0$, $\partial v/\partial z > 0$; accordingly, the effect of the second term on the right in (7) will involve a decrease in positive vorticity. Thus, lowering of the tropopause is an obstacle to formation of excessively great ζ ("infinitely great" in a nonviscous examination); this lowering is the more intense the more intense is the frontogenesis process. However, in region II

$$\frac{\partial w}{\partial z} < 0, \frac{\partial v}{\partial x} > 0,$$

and positive vorticity will increase under the influence of vertical circulation. Here the lowering effect is frontogenetic because more potentially warm stratospheric air subsides on the warm side of the high frontal zone.

Thus, the subsidence of stratospheric air acts as a regulator of the frontogenetic process, decreasing positive vorticity (and temperature contrasts) in the zone of maximum frontogenesis and at the same time increasing vorticity and temperature contrasts on the periphery of this zone. The subsidence of potentially warmer air, caused by dynamic factors, can be regarded as a branch of "thermally indirect" circulation only locally, in a limited sense. As was already demonstrated above in an analysis of a quasigeostrophic omega equation, subsidence on the cold side of a developing front is a branch of a frontolytic thermally direct circulation; but the same

descending branch, taking in stratospheric air, appears to be warmer than the tropospheric cold air (situated to the left of it in Fig. 2).

Now we will define the principal results of the study made here.

1. Proceeding on the basis of the quasigeostrophic omega equation in the form (2), it is demonstrated that the distribution of vertical movements in the free atmosphere, in particular, in jet stream zones, in a quasigeostrophic approximation is determined by divergence or convergence of the frontogenetic vector function, or, in other words, by the horizontal distribution of frontogenetic effects. With an accentuation of the high frontal zone the vertical circulation in the jet stream is thermally direct (in the sense that ascent occurs on the side of the warm air mass), and during blurring is thermally inverse (ascent on the side of the cold air) relative to the axis of the greatest intensity of frontogenesis or frontolysis respectively. If geostrophic movement leads only to a turning of the isotherms (without their significant squeezing together or spreading apart), then the developing circulation relative to the axis of maximum turning (line of zero advection) is thermally direct: ascent in the region of heat advection and descent in the region of cold advection.

2. As demonstrated by an analysis of the wind fields and vorticity within the framework of the approximation of "full" equations, as a result of essentially nongeostrophic movements in the neighborhood of the tropopause the descending branch of the circulation in an accentuating high frontal zone is intensified and takes in the region of most intensive frontogenesis. The subsidence of stratospheric air, potentially warmer, is locally perceived as a branch of thermally inverse circulation. This subsidence, accompanied by the drawing in of the tropopause, is a result of dynamic (not thermal) factors -- an increase in vorticity and wind velocity in the case of frontogenesis near the tropopause. Descent in the region of maximum frontogenesis appears as a regulator of the sharpness of fronts, constituting an obstacle to the formation of excessively sharp temperature contrasts and redistributing them horizontally.

BIBLIOGRAPHY

1. Vetlov, I. P., FRONTOGENEZ I PREOBRAZOVANIYE VYSOTNYKH DEFORMATSIONNYKH POLEY (Frontogenesis and the Transformation of High Deformation Fields), Leningrad, Gidrometeoizdat, 1951.

2. Dzhordzhio, V. A., "Jet Stream," METEOROLOGIYA I GIDROLOGIYA (Meteorology and Hydrology), No 6, 1956.

3. Pogosyan, Kh. P., Taborovskiy, N. L., "Advective-Dynamic Principles of Frontological Analysis," TRUDY TsIP (Transactions of the Central Institute of Forecasts), No 7(34), 1948.

4. Hoskins, B. J., "Atmospheric Frontogenesis Models: Some Solutions," QUART. J. ROY. METEOROL. SOC., Vol 97, No 412, 1971.

5. Hoskins, B. J., Bretherton, F. P., "Atmospheric Frontogenesis Models: Mathematical Formulation and Solution," J. ATMOS. SCI., Vol 29, No 1, 1972.

6. Hoskins, B. J., Draghici, J., Davies, H. C., "A New Look at the ω-Equation," QUART. J. ROY. METEOROL. SOC., Vol 104, No 439, 1978.

7. Reed, R. J., Danielssen, E. F., "Fronts in the Vicinity of the Tropopause," ARCH. MET. GEOPH. BIOKL., A, Vol 11, No 1, 1959.

UDC 551.524.73(215-13)

SEASONAL TEMPERATURE VARIATIONS IN THE SOUTHERN HEMISPHERE ATMOSPHERE AT ALTITUDES 25-80 KM

Moscow METEOROLOGIYA I GIDROLOGIYA in Russian No 4, Apr 80 pp 12-16

[Article by Candidate of Geographical Sciences Yu. P. Koshel'kov and A. I. Butko, Central Aerological Observatory, submitted for publication 7 July 1979]

Abstract: The amplitudes and phases of the annual and semiannual variations were computed on the basis of the mean monthly temperature values in the southern hemisphere at altitudes 25-80 km. The authors give a comparison with data for the northern hemisphere and describe great interhemispherical differences in the nature of the seasonal variations, confirming the necessity for creating reference models of the atmosphere separately for each hemisphere.

[Text] As is well known, seasonal temperature variations in the lower stratosphere in the southern hemisphere have been successfully investigated on the basis of radiosonde data (for example, see [1-4, 7, 14, 17, 21, 23]). The results of rocket sounding obtained at individual stations in the southern hemisphere and some satellite data have been used by a number of authors for an analysis of seasonal variations in the stratosphere and partially in the mesosphere [3, 9, 16-20, 22]. The limited volume of data gave these investigations a preliminary character. An empirical model of the temperature distribution at altitudes 25-80 km in the southern hemisphere [6], constructed recently on the basis of all available data from rocket sounding (up to 1977), makes it possible, in generalized form, to evaluate the peculiarities of temperature distribution in the upper atmosphere of this hemisphere. The reliability of the mean temperature values obtained in [6], at least to altitudes 50 km, to a definite degree is confirmed by the fact that the addition of supplementary observational data (for a two-year period) and a change in the method for the analysis of the data lead only to insignificant changes in mean temperature values (of

about 1-2°C), as indicated by a comparison with earlier results [5]. It can therefore be assumed that the amplitudes and phases of periodic temperature variations, computed using the data in [6], scarcely change significantly with a further increase in the mass of data from rocket sounding. Definite refinements (especially in the mesosphere) are possible, however, with the accumulation of the results of satellite observations, ensuring global coverage.

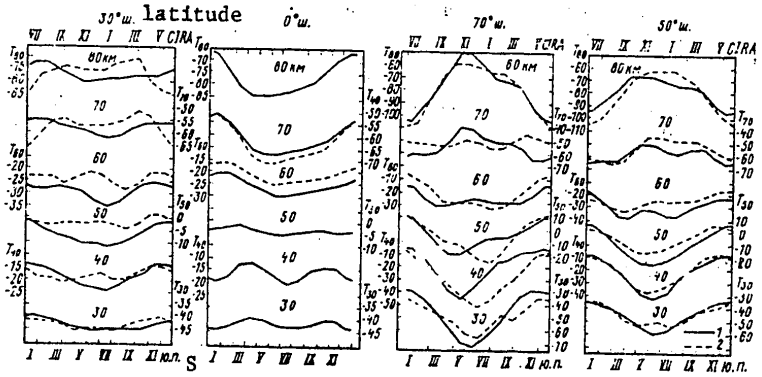

Fig. 1. Seasonal temperature variations in the southern hemisphere (1) [6] and according to model CIRA-1972 (with allowance for annual variation [10] at equator (2).

Figure 1 shows the seasonal variation of mean monthly temperature in the southern hemisphere. As a comparison we have also shown (with a six-month time shift) data from the International Reference Atmosphere COSPAR (CIRA 1972 [11]), based on data for the northern hemisphere (except for the mesosphere of the low and subtropical latitudes, where data for both hemispheres were used). Figure 2 shows the amplitudes and phases of the annual and semiannual variations in the southern hemisphere. Similar data for the northern hemisphere are available in the investigations of both Cole [10] and Nastrom and Belmont [19].

As is well known [21], the lower stratosphere of the equatorial zone is characterized by a similarity of the phase of the annual variation in regions situated to the north and south of the equator. As indicated in Fig. 2, the temperature maximum in the annual variation to the south of the equator is attained in the middle of the year, that is, in the same period as in the northern hemisphere.

Superposed on variations with an annual period are semiannual variations whose relative role is particularly significant in the low latitudes (Fig. 1). The amplitude of the semiannual variations in the stratosphere to the

south of the equator agrees with the results obtained for the northern hemisphere [10, 19]. In the equatorial stratosphere these variations for the most part determine the seasonal temperature changes at altitudes 30-50 km. A secondary maximum of the semiannual temperature variations is developed in the upper mesosphere over the equator. In the seasonal variations in this layer there are also well-developed variations with an annual period, the possible reasons for which are discussed below.

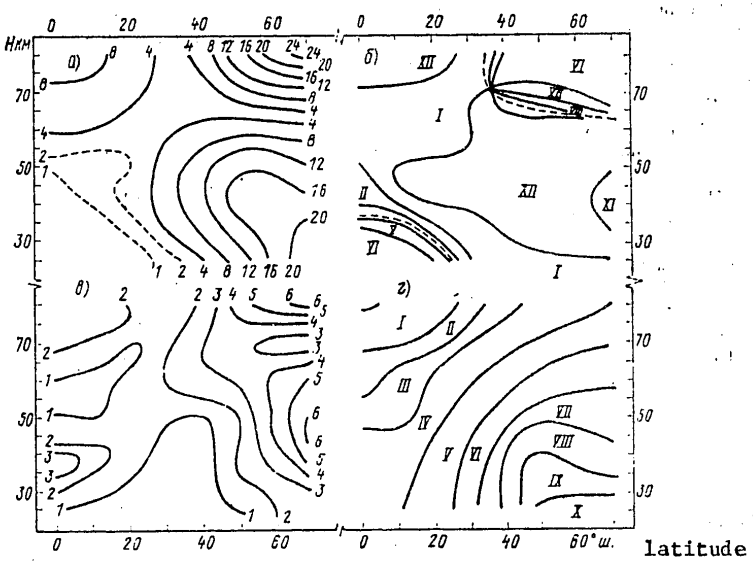

Fig. 2. Amplitude (°C) and phase (time of maximum, month) of annual (a,b) and semiannual (c,d) temperature variation in the southern hemisphere. The dashed line in Fig. 2b denotes regions of a jumplike phase change.

In the subtropical latitudes of the southern hemisphere in the seasonal temperature variation in the stratosphere there are definite differences from the northern hemisphere (Fig. 1). In particular, the lower temperature values during winter in the southern hemisphere upper stratosphere determine the greater amplitude of the seasonal variations in the southern hemisphere than in the northern hemisphere. The winter secondary temperature maximum, revealed from CIRA-1972 data and probably associated with large-scale processes in the northern hemisphere stratosphere, is not expressed in the southern hemisphere. According to our data, the amplitude of the semiannual variation at latitude 30° in the upper stratosphere in the northern hemisphere is greater and the amplitude of the annual variation is less than in the southern hemisphere.

According to satellite data for 1971 [9], the amplitude of the annual variation in the upper stratosphere at 30-40°S (and also in the higher latitudes) exceeds the corresponding value in the northern hemisphere; similar values in the two hemispheres were obtained for the semiannual variation. The analysis of Nastrom and Belmont [19] for the subtropical latitudes of the southern hemisphere reveals a good quantitative agreement with the results in this study for the annual variation, but reveals high values for the amplitude of the semiannual variation in the upper stratosphere at 30°S, exceeding the similar values in the northern hemisphere. According to the data published by Labitzke [17], the amplitude of the annual variation at the 2-mb level in the southern hemisphere is greater than in the northern hemisphere, at all latitudes exceeding 20°.

In the mesosphere of the subtropical latitudes the ratio of the amplitudes of the annual variation in the two hemispheres is the reverse of that which is observed in the stratosphere. In the northern hemisphere [10] at altitudes 75-80 km the amplitude between 30-40° latitude, like over the equator, is 8-10°C; the amplitude and phase of the annual variation change monotonically from the low to the high latitudes. In the southern hemisphere, at latitudes 30-40°, there is a minimum of the annual variation amplitude at the boundary of the two main regions of maximum amplitudes and opposite phases -- tropical and polar (Fig. 2).

The high temperature values in the polar mesosphere during winter, with which the annual variation in this region is associated, are usually attributed to dynamic or aeronomic effects [8]. The reasons for the appearance of the annual variation in the mesosphere over the equator are unclear. The onset of the temperature maximum in December-January, when the distance from the earth to the sun is minimum, is presumably due to the increased radiation heating during this season. It is not impossible that a definite role can also be played by dynamic processes associated with interhemispherical differences in large-scale synoptic processes and possibly with meridional circulation in the extratropical strato-mesosphere during winter. In a study by Labitzke and Barnett [18] the heating of the tropical stratosphere at altitudes 40-45 km at the beginning of the year is related to cooling of the arctic stratosphere after the ending of the winter warming. We note that according to rocket data [15] during a period of warming in the arctic stratosphere there can be a temperature increase in the low-latitude mesosphere. On the other hand, some satellite data indicate a temperature decrease in the upper mesosphere (during a period of stratospheric warming in the Arctic) not only in the high, but also in the low latitudes [13].

In the temperate latitudes of the southern hemisphere, especially at 50°S (Fig. 1), as in the subtropical latitudes, the amplitude of the annual variation is greater than in the CIRA-1972 model. The amplitude of the semiannual variation in the southern hemisphere is less than in the northern hemisphere.

The annual temperature variation in the stratosphere of both hemispheres attains maximum development in the polar regions. It is known that in the middle stratosphere the amplitude of the variation is greater in the southern hemisphere than in the northern hemisphere [2, 3, 14]. As indicated in Fig. 2, a peculiarity of the southern hemisphere is a decrease in amplitude with altitude above 25 km, which is related to the rapid temperature increase in the upper Antarctic stratosphere in the middle of winter. In the Arctic the increase in amplitude of the annual variation with altitude continues to altitudes 40-45 km. Below approximately 35 km the amplitudes of this variation are greater in Antarctica than in the Arctic, but at higher levels the reverse situation prevails.

The amplitude of the semiannual variation over Antarctica, according to data for Molodezhnaya station, attains a maximum in the upper stratosphere, in relation to the appearance of a relatively warm region in this layer in winter [12].

The winter minimum in the seasonal variation of temperature, delayed in the lower stratosphere in Antarctica relative to the Arctic [2], in the upper stratosphere is displaced (Fig. 1) to late autumn - early winter. This is related for the most part not to any change in the phase of the annual variation with altitude, but with an increase in the amplitude and a change in the phase of the semiannual variation with altitude. Figure 2 shows that in the stratosphere over Antarctica the onset of the temperature maximum in the semiannual variation lags with a decrease in altitude, reflecting subsidence of the region of relatively high temperatures during the winter-spring period. In the northern hemisphere, where the semiannual variation is associated primarily with winter stratospheric warmings and the development of a warm region in the northwestern part of the Pacific Ocean, the phase of this variation in the stratosphere, according to CIRA-1972 data, falls in January (July) and changes less with altitude.

It should be noted that in the subantarctic region and in Antarctica (as in the northern hemisphere [19]) in the annual variation a definite role is also played by the third harmonic. Its amplitude in the stratosphere attains 1°C at 70°S (maximum in March), whereas in the mesosphere above 60 km it increases to 2-3° at latitudes 50-70°S (maximum at the end of January).

A general conclusion following from this analysis is that the seasonal temperature variation in the stratosphere and mesosphere in the southern hemisphere has definite peculiarities in comparison with the northern hemisphere. These peculiarities are evidently associated with the interhemispherical differences in the nature of the underlying surface and the ellipticity of the earth's orbit. The existence of interhemispherical differences in the distribution of temperature and other meteorological elements in the middle atmosphere makes it necessary, in particular, to create reference models of the atmosphere separately for each hemisphere. A definite step in this direction is the totality of mean temperature values in the southern hemisphere at altitudes 25-80 km, represented in [6].

BIBLIOGRAPHY

1. Voskresenskiy, A. I., Chukanin, K. I., "Spring Transformations of Thermal Fields in the Lower Stratosphere of Eastern Antarctica," TRUDY AANII (Transactions of the Arctic and Antarctic Scientific Research Institute), Vol 327, 1976.

2. Gaygerov, S. S., AEROLOGIYA POLYARNYKH RAYONOV (Aerology of the Polar Regions), Moscow, Gidrometeoizdat, 1964.

3. Gaygerov, S. S., "Winter Stratospheric Warmings and Spring Restructurings in Antarctica and the Arctic," METEOROLOGIYA I GIDROLOGIYA (Meteorology and Hydrology), No 10, 1967.

4. Koshel'kov, Yu. P., "Peculiarities of the Temperature Field and the Geopotential Field of the 30-mb Surface in the Southern Hemisphere," TRUDY TsAO (Transactions of the Central Aerological Observatory), No 99, 1971.

5. Koshel'kov, Yu. P., "Mean Temperature in the Upper Stratosphere of the Southern Hemisphere," ANTARKTIKA (Antarctica), No 16, 1977.

6. Koshel'kov, Yu. P., "Mean Monthly Temperature in the Southern Hemisphere Mesosphere," TRUDY TsAO, No 140, 1978.

7. Lisogurskiy, N. I., TEMPERATURA I TSIRKULYATSIYA VOZDUKHA V STRATOSFERE ANTARKTIKI (Temperature and Circulation of Air in the Antarctic Stratosphere), Leningrad, Gidrometeoizdat, 1976.

8. Rakipova, L. R., Yefimova, L. K., DINAMIKA VERKHNIKH SLOYEV ATMOSFERY (Dynamics of the Upper Layers of the Atmosphere), Leningrad, Gidrometeoizdat, 1975.

9. Barnett, J. J., "The Mean Meridional Temperature Behaviour of the Stratosphere from November 1970 to November 1971 Derived from Measurements by the SCR on Nimbus IV," QUART. J. ROY. METEOROL. SOC., Vol 100, No 426, 1974.

10. Cole, A. E., "Periodic Oscillations in Stratosphere and Mesosphere," SPACE RES., Vol XV, 1975.

11. COSPAR INTERNATIONAL REFERENCE ATMOSPHERE 1972. CIRA 1972. Akademic Verlag, Berlin, 1972.

12. Gaigerov, S. S., Koshelkov, Yu. P., "Temperature and Wind in the Upper Atmosphere Over the Antarctic," SPACE RES., 1973.

13. Hirota, J., Barnett, J. J., "Planetary Waves in the Winter Mesosphere -- Preliminary Analysis of Nimbus-6 PMR Results," QUART. J. ROY. METEOROL. SOC., Vol 103, 1977.

14. Knittel, J., "Ein Beitrag zur Klimatologie der Stratosphare der Sudhalbkugel," MET. ABHANDL. INST. f. MET. u. INST. f. GEOPHYS. WISS., Ser. A, Bd 2/H 1, 1976, Berlin.

15. Labitzke, K., "The Interaction Between Stratosphere and Mesosphere in Winter," J. ATMOS. SCI., Vol 29, No 7, 1972.

16. Labitzke, K., "The Temperature in the Upper Stratosphere: Differences Between the Hemispheres," JGR, Vol 79, No 15, 1974.

17. Labitzke, K., "Comparison of the Stratospheric Temperature Distribution Over the Northern and Southern Hemispheres," Preprint to COSPAR XIX, Philadelphia, 1976.

18. Labitzke, K., Barnett, J. J., "Global Time and Space Changes of Satellite Radiances Received from the Stratosphere and Lower Mesosphere," JGR, Vol 78, No 3, 1973.

19. Nastrom, G. D., Belmont, A. D., "Periodic Variations in Stratospheric-Mesospheric Temperatures from 20-65 km at 80°N to 30°S," J. ATMOS. SCI., Vol 32, No 9, 1975.

20. Pearson, P. H., "Seasonal Variations of Density, Temperature and Pressure Between 40 and 90 km at Woomera, South Australia, March 1964-March 1965," WEAPONS RES. ESTAB. TECH. MEMO. PAD199, Australia, 1965.

21. Reed, R. J., Vlcek, Ch. L., "The Annual Temperature Variation in the Lower Tropical Stratosphere," J. ATMOS. SCI., Vol 26, No 1, 1969.

22. Rofe, B., "The Stratospheric and Mesospheric Circulation at Mid-Latitudes of the Southern Hemisphere," WEAPONS RES. ESTABL. TECHN. NOTE, PAD115, Australia, 1966.

23. Wexler, H., "Seasonal and Other Temperature Changes in the Antarctic Atmosphere," QUART. J. ROY. METEOROL. SOC., Vol 85, 1959.

UDC 551.515.2(267)

SOME FEATURES OF A TROPICAL CYCLONE OVER THE ARABIAN SEA IN 1977

Moscow METEOROLOGIYA I GIDROLOGIYA in Russian No 4, Apr 80, pp 17-27

[Article by Candidate of Physical and Mathematical Sciences L. I. Petrova, Institute of Experimental Meteorology, submitted for publication 17 July 1979]

Abstract: It is shown that the development of a tropical cyclone in the Arabian Sea during the summer monsoon of 1977 occurred during interaction of processes in the lower and upper troposphere and also the lower stratosphere. On the basis of data from the "Musson-77" expedition the author has made estimates of the components of the equations for the balance of latent heat and the sum of the internal and potential energy of the troposphere during the period of development of the tropical cyclone. There is an important peculiarity in the field of the radial component of wind velocity -- the presence of two layers of inflow. The first, known earlier, was observed in the boundary layer and the second was observed in the middle troposphere. The values of the parameters determining the development of tropical cyclones are computed and they are analyzed.

[Text] During the "bursting" of the summer monsoon of 1977 a tropical cyclone developed over the stationary observation polygon of the "Musson-77" expedition in the Arabian Sea.

A general description of the synoptic conditions for its development and structure were presented in [1, 9]. In this study we will examine a number of important characteristics of the development, structure and energy of this tropical storm, in particular, the relationship of processes in the lower and upper troposphere, the presence of a second layer of inflow in the field of the radial component of wind velocity and formation of a warm "core." In addition, we estimate the potential of development of a tropical cyclone proposed by Gray [13].

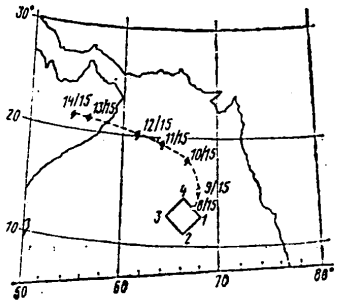

Fig. 1. Trajectory of hurricane in the Arabian Sea during period 8-14 June in 1977 (Moscow time). The rectangle represents the position of the stationary observation polygon of the "Musson-77" expedition formed by the ships: 1) scientific research ship "Akademik Shirshov," 2) scientific research weather ship "Priliv," 3) scientific research weather ship "Priboy," 4) scientific research weather ship "Okean."

Aerosynoptic Conditions

Over the Arabian Sea cyclones usually develop near the equatorial trough during the spring and autumn [17]. In this respect the examined cyclone was no exception. It was generated from a disturbance of the ICZ in the northern hemisphere directly over the stationary observation polygon of the expedition, developed near it into a tropical storm and later attained hurricane force [1]. According to the data in [19], with passage over Massira Island its maximum velocity was 45 m/sec and gusts attained 60 m/sec.

The trajectory of the tropical cyclone and the position of the observation polygon are shown in Fig. 1. The trajectory was plotted on TV photographs of cloud cover obtained from the "Meteor-2(2)" and "Meteor-27" satellites.

During the period directly preceding the development of the tropical cyclone there was a convergence of the convergence zones of the northern and southern hemispheres and there was a considerable intensification of the ICZ in the northern hemisphere: the vertical movements attained 80 x 10^{-4} mb/sec [1]. On the satellite photographs of 5-7 June in the zone of the later developing tropical cyclone it was possible to discriminate a thick cloud concentration of cumulus clouds. At the same time, approximately 2-3 days prior to the onset of active development of the tropical cyclone there was a high-altitude cyclonic eddy of small intensity (at AT_{300} it appeared for the first time on 5 June). Later the cyclonic circulation was propagated to lower levels and on the surface chart the cyclone made its appearance on 8 June.

Thus, the tropical cyclone over the Arabian Sea developed with superposing of cyclonic circulation in the upper troposphere on a region of intensive convection in the lower troposphere. To a certain degree such a process

occurred during the development of hurricane Alice (1-6 July 1973) [14].

Another peculiarity of development of the tropical cyclone is that its development occurred with the interaction of processes not only in the lower and upper troposphere, but also the lower stratosphere. Thus, data on the position of the ozone layer during this period over the investigated region, obtained using an ozonometric probe [7], indicated that the layer with the maximum ozone content descended from 16-19 to 40 mb by 6 June and to 60 mb on 8 June. For such displacements in the stratosphere there should be mean descending movements with a velocity of about 4 cm/sec. One of the possible mechanisms in the relationship between the movement of the layer with the maximum O_3 content and cyclogenesis can be the following. As is well known, among the conditions favorable for the development of tropical cyclones are those favoring the divergence (outflow) of air in the upper troposphere [5, 12]. Descending movements in the stratosphere, leading to the downward movement of the ozone layer, can favor divergence of flow in the upper troposphere. [On the "Musson-77" expedition ozonometric sounding was carried out by GDR specialists.]

The single case of observations undoubtedly does not make it possible to draw any unambiguous conclusions. However, it is possible that movement of the layer of the maximum ozone content can be one of the prognostic criteria for the development of tropical cyclones. It is interesting that during the development of a storm in the Bay of Bengal in August 1977 [17] there were changes in the distribution of ozone similar to those mentioned above. Here we note that on 6-7 June, with displacement of the ozone layer downward to altitudes 19-22 km, there was an increase in air temperature [1], which could be associated both with the absorption of UV radiation by the ozone layer and with adiabatic heating. If the above-mentioned relationships are confirmed in the future on the basis of greater statistical material, they can be used in predicting the development of a tropical cyclone.

Dynamic Characteristics

Figure 2a shows profiles of the radial component of wind velocity V_r at different distances from the center of the cyclone based on data from measurements in its rear part. The figure shows an interesting peculiarity of the V_r profile -- the presence of two layers of inflow: the first, known earlier, is observed in the boundary layer, whereas the second was at levels 500-200 mb. The intensity of the radial flow in the middle troposphere is commensurable with the flow in the boundary layer of the cyclone, and in a number of cases is even greater.

We note that the existence of a second intensive layer of inflow in the rear part of the periphery of a number of tropical cyclones at distances 500-1,000 km from the center was discovered for the first time on the basis of data from the expedition "Tayfun-75" [4]. On this expedition no measurements were made at closer distances.

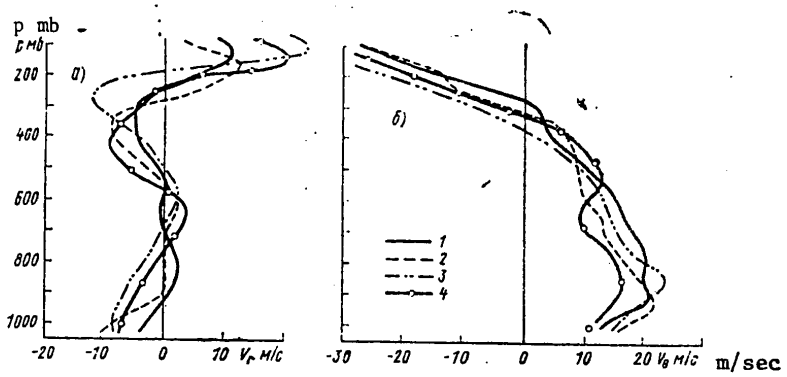

Fig. 2. Profiles of radial V_r (a) and tangential V_θ (b) wind velocity components in developing tropical cyclone at different distances from center. 1) 100 km, weak storm; 2) 250 km, storm; 3) 500 km, strong storm; 4) 700 km, storm of hurricane force

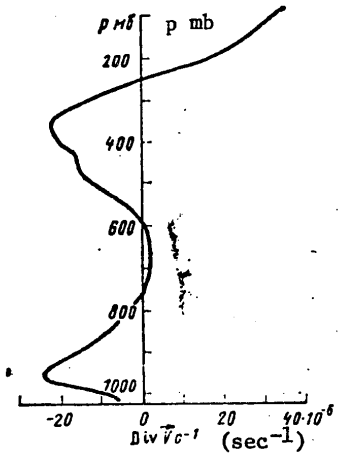

Fig. 3. Averaged profile of divergence of wind velocity Div $\vec{V}$ in tropical storm at distance 300-500 km from center.

The author of [6] analyzed available new experimental data on the structure of the periphery of a tropical cyclone from the point of view of the existence of two layers of inflow, evaluated some characteristics of these layers and expressed the hypothesis that there is a possible relationship between the second layer of inflow and the spiral-like bands in a tropical cyclone.

The profiles of the tangential component of wind velocity in the analyzed tropical cyclone have a "standard" form (see Fig. 2b).

The peculiarities of the radial component should also be manifested in the field of divergence of wind velocity Div $\vec{V}$. Figure 3 shows the mean (for eight sounding times) profile of Div $\vec{V}$ at a distance from the center 300-500 km. It follows from Fig. 3 that in the analyzed cyclone there are two layers of intensive convergence: in the boundary layer and in the middle troposphere.

Taking into account that the principal source of energy in a tropical cyclone is latent heat, it is interesting to compare the quantity of moisture entering the boundary and middle tropospheric layers of inflow. In the first layer the air density is $\rho_1 = 1.10$ kg/m^3 and specific humidity is $q_1 = 15.0$ g/kg. In the second layer $\rho_2 = 0.60$ kg/m^3 and $q_2 = 4$ g/kg. In such a case in a tropical cyclone with a radius R = 400 km, on the assumption of symmetry in the lower layer of inflow, there is entry of approximately $1.2 \cdot 10^5$ tons/sec of water vapor, and in the second layer -- $0.7 \cdot 10^5$ tons/sec, that is, their contribution is commensurable, at least in some cyclones.

An important conclusion can be drawn from the existence of a second layer of inflow in tropical cyclones. As indicated above, the second layer can introduce a quantity of moisture commensurable with that entering in the boundary layer of the tropical cyclone. It is natural to assume that this moisture, the same as that flowing into the first layer, is used in maintaining the vital cycle of a tropical cyclone. In the models of tropical cyclones existing at the present time an allowance is made only for the inflow of moisture in the boundary layer. A description of the process of interaction between the boundary layer and the higher layers is accomplished using the mechanism of conditional instability of the second kind (CISK) [8].

We note that according to this hypothesis the process of development of a tropical cyclone is based on the feedback between mesoscale circulations (clouds) and the large-scale circulation in a cyclone. A cyclonic eddy, as a result of friction against the surface, creates convergence in the boundary layer (so-called frictional convergence), which leads to an upward transfer of water vapor. Clouds develop in the convergence zone. Heat is released in them during condensation. Heating intensifies the cyclonic eddy, which, in turn, increases convergence in the boundary layer, etc. The layer of inflow of mass in the atmospheric boundary layer can serve as an illustration of the appearance of frictional convergence (Fig. 3). But the mentioned mechanism cannot explain the middle troposphere maximum and in general the thick inflow layer. A similar point of view on the CISK hypothesis was expressed in [11], where in a mean "composition" typhoon at a distance of 2-4 degrees in latitude from the center there was found to be a convergence layer extending to considerable heights (250-mb surface), but with a weak intensity. That this is not the only mechanism is also indicated by the noncorrespondence between the mean vertical

velocities at the upper boundary of the boundary layer to the values of the frictional convergence in this layer [20]. Here we should mention a study by Yamasaki [15] in which by means of numerical modeling the author obtained a cyclone even without allowance for friction. True, without friction a number of characteristic features of a tropical cyclone, such as the eye of the storm, are not reproduced.

The considered experimental data indicate that the structure of the inflow in a tropical cyclone can be complex. In the future it is necessary to refine the "statistics" of the second layer of inflow in the field of the radial component of wind velocity, as well as the reasons responsible for it. Evidently, in the middle troposphere of tropical cyclones in a number of cases there is a process (mechanism) acting similarly to friction, that is, which destroys the balance between the Coriolis force, centripetal force and pressure gradient.

Energy of a Tropical Cyclone

In the development of tropical cyclones one of the important and not completely explained problems is the process of formation of the warm "core" in the middle troposphere. We will examine the initial stage in its formation in the analyzed cyclone.

Table 1 gives the diurnal changes in enthalpy c_pT (heat content) of individual layers of the troposphere during the period 4-13 June. Enthalpy was computed using the formula

$$\int_{p_н}^{p_в} \overline{c_p T}^A \frac{dp}{g},$$

[H = lower, B = upper] where p is pressure, $\overline{c_pT}^A$ is the specific quantity of enthalpy averaged over the area A of the observed polygon; g is the acceleration of free falling; p_{lower} and p_{upper} are the isobaric surfaces, being the lower and upper boundaries of the computation layer.

Table 1

Changes in Layer-by-Layer Enthalpy Content in cal/(cm^2·day) in Period 5-13 June

Слои Layers	5—4	6—5	7—6	8—7	9—8	10—9	11—10	12—11	13—2
P_0—900	—65	10	—33	—65	—108	—97	—37	165	150
900—700	—2	39	—22	—38	16	19	49	—9	14
700—500	14	42	—26	—37	10	29	39	—17	—31
500—300	5	41	40	34	20	10	12	—2	—8
300—100	—16	—6	—14	7	36	23	5	—19	7
P_0—100	—64	126	—55	—99	—26	—16	68	119	132

Table 2

Components of Balance Equation ($c_pT + gz$) for Unit Column of Troposphere (from Sea Surface to 100-mb Level) During Period 6-12 June cal/(cm^2·day)

Дата, июнь 1	Общий приток c_pT+gz 2	H	Ra	$L(c-e)$	$\frac{\partial(c_pT+gz)}{dt}$	2+3+4+5	6—7
6	—2660	32	—179	186	216	—2621	2837
7	—2580	77	—134	2420	—144	—217	+73
8	—2190	105	—147	1980	—192	—252	60
9	—2730	84	—79	2620	—55	—105	50
10	190	18	—174	37	45	71	—26
11	390	—4	—232	7	144	161	—17
12	470	3	—252	0	182	221	—39

KEY:
1. Date, June
2. Total influx

Table 3

Components of Equation for Balance of Latent Heat Lq for Unit Column of Troposphere cal/(cm^2·day)

Дата, июнь 1	Общий приток Lq 2	LE	$L(c-e)$	$\frac{dLq}{dt}$	2+3+4	5—6
6	2860	456	—186	405	3130	—2725
7	1810	668	—2420	49	58	—9
8	1120	748	—1980	—136	—112	—24
9	1480	933	—2620	—224	—207	—17
10	—860	769	—37	—126	—128	2
11	—1000	704	—7	—292	—303	11
12	—440	512	—	90	72	18

KEY:
1. Date, June
2. Total influx

The table shows that a considerable increase in the heat content of virtually the entire troposphere over the polygon occurred on 6 June, which is associated with movement of the observation polygon into the active ICZ, where the temperature of the water surface attained 30.5°C [9]. Unfortunately, on 5 June the observations were made approximately 200 km to the south and it is impossible to determine more precisely how long the warm region existed prior to the onset of cyclogenesis. A stationary polygon was formed on 6 June [9]. On the two days which followed, 7-8 June, there was an increase in heat content only in the layer 500-300 mb, whereas the lower-lying layers were cooled. Later the "warming" was propagated downward and upward. After 9 June the hurricane withdrew from the polygon and

the measured data characterized the periphery of the tropical hurricane. The increase in enthalpy in the layer 1000-100 mb ceased in the polygon zone on 11 June, approximately 700 km from the center of the tropical cyclone. Thus, in the analyzed case in the zone of cyclone development several days prior to its development there was a warm zone. During cyclogenesis there was a further accumulation of enthalpy in the middle troposphere. We note that a similar picture was observed in 12 of the 13 analyzed Atlantic hurricanes during 1958-1962 [21]. An exception was hurricane Daisy (1962), before whose initial development a cold "core" was observed in the troposphere.

Now we will examine the dynamics of the components of the equations for the balance of dry static energy ($c_pT + gz$, where gz is potential energy) and moist static energy (Lq, where L is the latent heat of vaporization, q is specific humidity). As is well known [18], in a form convenient for computations on the basis of data from measurements in polygons, the expressions for the mentioned parameters in an isobaric coordinate system can be written in the form

$$\frac{\partial}{\partial t}\int_{p_н}^{p_в}\overline{(c_pT+gz)}\frac{dp}{g}=-\left\{\frac{1}{A}\int_{p_н}^{p_в}\oint_S(c_pT+gz)\,V_n\,dS\,\frac{dp}{g}+\right.$$

$$\left.+\left[\frac{\overline{(c_pT+gz)}_н\,\overline{W}_н}{g}-\frac{\overline{(c_pT+gz)}_в\,\overline{W}_в}{g}\right]\right\}+(\overline{Ra}_н-\overline{Ra}_в)+\overline{H}_н-\overline{H}_в)+ \qquad (1)$$

$$+\int_{p_н}^{p_в}\overline{L(c-e)}\frac{dp}{g},$$

$$\frac{\partial}{\partial t}\int_{p_н}^{p_в}L\overline{q}\,\frac{dp}{g}=-\left\{\frac{1}{A}\int_{p_н}^{p_в}\oint_S LqV_n\,ds\,\frac{dp}{g}+\left(\frac{L\overline{q}_н\,\overline{W}_н}{g}-\frac{L\overline{q}_в\,\overline{W}_в}{g}\right)\right\}+$$

$$+L\overline{E}-\int_{p_н}^{p_в}L\,\overline{(c-e)}\,\frac{dp}{g}. \qquad (2)$$

Here V_n is the wind velocity component normal to the S contour; W = dp/dt. The line at top denotes averaging over the polygon area A.

The mean diurnal values for all the components in formulas (1) and (2) for a unit column of the troposphere (from the sea surface to 100 mb) during the period 6-11 June are given in Tables 2 and 3 respectively. They were determined in the following way. The first terms on the right-hand sides of (1) and (2), representing the total energy influxes into the computation volume, except for vertical transfer by subgrid processes, were computed using data from radiosonde observations made four times a day by the method described in [18]. The turbulent fluxes of heat H and moisture LE, arriving from the ocean, were computed on the basis of standard meteorological measurements:

FOR OFFICIAL USE ONLY

APPROVED FOR RELEASE: 2007/02/08: CIA-RDP82-00850R000200100010-7

$$H = c_p \rho C_\theta (T_0 - T_a) U_a,$$

$$LE = \rho L C_e (q - q_a) U_a,$$

where T_0 is the temperature of the water surface, T_a is air temperature at the 10-m level, U_a is wind velocity at the 10-m level, q_a is specific air humidity at the 10-m level, q_0 is the specific humidity of saturation at $T = T_0$.

The Stanton number C_e and the Dalton number C_θ were estimated in accordance with [10].

An approximate estimate of radiation cooling in 24 hours was made using actinometric sounding data at nighttime [2].

The last term on the right-hand sides of (1) and (2), expressing the heat expenditure on the phase transitions of water (c is the evaporation rate, e is the condensation rate) was also evaluated roughly on the basis of the quantity of precipitation falling in a day. Despite the inadequate accuracy in evaluating a number of components, on all the days, other than 6 June, as follows from the data in Tables 2 and 3, the balance is satisfactorily satisfied for the mean daily values. We note that according to data registered at standard observation times the scatter is far greater. The considerable nonclosure in the balances ($c_pT + gz$) and Lq on 6 June is evidently caused by the falling of precipitation in the central zone of the polygon, beyond the measurement points.

It can be seen from the data in Table 2 that in the development of a tropical cyclone the determining components in the balance of dry static energy are the influxes due to large-scale movements and the release of heat in phase transitions. The same result is obtained in a model experiment [16]. The turbulent heat flux LE is commensurable with the above-mentioned components in the balance of latent heat (see Table 3). Considerable LE values are caused both by the high temperature of the water surface and the great wind velocities. We will also note the considerable variations in tropospheric moisture content.

In Tables 2 and 3, in addition, we give attention to the following peculiarity: through 9 June inclusive there was an influx Lq due to large-scale movements and outflow ($c_pT + gz$). During this period the measurements in the polygon characterized the central zone of a developing cyclone. After 9 June the situation in the polygon was opposite -- the outflow Lq and inflow ($c_pT + gz$). At this time the observation polygon was on the periphery of the intensifying tropical cyclone. This fact agrees with the tendency noted in [4] (on the basis of an analysis of data from the "Tayfun-75" expedition) for a predominance of outflows of latent heat Lq (inflows $c_pT + gz$) on the periphery of developing typhoons. Proceeding on the basis of the fact that the principal energy source for the active zone of a tropical cyclone is the moisture arriving from the periphery [5], it is natural to

assume that the absence of outflow Lq on the periphery is evidence of a decrease in the energy supply of the central zone, and accordingly, of an attenuation of the intensity of a tropical cyclone.

Table 4

Values of Parameters Determining the Development of Tropical Cyclones

	7 E 10^3 кал/см²	8 $\frac{\partial\Theta_e}{\partial p}$ + 5 K/500 мб	RH	9 TP кал/(см$^{+2}$ × K/500 мб)	10 ζ+5 10^{-6} с$^{-1}$	11 $\frac{1}{S_2+3}$ 750 мб/(м·с$^{-1}$)	10 f 10^{-5} с$^{-1}$	12 DP $\frac{10^{-11}\cdot с^{-2}}{м\cdot с^{-1}/750\ мб}$	13 G $\frac{1{,}5\cdot10^{-8}\ кал\cdot K}{см^3}$
5 июня 1	174	11	0,8	1,5	16	0,08	3,1	3	5
типичный неразв. кластер 2	100	20	1	2	12	0,10	3	3	6
6 июня 1	267	12	1	3,2	6	0,11	3,1	2	6
развив. кластер 1-й день 3	100	20	1	2	18	0,14	3	8	16
7 июня 1	331	9	1	3,0	15	0,14	3,1	7	21
развив. кластер 2-й день 4	100	20	1	2	30	0,15	3	15	30
8 июня 1	304	6	1	1,8	30	0,11	3,1	10	18
развив. кластер 3-й день 5	100	20	1	2	55	0,25	3	40	80
9 июня 1	295	10	1	2,9	18	0,16	3,1	9	26
тропический циклон (макс. скорость ветра 10 м/с при R=200 км) 6	100	20	1	2	100	0,33	3	100	200

Note: The values of the cyclogenesis parameters for clusters were taken from [13].

KEY:

1. ...June
2. Typical nondeveloping cluster
3. Developing cluster on first day
4. Developing cluster on second day
5. Developing cluster on third day
6. Tropical cyclone (maximum wind velocity 10 m/sec with R = 200 km)
7. cal/cm^2
8. mb
9. TP cal/(cm^{+2}·k/500 mb
10. sec^{-1}
11. mb/(m·sec^{-1})
12. DP 10^{-11}·sec^{-2}/m·sec^{-1}/750 mb
13. G $1.5\cdot10^{-8}$ cal·K/cm^3

Evaluation of Parameters Determining Development of a Tropical Cyclone

On the basis of a generalization of the results of numerous investigations of the conditions for the development of tropical cyclones Gray [13] proposed the following six parameters determining the development of a tropical cyclone:

1. The vorticity parameter ($\zeta_r + 5$), where ζ_r is relative vorticity at the boundary of the boundary layer (about 950 mb), expressed in 10^{-6} sec^{-1};
2. The Coriolis parameter $f = 2\omega \sin\varphi$, ω is the angular velocity of the earth's rotation, φ is latitude;
3. The vertical shear parameter $(\partial U/\partial p + 3)^{-1}$, where $\partial U/\partial p$ is the velocity gradient between the levels 950 and 200 mb, expressed in m/sec at 750 mb;
4. The ocean energy parameter

$$E = \int_{z_T = 26\,^\circ C}^{\text{пов}} \rho_w c_w (T_z - 26)\, dz,$$

[ПОВ = sur(face)] where ρ_W is water density in the ocean, c_W is the specific heat capacity of water, T is ocean temperature.
5. The moist stability parameter $(\partial \theta_e/\partial p + 5)$, where $\partial \theta_e/\partial p$ is the gradient of equivalent-potential temperature in the surface - 500-mb layer, expressed in K/500 mb;
6. The humidity parameter RH - 40/30, where RH is the mean relative humidity in the layer 700-500 mb.

The physical sense of each of the mentioned parameters was discussed in detail in [13]. In the cited study the product of the first three parameters is called the dynamic potential DP and the next three are called the thermal potential TP of generation of a tropical cyclone. The parameter G = TP·DP has been proposed as the generation potential. A climatological evaluation of G gives a good correspondence with the frequency of occurrence of a tropical cyclone.

Gray also carried out computations of the diurnal values of potential of generation for individual clusters later developing into tropical cyclones. Taking advantage of the fact that there are measurement data for the zone of hurricane development, we will evaluate the diurnal values of generation potential and compare them with the corresponding values given in [13]. Table 4 gives the diurnal values of individual parameters and the potential of formation of the analyzed tropical cyclone (numerator) and for clusters (denominator). As the critical value, indicating the further development of a disturbance into a hurricane, Gray obtained a value equal to 30. Table 4 shows that according to measurements made in the polygon during the period directly preceding intensification of the disturbance of 6-7 June the potential did not attain the mentioned critical value, although the disturbance then developed to a hurricane. According to Gray's data, in a developing tropical cyclone with winds up to

10 m/sec at a distance of 200 km from the center the generation potential value attains 200, whereas according to measurement data in the polygon at approximately this same distance from the center of a tropical cyclone in the storm stage G = 26.

Now we will examine individual parameters. The ocean energy parameter E is very high; it exceeds Gray's evaluations by a factor of approximately three. This is attributable to the fact that in the formation zone, as already mentioned, the temperature of the water surface was very high and there was a thick layer of the ocean with $T_w > 26.5°C$. We note that Gray concluded that E has a small variability. The analyzed case indicates that this is not always the case. At first glance it is surprising that there are such relatively low values of the instability parameter $\partial\theta_e/\partial p$, but in our opinion this is caused by intensive vertical exchange. The humidity parameter is evidently a conservative characteristic. In general, the thermal potential in the considered case is greater.

The vorticity parameter merits particular attention among the parameters determining the dynamic potential. Table 4 shows that its value is 3-6 times less than the values obtained in [13]. In addition, we note that at the 950-mb level it was not rare on the basis of polygon measurements to obtain $\zeta < 0$. Table 4 gives mean ζ values for the layer 950-900 mb. In principle it is not at all surprising that in the presence of a cyclonic circulation in individual zones there will be negative vorticity. As is well known, in a cylindrical coordinate system vorticity is determined using the formula

$$\zeta_r = \frac{1}{r}\left[\frac{\partial (rV_\varphi)}{\partial r} - \frac{\partial V_r}{\partial \varphi}\right],$$

where r is the radius.

For an axially symmetric case $\partial V_r/\partial\varphi = 0$ and

$$\zeta_r = \frac{V_\varphi}{r} + \frac{\partial V_\varphi}{\partial r}.$$

With a distribution of the tangential velocity in accordance with the law $V_\varphi = cr^{-x}$, where $x > 1$, the vorticity will be negative when there is a cyclonic circulation.

Such a $V\varphi$ distribution can be observed precisely in the boundary layer of a hurricane (typhoon) at distances exceeding (excluding the periphery) the radius of the maximum winds.

The authors of [3], in an analysis of data from the expedition "Tayfun-75," also pointed out the negative vorticity value (on the basis of polygon measurements) in tropical lows. The noncorrespondence between the sign of vorticity and the type of circulation disappears if vorticity is computed along the contour taking in the center of circulation. We note that in evaluating the Gray parameters over the course of a two-week period in

the zone of potential formation of tropical cyclones on the basis of data from the "Tayfun-78" expedition [3] it was found that the vorticity parameter (evaluated on the basis of polygon measurements) in many cases had a negative value and in general was characterized by a very great dispersion.

The wind shear parameter was somewhat less (the shear was greater) than in the investigations in [13]. The Coriolis parameter, naturally, differs little and it can be regarded as a scaling factor. In general, the DP value was lower and the TP value was higher than according to the data in [13].

Thus, the investigation carried out in this section indicates that the generation potential for a tropical cyclone proposed in [13], which is well confirmed on the basis of climatological data, cannot be directly used in corresponding evaluations on the basis of local (polygon) measurements. In particular, attention must be given to relative vorticity, and possibly a refinement should be made in the region of its determination. A further checking of potential in other individual cases of hurricane development is necessary.

BIBLIOGRAPHY

1. Veselov, Ye. P., Bel'skaya, N. N., Petrova, L. I., Papezh, A., "Peculiarities in the Development of a Tropical Cyclone Over the Arabian Sea During the Period of 'Bursting' of the Monsoon in June 1977," METEOROLOGICHESKIYE ISSLEDOVANIYA (Meteorological Investigations), No 24, 1979.

2. Zaytseva, N. A., "Spatial-Temporal Variability of Long-Wave Radiation Fluxes and Heat Influxes Under Conditions of Monsoonal Circulation," METEOROLOGICHESKIYE ISSLEDOVANIYA, No 24, 1979.

3. Ivanov, V. N., Mikhaylova, L.A., Nekrasov, I. V., "Some Statistical Properties of the Phenomenological Parameters of Cyclogenesis in the Tropical Zone," TAYFUN-78 (Typhoon-78), Leningrad, Gidrometeoizdat, 1980.

4. Nesterova, A. V., Petrova, L. I., "Dynamics and Energy of the Troposphere According to Data from the 'Tayfun-75' Expedition," TRUDY IEM, No 22(87), 1979.

5. Pal'men, E., N'yuton, Ch., TSIRKULYATSIONNYYE SISTEMY ATMOSFERY (Circulation Systems in the Atmosphere), Leningrad, Gidrometeoizdat, 1973.

6. Petrova, L. I., Nesterova, A. V., "Inflow Layer on the Periphery of Tropical Cyclones," TAYFUN-78, Leningrad, Gidrometeoizdat, 1980.

7. Plessing, P., Fayster, U., Peters, E., "Results of Ozone Radiosonde Measurements in the International Experiment 'Musson-77'," METEOROLOGICHESKIYE ISSLEDOVANIYA, No 25, 1980.

8. Khain, A. P., "Methods for the Parameterization of Convection Used in the Modeling of Tropical Cyclones," TAYFUN-75, Vol 2, Leningrad, Gidrometeoizdat, 1978.

9. Chuchkalov, B. S., "First Results of Experiment 'Musson-77'," METEOROLOGICHESKIYE ISSLEDOVANIYA, No 24, 1979.

10. Bunker, A. F., "Computations of Surface Energy Flux and Annual Air-Sea Interaction Cycles of the North Atlantic Ocean," MON. WEATHER REV., Vol 104, 1976.

11. Frank, W. M., "The Structure and Energetics of a Tropical Cyclone," ATMOS. SCI. PAPER, No 258, Colorado State University, 1976.

12. Gautier, M. C., "Cyclogenese Tropicale," METEOROLOGIE, No 6, 1976.

13. Gray, W. M., "Tropical Cyclone Genesis," ATMOS. SCI. PAPER, No 234, Colorado State University, 1975.

14. Herbert, P. Y., Frank, N. L., "Atlantic Hurricane Season of 1973," MON. WEATHER REV., Vol 102, No 4, 1974.

15. Yamasaki, M., "The Rate of Surface Friction in Tropical Cyclones," J. METEOROL. SOC. JAPAN, Vol 56, No 6, 1977.

16. Kurihara, Y., "Budget of Tropical Cyclone Simulated in an Axisymmetric Numerical Model," J. ATMOS. SCI., Vol 32, No 1, 1975.

17. Ramage, C. S., "Monsoonal Influence of the Annual Variation of Tropical Cyclone Development Over the Indian and Pacific Oceans," MON. WEATHER REV., Vol 102, No 11, 1974.

18. Rasmusson, E. M., "Mass Momentum and Energy Budget Equations for BOMAP Computations," NOAA TECHNICAL MEMORANDUM ERL, BOMAP-3, 1971.

19. Watts, D., "Severe Cyclones in the Arabian Gulf - June 1977," WEATHER, Vol 33, No 3, 1978.

20. Williams, K. T., Gray, W. M., "A Statistical Analysis of Satellite-Observed Trade Wind Cloud Clusters in the Western North Pacific," TELLUS, Vol 21, 1973.

21. Zipser, E. J., "On the Thermal Structure of Developing Tropical Cyclones," Nat. Hurric. Res. Proj. Preprint, No 67, 1964.

UDC 551.(521.3:510.42)

INFLUENCE OF ATMOSPHERIC CONDENSATION NUCLEI ON THE ATTENUATION OF SOLAR AND LONG-WAVE RADIATION

Moscow METEOROLOGIYA I GIDROLOGIYA in Russian No 4, Apr 80 pp 28-39

[Article by Candidate of Physical and Mathematical Sciences V. I. Khvorost'yanov, Ukrainian Scientific Research Hydrometeorological Institute, submitted for publication 27 July 1979]

Abstract: The microphysical model of condensation nuclei proposed by L. M. Levin, Yu. S. Sedunov and V. I. Smirnov is used in computing the aerosol sections of attenuation and absorption of solar and long-wave radiation and also spectral optical thicknesses. It is shown that the dependence of these characteristics on wavelength and relative humidity is described by power laws and the parameters determining them are related to one another and can be expressed through the microphysical characteristics of the aerosol. The computed values agree well with the experimental data. By means of averaging in the wavelength spectrum it was possible to derive expressions for the integral optical thickness of the effective wavelength of aerosol scattering and the aerosol part of the Linke turbidity factor.

[Text] The determination of interrelationships between microphysical and optical properties of atmospheric condensation nuclei is of interest both for cloud physics and for atmospheric optics because it makes it possible, using optical measurements, to investigate the characteristics of condensation nuclei and processes leading to cloud formation and also makes it possible to improve optical methods for monitoring atmospheric contamination.

Two of the most important optical characteristics of atmospheric aerosol, making it possible to judge its microstructure, are the dependence of the attenuation cross section σ and the dependence of optical thickness τ on radiation wavelength λ and on humidity H. The $\sigma(\lambda)$ and $\tau(\lambda)$

dependences, determined by the empirical Angstrom law $\sigma(\lambda)$, $\tau(\lambda)\sim\lambda^{-Q}$ were experimentally investigated in [4, 6, 7, 22]. In [22] the Angstrom law was theoretically related to the existence of the Junge aerosol spectra (see also [8, 18]), but with such an approach it is not possible to describe the dependences $\sigma(H)$, $\tau(H)$, although these parameters, according to experimental data [3, 4, 6, 16], with an increase in humidity, can increase by a factor of several times. In [19-21] the $\sigma(H)$ dependence was computed using empirical formulas correctly describing the growth of nuclei with an increase in humidity, but not relating it to the microstructure of an aerosol, and in [1] -- with an allowance for microphysical processes. In these cases the Mie function was assumed to be equal to two, but numerical computations do not always make it possible to detect functional dependences between radiation and microphysical properties of nuclei.

In an earlier communication [17] there was a brief exposition of the results obtained when using a microphysical model of condensation nuclei formulated by L. M. Levin, Yu. S. Sedunov [11, 13] and V. I. Smirnov [15] for computing the optical attenuation cross sections. In this article, in addition to the optical cross sections, this model is used in computing the spectral optical thicknesses and the coefficients of absorption of long-wave radiation. It is shown that the dependences of these parameters on wavelength and on humidity are described by power laws; a correlation is established between them and the parameters determining them are expressed through the microphysical characteristics of the aerosol. By means of averaging in the wavelength spectrum it was possible to derive expressions for the integral optical thickness, the effective wavelength and the aerosol part of the Linke turbidity factor.

Short-Wave Radiation Attenuation Cross Sections

The process of formation of the aerosol spectrum is essentially dependent on relative humidity H. With $H > 70\%$ (only such a case is considered in this article) the supersaturation value $\delta = e_\infty - e_r/e_\infty$, regulating the rate of growth of particles, is determined by the hygroscopicity and surface tension effects [13:

$$\delta(r) = 1 - (1 - \delta_0)\exp\left(\frac{B}{r}\right)\left(1 - \frac{C}{r^3}\right), \qquad (1)$$

where e_r and e_∞ are the vapor pressures over the surface of a droplet of the radius r and at infinity, $B = 2\sigma/R_v T\rho_w \approx 1.2\cdot10^{-7}$ cm is the Kelvin parameter, σ is surface tension, R_v is the gas constant of vapor, $C = br_0^{3(1+\alpha)}$ is the activity of the nucleus, r_0 is the radius of a dry nucleus, δ_0 is supersaturation over the plane surface of the water.

The mass of the soluble part of the nucleus is proportional to its activity, that is, with $\alpha = 0.5$ -- to the volume of the nucleus and with $\alpha = 0$ -- to its surface [9].

The equilibrium size of the particle is determined from the condition $\delta(r) = 0$. If the spectrum of dry aerosol is described by a Junge distribution $f(r_0) = ar_0^{-\nu}$, then, as indicated in [11, 13, 15], with $H > 70\%$ the size distribution function for aerosol particles $f(r)$ will be as follows:

$$[\Gamma p = gr] f(r) = \frac{a}{1+\alpha}\left(\frac{b}{B}\right)^{(\nu-1)/2(1+\alpha)} \left(1-\frac{2}{3}\frac{r}{r_{rp}}\right)^{-\frac{\nu+2\alpha+1}{2(1+\alpha)}} \left(1-\frac{r_*}{r_{rp}}\right) r^{-\frac{\nu+\alpha}{1+\alpha}}; \quad (2)$$

$$r_{rp} = \frac{2B}{3}\frac{1-\delta_0}{\delta_0}.$$

The attenuation cross section σ_λ^{at} and the absorption coefficient $\sigma_{a\lambda}$ can be computed using the known formulas

$$\sigma_\lambda^{at} = \pi \int_{r_{min}}^{r_{max}} dr r^2 f(r)\, K_{at}(2\pi r/\lambda), \quad (3)$$

$$\alpha_{a\lambda} = \pi \int_{r_{min}}^{r_{max}} dr r^2 f(r)\, K_{abs}(2\pi r/\lambda). \quad (4)$$

The distribution (2) is not a power-law distribution and the dependences $\sigma(\lambda)$, $\sigma(H)$ obtained using it, employing (3), also must not be power-law dependences, as in [1, 19-21]. But it is found that in this problem it is possible to use the power-law approximations (2). In actuality, when $H < 100\%$ $r_{gr} < 0$ and in the humidity range 70-97% the $|r_{gr}|$ value falls in the range $2 \cdot 10^{-7}$-$2.6 \cdot 10^{-6}$ cm. As indicated by numerical computations with the use of (2) and the $K(2\pi r/\lambda)$ values computed using the Mie theory, the maximum of the integrand in formula (3) for σ_λ^{at} with $\lambda = 0.5\,\mu m$ is near $r \sim 0.2\,\mu m$ (curves 1, 2 in Fig. 1), and more than 95% of the contribution to the integral (3) for σ_λ^{at} is from the region $r > 0.06\,\mu m$. But in this region in the indicated range of humidities $r \gg |r_{gr}|$ and by analogy with [15] with an accuracy to first-order terms for $|r_{gr}|/r$ and taking into account the expression $(1-\delta_0)/[\delta_0 = (H-1)^{-1}]$ the $f(r)$ function can be represented in the form

$$f(r) = \frac{3}{2}\frac{a}{1+\alpha}\left(\frac{b}{1-H}\right)^R \left[1-\left(R+\frac{1}{3}\right)\frac{B}{r}(1-H)^{-1}\right] r^{-\frac{3\nu+2\alpha-1}{2(1+\alpha)}}. \quad (5)$$

******

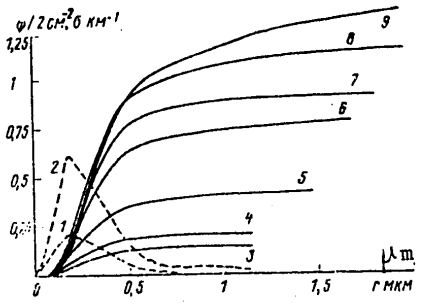

Fig. 1. Dependence of attenuation cross sections σ^{at} on the upper integration limit making computations using (6)-(10) and integrand ψ in (3), computed using (2) with H = 70% (curve 1) and H = 90% (2). Curves 3-6: ν = 4 and H corresponding to 70, 80, 90 and 95%; curves 7-9: H = 97% and ν corresponding to 4.5, 4 and 3.5.

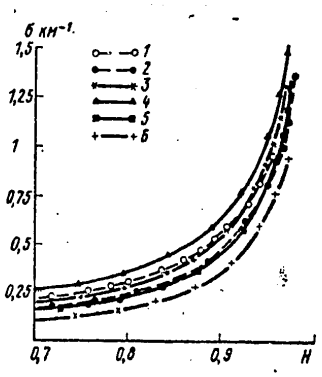

Fig. 2. Dependence of experimental cross sections σ^{at} and those computed using (6)-(10) on humidity. 1, 3) experiment [4] and computations with λ = 0.5 μm; 2, 5) experiment [16] and computations with λ = 0.59 μm; 4, 6) computations with λ = 0.59 μm, α = 0.5 and ν corresponding to 3.5 and 4.5.

The a value can be determined from the condition of normalization to the concentration of dry aerosol:

$$a = N(\nu - 1) r_{min}^{\nu-1}\left[1 - \left(\frac{r_{min}}{r_{max}}\right)^{\nu-1}\right].$$

Substituting (5) into (3), for σ_λ^{at} we obtain

$$\sigma_\lambda^{at}(H) = D_1(\nu, \alpha) N\lambda^{-Q}(1-H)^{-R} - \\ - D_2(\nu, \alpha) N\lambda^{-(Q+1)}(1-H)^{-(R+1)}, \quad (6)$$

where D_1, D_2, R, Q are constants dependent on aerosol microstructure:

$$D_1(\nu, \alpha) = 3 \cdot 2^Q \cdot \pi^{Q+1} b^R r_{min}^{\nu-1}\left[1 - \left(\frac{r_{min}}{r_{max}}\right)^{\nu-1}\right] RI_1, \quad (7)$$

$$D_2(\nu, \alpha) = 3 \cdot 2^{Q+1} \pi^{Q+2} b^R r_{min}^{\nu-1}\left[1 - \left(\frac{r_{min}}{r_{max}}\right)^{\nu-1}\right] R\left(R + \frac{1}{3}\right) I_2, \quad (8)$$

$$R = (\nu - 1)/2(1 + \alpha), \quad Q = (3\nu - 4\alpha - 7)/2(1 + \alpha), \quad (9)$$

I_1, I_2 are dimensionless integrals:

$$I_1 = \int_{x_{min}}^{x_{max}} dx\, x^{-(Q+1)} K_{at}(x), \quad I_2 = \int_{x_{min}}^{x_{max}} dx\, x^{-(Q+2)} K_{abs}, \quad x_{min,\,max} = 2\pi r_{min,\,max}/\lambda. \quad (10)$$

Figure 1 shows that the integrand (3) for the visible region of the spectrum decreases rapidly outside the region $0.06 < r < 0.6\,\mu m$; therefore, we can accomplish the transition $x_{min} \to 0$, $x_{max} \to \infty$, after which the integrals are not dependent on the limits. Computations indicated that this exerts no influence on the results.

Formula (6) shows that the dependence of σ^{at} on wavelength (Angstrom law) and on relative humidity are expressed by power laws; as can be seen from (9), the corresponding exponents are linearly related: Q = 3R - 2. The Q and R values for different ν, α are given in Table 1.

Table 1 shows that in the Junge model of dry aerosol $\nu = 4$ in the case of the soluble part, proportional to the volume of the nucleus, $\alpha = 0.5$ (and also for $\nu = 3$, $\alpha = 0$), Q = R = 1, $\sigma(\lambda) \sim \lambda^{-1}$, $\sigma(H) \sim (1 - H)^{-1}$. This case evidently is encountered most frequently in the atmosphere. We made computations of σ^{at} using (6)-(10) with $\alpha = 0.5$, b = 0.25 [11, 13] and the mean values of continental aerosol $r_{min} = 10^{-5}$ cm, $N = 10^3$ cm^{-3} [18]. The results are presented in Figures 1 and 2. Figure 1 shows that the principal contribution to the attenuation of solar radiation is from particles in the range of radii 0.1-0.6μm, which agrees with the observational data [4, 6]. This interval is broadened with an increase in H and a decrease in ν. Figure 2 illustrates the dependence $\sigma(H)$. The theoretical curves are close to the experimental curves with $\nu = 4$.

The good agreement of the curves indicates the following: 1) atmospheric turbidity with H > 70% is due to an increase of cloud condensation nuclei measuring 0.1- 1 μm; 2) although atmospheric aerosol is a complex multicomponent mixture [7, 12, 18], the dependences $\sigma(\lambda)$, $\sigma(H)$ with H > 70% can be described using one or two distribution functions with some effective ν, α, N.

Table 2 gives the D_1, D_2 values, by using which, with formula (6) it is easy to compute σ^{at} with different ν, λ and N. In this case $[\lambda]$ = cm^{-1}, [N] = cm^{-3} and $[\sigma^{at}]$ = cm^{-1}.

The contribution of the second term in (6) attains 8% with H = 90% and 18% with H = 95%, that is, in evaluations of σ^{at} with the corresponding error this can be neglected. In the case H→100%, when $|r_{gr}|$ is great, expression (5) loses sense and for f(r) it is possible to use (2) with the neglecting of $r/|r_{gr}|$. Substituting it into (3), we obtain

$$\sigma_1^{at} = D_3 \lambda^{-p}; \quad D_3 = \frac{a}{1+\alpha}\left(\frac{b}{B}\right)^R 2^p \pi^{p+1}; \quad I_3 = \int_{x_{min}}^{x_{max}} dx\, x^{-(p+1)} K_{at}, \tag{11}$$

where $p = (\nu - 2\alpha - 3)/(1+\alpha)$, that is, with H→100% σ^{at} does not tend to infinity, but tends to a finite limit σ_1. As can be seen from (9) and (11), p = 2R - 2, p = Q - R and since in all cases R > 0, p < Q, that is, with an increase in humidity, the dependence of attenuation on wavelength decreases, which agrees with the observations in [18]. This is illustrated by Table 1, where p < Q for all ν and α. With ν = 4, α = 0.5 (or ν = 3, λ = 0) p = 0, that is, a transition of attenuation to neutral, observed in clouds and fog (white light) [10], already occurs in the stage of inadequate saturation, which agrees with observations [10, 18]. With α = 0.5 and ν = 3 (or ν = 3.5) p < 0, attenuation increases with wavelength; this effect should be observed when H→100% in hazes containing a sufficient number of large particles (for example, some sea hazes), as can be seen from the ν values. With ν = 4.5 σ_1 = 2.7 km^{-1} (visibility range V = 1.4 km), with ν = 5 σ_1 = 2.2 km (V = 1.8 km). A further deterioration of visibility occurs in the case of a positive supersaturation, that is, the existence of dense clouds (V ~ 100 m) when incomplete saturation is impossible.

The visibility range in a homogeneous air mass with 70% < H < 95% is

$$V(H) = 3{,}91/\sigma = A(1-H)^R, \tag{12}$$

where $A = 3.91\,\lambda^Q/D_1$. For λ = 0.5 μm, ν = 4, α = 0.5, the value A ≈ 73 km, R = 1. Formula (12), like in [19, 20], can be used in predicting the visibility range.

Using (6)-(10) with σ^{at} measurement data in the case H < 95% it is easy to determine Q and R:

$$Q = \ln \frac{\sigma^{at}(\lambda_1)}{\sigma^{at}(\lambda_2)} \Big/ \ln \frac{\lambda_2}{\lambda_1}; \quad R = \ln \frac{\sigma^{at}(H_1)}{\sigma^{at}(H_2)} \Big/ \ln \frac{1-H_2}{1-H_1},$$

and then N. The correlation between Q and R makes it possible, using σ_{at} measurements for two wavelengths, to establish the dependence $\sigma^{at}(H)$ and to predict V. Knowing one of the values Q or R, it is possible to determine the other, washing the soluble part from the aerosol sample and determining α.

The cited σ^{at} values were obtained with a refractive index of aerosol matter n = 1.5. For taking the dependence n(H) into account, we will assume, as in [19], that

$$n(H) = n_1 \frac{r^3(H_1)}{r^3(H)} + n_w \frac{r^3(H) - r^3(H_1)}{r^3(H)},$$

where n_w is the index for water, $n_1 = n(H_1)$. Here $H_1 = 70\%$. Using [11, 13, 15] we obtain

$$r(H) = C^{1/3}(1-H)^{-1/3}[1+(B/3C^{1/3})(1-H)^{-2/3}]^{-1},$$

which gives

$$n(H) = n_w + (n_1 - n_w)\frac{\theta(H)}{\theta(H_1)}, \theta(H) = (1-H)[1+(B/3C^{1/3})(1-H)^{-2/3}]^3$$

The dependence n(H) can be taken into account by substituting in the Mie functions in (3) the argument:

$$K\left(\frac{2\pi r}{\lambda}\frac{n(H)-1}{n_1-1}\right),$$

as follows, for example, from the Van de Hulst formula [8]. This essentially involves multiplying the first term in (6) by

$$\left(\frac{n(H)-1}{n_1-1}\right)^Q \text{ and the second term by } \left(\frac{n(H)-1}{n_1-1}\right)^{Q+1}.$$

The evaluations indicated that allowance for n(H) in the considered humidity range gives corrections to σ^{at} less than 14%.

Table 1

Q Values (Numerator), P (Denominator) and R (After Semicolon)

α	ν				
	3	3,5	4	4,5	5
0	$\frac{1}{0}$; 1	$\frac{1,75}{0,5}$; 1,25	$\frac{2,5}{1}$; 1,5	$\frac{3,25}{1,5}$; 1,75	$\frac{4}{2}$; 1,33
0,5	$\frac{0}{-0,67}$; 0,67	$\frac{0,5}{-0,33}$; 0,83	$\frac{1}{0}$; 1	$\frac{1,5}{0,33}$; 1,17	$\frac{2}{0,67}$; 1,33

Table 2

D_1, D_2 Values in Formula (6) With $\alpha = 0.5$ and Different ν

	ν				
	3	3,5	4	4,5	5
D_1	$0,23\cdot10^{-8}$	$0,75\cdot10^{-11}$	$0,29\cdot10^{-13}$	$0,13\cdot10^{-16}$	$0,72\cdot10^{-18}$
D_2	$0,37\cdot10^{-13}$	$0,21\cdot10^{-17}$	$0,14\cdot10^{-19}$	$0,68\cdot10^{-21}$	$0,6\cdot10^{-23}$

Aerosol Absorption of Long-Wave Radiation

In a similar way it is possible to examine aerosol absorption in the window of transparency 8-12μm. According to K. S. Shifrin [8], the absorption section is

$$\sigma_\lambda(r) = \pi r^2 \left(1 - \exp\left(-\frac{8\pi\varkappa r}{\lambda}\right)\right), \tag{13}$$

where $\varkappa$ is the fictitious part of the refractive index of aerosol matter. For the most common case R = 1 (that is, $\nu = 4$, $\alpha = 0.5$ or $\nu = 3$, $\alpha = 0$) the substitution of (13) into (4), integration and use of asymptotic formulas for the integral exponents $\mathrm{Ei}(-x) \approx c + \ln x$ with

$$x = \frac{8\pi\varkappa r_{\min}}{\lambda} \ll 1 \quad \text{and} \quad \mathrm{Ei}(-x) \approx -\frac{\exp(-x)}{x} \quad \text{with} \quad x = \frac{8\pi\varkappa r_{\max}}{\lambda} \gg 1$$

gives for the absorption coefficient

$$\alpha_{a\lambda} = \frac{12\pi^2\varkappa N(\nu-1)\, r_{\min}^{\nu-1}}{\lambda(1+\alpha)} \frac{b}{1-H}\left[1 - c - \ln\frac{8\pi\varkappa r_{\min}}{\lambda} - \frac{\lambda}{8\pi\varkappa r_{\max}} - \left(R + \frac{1}{3}\right)(1-H)^{-1}\frac{B}{r_{\min}}\right], \tag{14}$$

where c = 0.577 is the Euler constant. The main contribution in the brackets is from the third term, describing the contribution to absorption from the finely disperse fraction: $-\ln 8\pi\varkappa r_{\min}/\lambda \approx 4$ with $\varkappa = 0.1$, $r_{\min} = 10^{-5}$ cm, $\lambda = 10\mu$m. The fourth term, describing the contribution of the coarsely disperse fraction, is equal to 0.4 with $r_{\max} = 10\mu$m. Thus, the greatest contribution to absorption is from the finely disperse aerosol and the correlation of the absorption coefficient with the finely disperse fraction must be far greater than with the coarsely disperse fraction, which agrees with the experimental data [12, 16]. Table 3 gives the coefficients of aerosol absorption of radiation with a wavelength $\lambda = 10\mu$m, computed with $r_{\min} = 0.1\mu$m, $r_{\max} = 10\mu$m, $\varkappa = 0.1$; $N = 10^3$ cm^{-3}, $\alpha = 0.5$, $\nu = 4$. Here we have also given, as a comparison, the volume coefficients of vapor absorption $\alpha_V = \tilde{\alpha}_V \rho_V$, where $\tilde{\alpha}_V = 0.1$ cm^2/g is the mass vapor absorption coefficient [8], ρ_V (T) is vapor density.

Absorption by vapor increases with absolute humidity, that is, with temperature, whereas absorption by aerosol is determined by the relative humidity, regardless of temperature. Therefore, the ratio $\alpha_{a\lambda}/\alpha_V$ in the humidity range 70-95% varies from 12 to 54% with T = 10°C and from 25 to 104% with T = 0°C. The contributions of both factors to absorption are comparable. With a decrease in temperature there is an increase in the relative contribution of aerosol to total absorption, that is, there is an intensification of the dependence of total absorption on relative humidity, which explains the experimental data [2].

With a small change in temperature δT, as can be seen from (14), the change in the aerosol absorption coefficient $\delta\alpha_{a\lambda}$ is determined by the factor $\delta(1 - H)^{-1}$. With an accuracy to values of the first order of magnitude, using the Clausius-Clayperon formula, for the relative change in $\alpha_{a\lambda}$ we obtain:

$$\frac{\delta\alpha_{a\lambda}}{\alpha_{a\lambda}} = -\frac{H}{1-H}\frac{1}{q_s}\frac{dq_s}{dT}\delta T = -\frac{H}{1-H}\frac{L}{R_n T^2}\delta T, \qquad (15)$$

where L is the heat of vaporization, q_s is saturating humidity (a similar formula is also correct for the attenuation coefficient (6) with $H < 95\%$). With H = 80% and T = 30° computations made using (15) show that with an increase in temperature by 1°C $\delta\alpha_a / \alpha_{a\lambda} \approx -30\%$; the contribution of aerosol to the total absorption coefficient is about 6%, that is, the total absorption coefficient has an additional negative temperature dependence -- 2% per 1°C when T = 30°C. The determined value agrees well with the experimental value [7], an explanation of which usually requires invoking of the hypothesis of a contribution of water vapor dimers to absorption. We see that the effect of a negative temperature dependence of absorption in the window can be attributed to aerosol absorption without the dimer hypothesis. Table 3 shows that the effect must be intensified with a decrease in temperature and an increase in relative humidity. For example, with T = 0°C and H = 95% the decrease of the absorption coefficient can be 30-40% with a temperature increase by 1°C.

Table 3

Absorption Coefficients in km^{-1} for Aerosol (Numerator) and Water Vapor (Denominator) for $\lambda = 10\,\mu m$

T°C	H% 70	80	90	95
0	0,008 / 0,033	0,013 / 0,037	0,023 / 0,041	0,045 / 0,043
10	0,008 / 0,067	0,013 / 0,075	0,023 / 0,083	0,045 / 0,086

Table 4

H%	λ мкм μm 0,4	0,5	0,6	0,7	0,8	0,9	1
70	0,24	0,19	0,16	0,14	0,12	0,11	0,1
80	0,36	0,29	0,24	0,21	0,18	0,16	0,15
90	0,68	0,54	0,45	0,39	0,34	0,30	0,27
95	1,20	0,96	0,80	0,69	0,60	0,53	0,48
$\tau_{R\lambda}$	0,36	0,14	0,013	0,04	0,02	0,013	0,009

Spectral Optical Thickness

This parameter can be computed using the formula

$$\tau_{a\lambda}(z) = \int_z^\infty \sigma_\lambda^{at}(z)\, dz, \tag{16}$$

and, as indicated by (6), with vertically constant ν, α is determined by the N(z) and H(z) profiles. We will assume that $N(z) = N_0 \exp(-z/l)$ and that specific humidity is described by the Hann formula $q(z) = q_0 \exp(-\mu z)$ or for vapor density $\rho_v(z) = \rho_{v0} e^{-\tilde{\mu} z}$. If temperature decreases linearly with altitude, $T(z) = T_0 - \gamma z$, then, using for the pressure of saturated vapor the Clausius-Clayperon formula, and for pressure the barometric formula, for q we obtain

$$q_s(z) = q_{s0} \exp(-dz), \quad d = \frac{L\gamma}{R_n \overline{T}^2} - \frac{g}{R_c \overline{T}}, \tag{17}$$

[π= v(apor] where R_c is the gas constant of air, g is the acceleration of free falling, $\overline{T}$ is mean temperature.

Jointly with the Hann formula this gives

$$H(z) = H_0 \exp(-(\mu - d)\, z). \tag{18}$$

With H<95%, neglecting the second term in expression (6), substituting it into (16) together with N(z) and H(z) and integrating, we obtain

$$\tau_{a\lambda}(0) = \sigma_\lambda^{ai}(z=0)\, l\varphi(H), \quad \varphi(H) = l^{-1}(1-H)^{-1} \sum_{k=1}^{\infty} \frac{H_0^k}{l^{-1} + k(\mu - d)}. \tag{19}$$

With $\overline{T}$ = 0°C computations using (17) give d = 0.32 km^{-1}. According to [8] $\tilde{\mu} \approx 0.45$-0.5 km^{-1}, which corresponds to $\mu \approx 0.32$-0.37 km^{-1}. With μ= 0.32 km^{-1} = d, H(z) = const, a series in φ(H) is reduced to a geometrical progression and φ = 1. With $\mu > d$, when H decreases with altitude, as can be seen from (19), $\varphi < 1$, that is, allowance for a decrease in H with altitude leads to a decrease in τ_λ by 10-30%.

With μ= d and H(z) = const (this assumption is frequently made in models of the atmosphere [8]), the substitution of (6) into (16) gives

$$\tau_{a\lambda}(z) = [D_1 N_0 \lambda^{-Q}(1-H)^{-R} - D_2 N_0 \lambda^{-(Q+1)}(1- \\ -H)^{-(R+1)}]\, l e^{-z/l}. \tag{20}$$

The results of computation of $\tau_{\alpha\lambda}$ for this case, using (20), with l = 1 km, ν = 4, α = 0.5, $N_0 = 10^3$ cm^{-3} are given in Table 4.

The last line gives the Rayleigh optical thicknesses from [8]. As indicated by Table 3, except for the case λ= 0.4 μ m, H<80%, the aerosol optical thickness is greater than the Rayleigh thickness and their difference increases with wavelength and humidity. With fixed λ and an increase in

humidity from 70 to 90% $\tau_{a\lambda}$ approximately adheres to the law $(1 - H)^{-1}$, whereas with H = 95% $\tau_{a\lambda}$ already is appreciably less, which is caused by the second term in (6).

Integral Optical Thickness and Effective Wavelength of Aerosol Scattering

In order to compute the integral attenuation of each of the components in the real atmosphere it can be assumed, as is frequently done (for example, in [14]), that attenuation occurs alternately by each component: molecular scattering (ideal atmosphere); aerosol scattering; absorption by water vapor.

Then the integral optical thickness of the ideal (Rayleigh) atmosphere is $\tau_R = 0.1$ and the effective wavelength is $\lambda = 0.55\,\mu m$ [14]In computations of similar parameters for aerosol attenuation as the initial parameters we use radiation intensity in the ideal atmosphere. The spectral solar constant at the upper boundary of the atmosphere is

$$I_{0\lambda} = (a/r_0)^2 B_\lambda (T_s),$$

where $B\lambda$ is the Planck function with a temperature of the solar surface $T_s = 6000$ K, r_0 is the distance from the earth to the sun. Neglecting the distortion of the spectrum in the case of Rayleigh scattering for small atmospheric masses, we will assume that after passage through the ideal atmosphere the spectral intensity $I_{0\,R}$ is also proportional to the intensity of a black body, but with some (lesser) effective temperature $\tilde{T}$, that is,

$$I_{R\lambda} = (a/r_0)^2 B_\lambda (\tilde{T}).$$

The integral solar constants at the upper boundary of the atmosphere are

$$I_0 = (a/r_0)^2 \sigma T_s^4,$$

and after passage through the ideal atmosphere $I_R = (a/r_0)^2 \sigma \tilde{T}^4$ are related by the ordinary expression $I_R = I_0 e^{-m\tau_R}$, where m is atmospheric mass, is the Stefan-Boltzmann constant. Hence:

$$\tilde{T} = T_s (I_R/I_0)^{1/4} = T_s \exp(-m\tau_R/4). \qquad (21)$$

For example, with m = 2 $\tilde{T}$ = 5710 K. The integral aerosol optical thickness τ_a can now be determined by the expression

$$e^{-\tau_a} = \frac{\int_0^\infty d\lambda\, e^{-\tau_\lambda} I_{0\lambda}(\tilde{T})}{\int_0^\infty d\lambda\, I_{0\lambda}(\tilde{T})} = \frac{\int_0^\infty d\lambda\, e^{-\tau_\lambda} B_\lambda(\tilde{T})}{\int_0^\infty d\lambda\, B_\lambda(\tilde{T})}. \qquad (22)$$

For the most frequently encountered case $\tau_\lambda \sim \lambda^{-1}$, that is, with $\nu = 4$, $\alpha = 0.5$, the integrals in (22) can be computed analytically. In this case with H< 95% $\tau_\lambda(0)$, in accordance with (20) can be represented in the form

$$\tau_\lambda = \beta/\lambda, \quad \beta = D_1 \cdot N_0 (1-H)^{-1} l \tag{23}$$

and is computed using Table 2 with different N_0 and H.

Denoting the integrals in the numerator and denominator (22) by J_1 and J_2, substituting (23) and the expression for $B_\lambda(\tilde{T})$ into (22), we obtain

$$e^{-\tau_a} = \frac{J_1}{J_2}, \quad J_1 = G \int_0^\infty e^{-gx} \frac{x^3}{e^x - 1}\, dx, \quad J_2 = J_1 (g=0), \tag{24}$$

where

$$G = \frac{2k^4 \tilde{T}^4}{c^2 h^3}, \quad g = \beta k \tilde{T}/ch,$$

c is the speed of light, h is the Planck constant, k is the Boltzmann constant.

Then we will expand the integrand in J_1 into a series in powers of e^{-x}:

$$J_1 = G \sum_{n=0}^{\infty} \int_0^\infty e^{-(g+n+1)x} x^3\, dx. \tag{25}$$

Each of the integrals in the sum is reduced to a Γ-function and now

$$J_1 = \Gamma(4) \sum_{n=0}^{\infty} (g+n+1)^{-4} = G\Gamma(4)\zeta(4, g+1), \tag{26}$$

where $\zeta(x, y)$ is the Riemann zeta function. Thus,

$$\tau_a = \ln (J_2/J_1) = \ln |(\zeta(4, 1)/\zeta(4, g+1)|. \tag{27}$$

The series for the ζ-function in (26) converges very rapidly and allowance for the first three terms ensures an accuracy above one percent. But the quite simple formula (27) can be further simplified. For example, with $\tau(\lambda = 0.5\,\mu m) = 0.5$, the value $\beta \sim 0.25 \cdot 10^{-4}\,\mu m$ and $g \sim 0.1$. Each of the terms of the series in (26) for the ζ-function can be represented in the following way:

$$(n+g+1)^{-4} \approx (n+1)^{-4} \left(1 - \frac{4g}{n+1}\right)$$

and expression (27) is transformed:

$$\tau_a \cong -\ln\left(1 - 4g \frac{\zeta(5, 1)}{\zeta(4, 1)}\right) \approx 4g \frac{\zeta(5, 1)}{\zeta(4, 1)}. \tag{28}$$

Substituting (23) into (28) and the value $4\zeta(5)/\zeta(4) = 3.86$, we obtain

$$\tau_a = 4 \frac{\beta k \tilde{T}}{ch} \frac{\zeta(5)}{\zeta(4)} = 3{,}86 \frac{D_1 N_0 l k T_s}{(1-H)\, ch} e^{-m\tau_R/4}. \tag{29}$$

Using (29) and Table 2, for D_1 it is easy to compute the integral aerosol optical thickness τ_a with different concentrations and the microstructure of aerosol and atmospheric masses. The effective wavelength λ_a can be introduced using the expression $\tau_a = \beta/\lambda_a$. Then for λ_a from (29) it follows

$$\lambda_a = \frac{ch}{4k\tilde{T}} \frac{\zeta(4)}{\zeta(5)} = 0{,}26 \frac{ch}{kT_s} e^{m\tau_R/4}. \tag{30}$$

For example, $\lambda_a = 0.614\,\mu m$ when m = 1 and $\lambda_a = 0.645$ when m = 2. We note as a comparison that the λ_a values obtained in [14] on the basis of data from spectral computations are 0.61, 0.63, $0.65\,\mu m$ for optical thicknesses at $\lambda = 0.5\,\mu m$ of 0.2, 0.3 and 0.5 respectively. The close agreement of these values and those obtained using formula (30) indicate a good accuracy of the latter. We note that with an increase in atmospheric mass the integral optical thickness decreases and the effective wavelength increases, that is, aerosol attenuation experiences a "red shift."

Influence of Humidity on the Linke Turbidity Factor

One of the most important characteristics of atmospheric transparency is the Linke turbidity factor P_m, which is determined as the ratio of the optical thicknesses of the real and ideal atmospheres: $P_m = 1 + W_m + R_m$, where $W_m = \tau_V / \tau_R$ is the moist turbidity factor characterizing attenuation by water vapor, $R_m = \tau_a / \tau_R$ is the aerosol or residual turbidity factor. Usually aerosol attenuation is determined as the residual term in the formula for F_m with known P_m and W_m; P_m is computed using data for measurements of integral radiation at the surface and W_m is computed using empirical formulas, for example, in [5] with m = 2: $W_2 = 0.367\, e_0^{0.4}$, where e_0 is the elasticity of saturated vapor at the surface in millibars. The method developed above makes possible the direct computation of R_m. According to (29)

$$R_m = 3{,}86\,\frac{\beta\, k T_s}{ch\,\tau_R}\, e^{-m\tau_R/4} = 3{,}86\,\frac{D_1 N_0 l k T_s}{(1-H)\,ch\,\tau_R}\, e^{-m\tau_R/4}. \qquad (31)$$

Examples of computation of R_m from (32) for different H are given in Table 5 for values of the parameters $N_0 = 10^3\ cm^{-3}$, $l = 1$ km, $\nu = 4$, $\alpha = 0.5$, m = 2. Here, as a comparison, we give the values of the moist turbidity factor W_2 (denominator), computed using the formula cited above.

Table 5 shows that the values of aerosol and moist turbidity are comparable only with T = 20°C and H = 70%; at lesser temperatures and higher humidities R_2 should appreciably exceed W_2. Thus, with an increase in relative humidity, however paradoxical it may seem, the role of water vapor in the direct attenuation of solar radiation decreases and processes of vapor absorption by aerosol begin to play the main role, leading to its enlargement. These factors also cause high values of the turbidity factor P in moist equatorial air masses, which in Table 5 can correspond to the case T = 20°C, H = 90%. In this case $P_2 = 6.47$ and 65% of the total attenuation is caused by aerosol scattering.

Using (32) for the number of aerosol particles in a unit air column $M = N_0 l$ we can derive the formula

$$M = 0{,}26\,\frac{R_m \tau_R\, ch\,(1-H)}{D_1 k T_s}\, e^{m\tau_R/4}, \qquad (32)$$

Table 5

Aerosol (Numerator) and Moist (Denominator) Turbidity Factors

T°C	H%		
	70	80	90
0	1.55 / 0.66	2.33 / 0.70	4.19 / 0.74
20	1.55 / 1.15	2.33 / 1.21	4.19 / 1.26

The above formula makes it possible to evaluate aerosol contamination of the atmosphere by the ordinary method of determining the aerosol turbidity factor R_m, that is, using measurements of temperature, humidity and integral intensity of solar radiation at the surface.

In conclusion I consider it my pleasant duty to thank K. Ya. Kondrat'yev, M. V. Buykov, L. M. Levin and N. I. Goysa for useful discussion and comments.

*****

BIBLIOGRAPHY

1. Aleksandrov, E. L., Klepikova, N. V., "Deformation of the Spectrum of Condensation Nuclei During the Water Encasement Process and Evaluation of its Influence on Visibility," TRUDY IEM (Transactions of the Institute of Experimental Meteorology), No 20, 1971.

2. Aref'yev, V. N., Dianov-Klokov, V. I., Sizov, N. I., "Laboratory Investigations of the Role of Aerosol in the Attenuation of Radiation at 10.6μm by Water Vapor," IZV. AN SSSR, FIZIKA ATMOSFERY I OKEANA (News of the USSR Academy of Sciences, Physics of the Atmosphere and Ocean), No 12, 1978.

3. Balin, Yu. S., Krekov, G. M., Samokhvalov, I. V., Rakhimov, R. F., "Influence of Humidity on Radar Scattering in the Atmosphere," METEOROLOGIYA I GIDROLOGIYA (Meteorology and Hydrology), No 8, 1978.

4. Georgiyevskiy, Yu. S., Rozenberg, G. V., "Humidity as a Factor in the Variability of Aerosol," IZV. AN SSSR, FIZIKA ATMOSFERY I OKEANA, No 2, 1973.

5. Goysa, N. I., Zheleznyakova, T. V., Shoshin, V. M., "Influence of Air Humidity and Aerosol Content on Atmospheric Transparency," TRUDY UkrNIGMI (Transactions of the Ukrainian Scientific Research Hydrometeorological Institute), No 77.

6. Zuyev, V. Ye., et al., "Some Results of Investigations of the Optical Properties of Seashore Haze," IZV. AN SSSR, FIZIKA ATMOSFERY I OKEANA, No 12, 1978.

7. Kondrat'yev, K. Ya., et al., "Climate and Aerosol," TRUDY GGO (Transactions of the Main Geophysical Observatory), No 381, 1976.

8. Kondrat'yev, K. Ya., AKTINOMETRIYA (Actinometry), Leningrad, Gidrometeoizdat, 1965.

9. Laktionov, A. G., "Content of Water-Soluble Substances in Particles of Atmospheric Aerosol," IZV. AN SSSR, FIZIKA ATMOSFERY I OKEANA, No 4, 1972.

10. Levin, L. M., FIZIKA GRUBODISPERSNYKH AEROZOLEY (Physics of Coarsely Disperse Aerosols), Moscow, Izd-vo AN SSSR, 1961.

11. Levin, L. M., Sedunov, Yu. S., "Some Problems in the Theory of Atmospheric Condensation Nuclei," DOKLADY AN SSSR (Reports of the USSR Academy of Sciences), Vol 170, No 1, 1966.

12. Rozenberg, G. V., et al., "Submicron Fraction of Aerosol and Light Absorption in the Transparency Window 8-12μm," IZV. AN SSSR, FIZIKA ATMOSFERY I OKEANA, No 11, 1977.

13. Sedunov, Yu. S., FIZIKA OBRAZOVANIYA ZHIDKOKAPEL'NOY FAZY V ATMOSFERE (Physics of Formation of the Liquid-Droplet Phase in the Atmosphere), Leningrad, Gidrometeoizdat, Leningrad, Gidrometeoizdat, 1972.

14. Sivkov, V. I., METODY RASCHETA KHARAKTERISTIK SOLNECHNOY RADIATSII (Methods for Computing the Characteristics of Solar Radiation), Leningrad, Gidrometeoizdat, 1968.

15. Smirnov, V. I., "Equilibrium Sizes and Spectrum of Sizes of Aerosol Particles in the Moist Atmosphere," IZV. AN SSSR, FIZIKA ATMOSFERY I OKEANA, No 10, 1978.

16. Filippov, V. L., Mirumyants, S. O., "Investigation of the Dependence of Aerosol Attenuation of Visible and IR Radiation on Air Humidity," IZV. AN SSSR, FIZIKA ATMOSFERY I OKEANA, No 9, 1972.

17. Khvorost'yanov, V. I., "Attenuation of Optical Radiation by Atmospheric Aerosol," DOKLADY AN SSSR, Vol 247, No 2, 1979.

18. Yunge, Kh., KHIMICHESKIY SOSTAV I RADIOAKTIVNOST' ATMOSFERY (Chemical Composition and Radioactivity of the Atmosphere), Moscow, Mir, 1965.

19. Hanel, G., "New Results Concerning the Dependence of Visibility on Relative Humidity and Their Significance in a Model for Visibility Forecast," BEITR. PHYS. ATMOS., No 2, 1971.

20. Kasten, F., "Visibility Forecast in the Phase of Pre-condensation," TELLUS, Vol 21, No 5, 1969.

21. Tuomi, T. J., "Backscatter of Light by Aerosol at High Relative Humidity," J. AEROSOL. SCI., Vol 7, No 6, 1976.

22. Volz, F., "Optik des Dunstes," HANDBUCH DER GEOPHYSIK, Borntrager, Berlin, 1956.

UDC 551.510.42

IMPROVING ESTIMATES OF ATMOSPHERIC AEROSOL TURBIDITY

Moscow METEOROLOGIYA I GIDROLOGIYA in Russian No 4, Apr 80 pp 40-46

[Article by Candidate of Geographical Sciences L. D. Krasnokutskaya and Doctor of Physical and Mathematical Sciences Ye. M. Feygel'son, Institute of Atmospheric Physics, submitted for publication 30 July 1979]

Abstract: A study was made of the possibility of determining the spectral optical thickness of aerosol attenuation on the basis of data from standard measurements of direct solar radiation. Different methods are compared and their error is estimated. The article gives a detailed table of data from computations of direct solar radiation used for improving the method for determining aerosol optical thickness.

Introduction

Modern problems in the theory of climate require a knowledge of the aerosol composition of the atmosphere and the optical properties of aerosol. It is necessary to create models of global "aerosol climate," and in particular it is necessary to know "aerosol transparency" P_a of the atmosphere for solar radiation.

Evidently, the principal source of extensive information on the parameter P_a is the world actinometric network, including shipboard actinometric measurements.

In the Soviet Union the actinometric network is extensive and actinometric measurements are systematically carried out on scientific research ships.

Many data are furnished by expeditions; one of the most important was the international expedition GATE-74.

Standard actinometric observations include measurements of integral direct solar radiation I in the spectrum of wavelengths. These data are a source of information on the P_a parameter.

The State Committee on Hydrometeorology has a method for determining P_a using data from measurements of I developed by S. I. Sivkov [9] and used in the actinometric network.

Z. I. Pivovarova [4] used her own method for computing the seasonal distribution of P_a over the territory of the USSR on the basis of long-term data from actinometric stations.

Ways in which to improve the method in [9] for computing P_a are presented in an article by A. S. Averkiyeva and T. V. Yevnevich [1].

N. A. Timofeyev formulated algorithms for determining the characteristics of atmospheric turbidity using data from shipboard actinometric observations [10].

Abroad G. Yamamoto, et al. [12] proposed his method for determining turbidity parameters using I measurements. He used this method in processing data from the International Geophysical Year (1962).

All the enumerated and many other methods for determining P_a are based on a number of simplifying assumptions. The objective of our work was to systematize the latter, evaluate the error, compare different methods and introduce some improvements.

Principal Expressions and Simplifying Assumptions

The actinometer aperture angle is 10°. In addition to direct solar radiation which falls into this angle there is also scattered radiation -- a considerable fraction of all the scattered light, but a small (less than 5%) fraction of the direct solar radiation.

Neglecting the scattered radiation, we write:

$$I = \int_0^\infty I_{0,\lambda} \exp\left[-m\left(\tau_{O_3,\lambda} + \tau_{R,\lambda} + \tau_{v,\lambda} + \tau_{a,\lambda}\right)\right] d\lambda. \qquad (1)$$

Here $I_{0,\lambda}$ is the spectral component of the solar constant; m is the air mass; $m = \sec \zeta$ with $\zeta \lesssim 75°$; ζ is the solar zenith angle; $\tau_{O_3,\lambda}$; $\tau_{R\lambda}$; $\tau_{v,\lambda}$; $\tau_{a,\lambda}$ are the spectral optical thicknesses of attenuation as a result of absorption in the ozone layer, molecular scattering, absorption by water vapor, scattering and absorption by aerosol particles.

The I value is measured, $\tau_{R,\lambda}$ is known. If the ozone content m_{O_3} and water vapor content m_v in the atmosphere are stipulated, as well as the position of the sun ζ at the time of the measurements, then $\tau_{a,\lambda}$ remains unknown.

Different methods for determining $\tau_{a,\lambda}$ or $P_{a,\lambda} = e^{-\tau_{a,\lambda}}$ are based on various of the simplifying assumptions enumerated below:

1) It is surmised that m_{O_3} is stipulated on the basis of mean climatic data, as is justified by the following circumstances:
a) m_{O_3} as a rule is not measured simultaneously with I.
b) The real changes in the content of O_3 absorbed in the Huggins and Chappuis bands exert virtually no influence on the I value.

2) The data from measurements of I for different solar altitudes are reduced to an air mass m = 2 in accordance with [6] on the basis of the empirical fact cited by S. I. Sivkov [8] that:

$$\Delta I(\zeta_1;\ \zeta_2) = I(\zeta_1) - I(\zeta_2) \approx \text{const}, \tag{2}$$

if ζ_1 = const and ζ_2 = const.

In order to reduce $I(\zeta)$ to $I(60°)$ use is made of tables of the mean (based on extensive measurement data) differences $\Delta I(\zeta;\ 60°)$. Using them we obtain

$$I(60°) = I(\zeta) \pm \Delta I(\zeta;\ 60°). \tag{3}$$

Thus, the diurnal variation $I(\zeta)$ is disposed of, and presumably we are freed of the Forbes effect (different spectral composition of radiation for different ζ). The second is not validated; the first is not mandatory and leads to errors, as will be evident below (see Table 3).

3) The rigorous equation (1) is replaced by an approximate equation

$$I = \tilde{I}_0 P_R P_v P_a = I_{ид} P_v P_a, \tag{4}$$

where

$$\tilde{I}_0 = \int_0^\infty I_{0,\lambda} \exp[-m\tau_{O_3,\lambda}]\, d\lambda$$

[ИД = ideal] is the "subozone" solar constant, corresponding to the mean ozone content;

$$I_{ид} = \int_0^\infty I_{0,\lambda} \exp[-m(\tau_{O_3,\lambda} + \tau_{R,\lambda})]\, d\lambda$$

is the intensity of direct solar radiation in an "ideal" (purely gas) atmosphere;

P_R, P_V, P_a are the integral transmission functions for individual components of atmospheric attenuation.

4) On the assumption of a nondependence of $\tau_{a,\lambda}$ on wavelength, that is, in the case $\tau_{a,\lambda} = \tau_{a,int} = \tau_a$ (τ_a is the integral optical thickness of aerosol attenuation), from (1) we obtain

$$P_a = e^{-\tau_a} = \frac{I}{\int_0^\infty \tilde{I}_{0,\lambda} \exp[-m(\tau_{R,\lambda} + \tau_{v,\lambda})]\, d\lambda}. \tag{5}$$

Combining (5) and (4), we have

$$P_a = \frac{I}{\tilde{I}_0 P_R P_v}. \tag{6}$$

5) The spectral dependence of aerosol attenuation is stipulated in the form

$$\tau_{a,\lambda} = \tau_{a,\lambda_0}\left(\frac{\lambda_0}{\lambda}\right)^n = \beta\lambda^{-n} \tag{7}$$

when $\lambda_0 = 0.55\,\mu m$.

Here β is the Angstrom turbidity coefficient; n is a parameter dependent on the size distribution of particles. Under real conditions there is frequently realization of the case $n \approx 1$ (for example, see [5, 7, 9]).

The simplifications set forth above in 1) - 4) are proposed in [4, 9] and are used in the network of actinometric stations. In [4], in addition, the product (4) is replaced by the difference

$$\Pi_a = I_{ид} - I - \Pi_v, \tag{8}$$

[ид = ideal] where $\Pi_a = 1 - P_a$, Π_V is absorption by water vapor.

Expression (8) approximately corresponds to a linear approximation of formula (1).

Expressions (4) and (7) are used in [1, 10]. In (4) the functions P_R, P_V, P_a are replaced approximately by others taking into account the impossibility of a rigorous separation of variables in (1). Source [1] gives approximate tables of the dependence of I on the mass of water vapor m_V and on τ_{a,λ_0} with $\zeta = 60°$ and n = 1. Source [10] gives empirical formulas which can be used in computing β and n in (7). In [12] use was made of simplifications of (4) and (7) with n = 1. Nomograms are given for determining β in formula (7).

Tables of I Value and Estimates of Aerosol Attenuation

We carried out detailed computations of I using formula (1) using stipulated values $\tilde{I}_{0,\lambda}$ (simplification of I) from [11] on the assumption of satisfaction of formula (7). The computations were made in the following range of change of the input parameters: $0.05 \leqslant \tau_{a,\lambda_0} \leqslant 0.8$; n = 0; 0.5; 1; 2; $0 \leqslant \zeta \leqslant 75°$; $0 \leqslant m_V \leqslant 5$ g/cm^2. We used the spectral transmission functions for water vapor from [2]. It was assumed that $\tau_{R,\lambda_0} = 0.098$ in accordance with [3].

The computation data are presented in Table 1. If I, ζ and m_V are known, using Table 1 it is possible to determine τ_{a,λ_0} in dependence on the choice of the n parameter. Examples of determining τ_{a,λ_0} are given in

Table 1

Computation of I Values With Stipulated ζ, m_v, τ_a, λ_0, n

m_v	n = 0	0,5	1	2	0	0,5	1	2	0	0,5	1	2
	$\zeta = 0°$											
	$\tau_a, \lambda_0 = 0.05$				$\tau_a, \lambda_0 = 0,10$				$\tau_a, \lambda_0 = 0,2$			
0	1,587	1,600	1,609		1,510	1,535	1,554		1,366	1,412	1,443	
0,5	1,448	1,458	1,465		1,377	1,397	1,410		1,246	1,282	1,308	
1	1,422	1,432	1,438		1,353	1,372	1,384		1,224	1,259	1,283	
2	1,395	1,404	1,410		1,327	1,345	1,357		1,200	1,234	1,257	
3	1,375	1,384	1,390		1,308	1,325	1,337		1,183	1,215	1,238	
5	1,347	1,356	1,361		1,281	1,298	1,309		1,159	1,190	1,211	
	$\tau_a, \lambda_0 = 0,3$				$\tau_a, \lambda_0 = 0,5$				$\tau_a, \lambda_0 = 0,8$			
0	1,236	1,300	1,344		1,012	1,102	1,168		0,750	0,862	0,953	
0,5	1,127	1,178	1,213		0,923	0,994	1,047		0,684	0,772	0,845	
1	1,105	1,156	1,190		0,907	0,975	1,026		0,672	0,754	0,826	
2	1,086	1,132	1,165		0,889	0,954	1,003		0,659	0,740	0,806	
3	1,071	1,114	1,147		0,877	0,939	0,987		0,649	0,728	0,792	
5	1,049	1,091	1,122		0,859	0,919	0,964		0,636	0,711	0,772	
	$\zeta = 60°$											
	$\tau_a, \lambda_0 = 0,05$				$\tau_a, \lambda_0 = 0,10$				$\tau_a, \lambda_0 = 0,2$			
0	1,427	1,452	1,469	1,487	1,291	1,337	1,369	1,405	1,057	1,136	1,192	1,261
0,5	1,271	1,290	1,303	1,318	1,150	1,185	1,209	1,238	0,941	1,000	1,045	1,100
1	1,245	1,263	1,276	1,290	1,126	1,160	1,184	1,211	0,922	0,979	1,021	1,074
2	1,213	1,231	1,242	1,256	1,098	1,130	1,152	1,178	0,899	0,953	0,993	1,043
3	1,192	1,208	1,220	1,233	1,078	1,109	1,130	1,156	0,883	0,935	0,973	1,021
5	1,165	1,180	1,195	1,204	1,054	1,083	1,103	1,127	0,863	0,912	0,949	0,995
	$\tau_a, \lambda_0 = 0,3$				$\tau_a, \lambda_0 = 0,5$				$\tau_a, \lambda_0 = 0,8$			
0	0,965	0,965	1,042	1,139	0,580	0,700	0,803	0,946	0,318	0,437	0,556	0,742
0,5	0,771	0,846	0,905	0,984	0,517	0,607	0,686	0,801	0,283	0,372	0,462	0,611
1	0,764	0,827	0,884	0,959	0,506	0,593	0,668	0,778	0,278	0,363	0,449	0,592
2	0,744	0,804	0,858	0,929	0,493	0,575	0,647	0,751	0,271	0,351	0,422	0,568
3	0,728	0,789	0,840	0,909	0,484	0,563	0,632	0,733	0,266	0,343	0,422	0,552
5	0,714	0,769	0,818	0,884	0,474	0,548	0,614	0,710	0,260	0,333	0,408	0,533
	$\zeta = 75°$											
	$\tau_a, \lambda_0 = 0,05$				$\tau_a, \lambda_0 = 0,10$				$\tau_a, \lambda_0 = 0,2$			
0	1,157	1,232	1,263	1,300	0,980	1,056	1,112	1,180	0,667	0,779	0,868	0,988
0,5	1,024	1,057	1,080	1,108	0,845	0,901	0,942	0,996	0,575	0,656	0,723	0,816
1	0,995	1,026	1,048	1,075	0,821	0,875	0,913	0,964	0,559	0,635	0,697	0,787
2	0,962	0,992	1,012	1,038	0,794	0,844	0,881	0,929	0,541	0,613	0,672	0,755
3	0,943	0,974	0,994	1,018	0,780	0,828	0,864	0,910	0,531	0,601	0,658	0,739
5	0,915	0,944	0,963	0,986	0,757	0,802	0,836	0,880	0,515	0,581	0,636	0,712
	$\tau_a, \lambda_0 = 0,3$				$\tau_a, \lambda_0 = 0,5$				$\tau_a, \lambda_0 = 0,8$			
0	0,454	0,577	0,685	0,843	0,210	0,321	0,440	0,639	0,0663	0,137	0,242	0,456
0,5	0,391	0,480	0,565	0,618	0,181	0,260	0,347	0,498	0,0572	0,107	0,180	0,338
1	0,381	0,464	0,540	0,612	0,176	0,251	0,332	0,476	0,0556	0,102	0,172	0,321
2	0,368	0,447	0,518	0,588	0,170	0,240	0,317	0,452	0,0538	0,0978	0,162	0,302
3	0,360	0,436	0,506	0,655	0,168	0,235	0,309	0,440	0,0528	0,0953	0,158	0,292
5	0,351	0,423	0,488	0,627	0,162	0,226	0,296	0,420	0,0513	0,0914	0,150	0,278

Table 2 for conditions of weak, moderate and strong aerosol turbidity.

Table 2

Spectral τ_{a,λ_0} and Integral $\tau_{a,int}$ Optical Thicknesses of Aerosol Attenuation

ζ°	I кал/(см²·мин) 1	m_v г/см² 2	n: 0	n: 0,5	n: 1	n: 2
			c(n): 1	c(n): 0,856	c(n): 0,754	c(n): 0,664
			τ_{a,λ_0} ($\tau_{a.\,инт}$) 3			
22	1,26	2,2	0,11	0,13(0,11)	0,15(0,11)	0,18(0,11)
41	1,13	2,4	0,17	0,20(0,17)	0,23(0,17)	0,26(0,17)
58	1,10	3,7	0,10	0,12(0,10)	0,13(0,10)	0,15(0,10)
34	1,05	2,4	0,25	0,28(0,24)	0,31(0,23)	0,39(0,26)
43	1,05	2,7	0,27	0,34(0,29)	0,37(0,28)	0,46(0,30)
59	0,75	2,4	0,32	0,35(0,30)	0,41(0,31)	0,49(0,32)
76	0,56	6,0	0,19	0,23(0,20)	0,27(0,20)	0,33(0,22)
43	0,85	2,9	0,38	0,43(0,37)	0,50(0,38)	0,60(0,40)
43	0,74	3,2	0,48	0,57(0,49)	0,66(0,50)	0,77(0,51)
59	0,54	3,2	0,50	0,59(0,50)	0,70(0,53)	—

KEY:
1. cal/(cm^2·min)
2. g/cm^2
3. int

Table 2 shows the considerable uncertainty of τ_{a,λ_0} introduced by the choice of the n parameter. It is evidently necessary to have some additional information about particle size. For example, the case n = 0 probably corresponds to large particles, or small particles, if there are few of them.

An approximate method for determining n is given in [10]. Nevertheless, even in the absence of additional information by the use of Table 1 it is possible to separate cases with different degrees of turbidity. In addition, the n = 2 value is not too realistic and the $\tau_{a,\lambda 0}$ values differ little with n = 1/2 and n = 1.

Next some nontrivial circumstance is discovered. We will determine the integral optical thickness of aerosol attenuation $\tau_{a,\,int}$ using the formula

[И НТ = int]

$$\tau_{a,\,инт} = \frac{\int_0^\infty I_{0,\lambda}\,\tau_{a,\lambda}(n)\,d\lambda}{I_0}. \qquad (9)$$

Table 3

Comparison of Different Methods for Computing τ_{a,λ_0}

	Настоящая работа 1	Актин. сеть ** 2	[4]	[12]	[1]	[10]
	I=0,74 кал/(см²·мин) *; ζ=43°; m_v sec ζ=2,2 г/см² 4					
n=0	0,48/0,49	0,48(0,45) 3	0,40(0,38)	—	—	—
n=1	0,66/0,68	—	—	0,68	—	0,63
	I=0,96 кал/(см²·мин) *; ζ=60°; m_v sec ζ=1 г/см² 4					
n=0	0,22/0,19	0,19 3	0,14	—	—	—
n=1	0,26/0,25	—	—	0,28	0,27	0,24
	I=0,56 кал/(см²·мин) *; ζ=76°; m_v sec ζ=6 г/см² 4					
n=0	0,19/0,19	0,18(0,21) 3	0,10(0,16)	—	—	—
n=1	0,27/0,25	—	—	0,25	(0,29)	0,20

KEY:
1. This study
2. Actinometric network
3. cal/(cm^2·min)
4. g/cm^2

*I, together with the corresponding m_v and ζ were furnished through the kindness of T. V. Yevnevich.

**Data from the actinometric network and [4] can be regarded as τ_{a,λ_0} when n = 0.

The figures in parentheses were obtained by reducing I, P, P_R, P_a, P_v to m = sec ζ = 2.

Substituting into the latter the relationship $\tau_{a,\lambda}(n)$, expressed by formula (7), we obtain

[И НТ = int]

$$\tau_{a,\text{инт}} = c(n)\,\tau_{a,\lambda_0}(n) \tag{10}$$

with

$$c(n) = \int_0^\infty I_{0,\lambda} \left(\frac{\lambda_0}{\lambda}\right)^n d\lambda. \tag{11}$$

Table 2 gives the c(n) and $\tau_{a,\text{int}}$ values (numbers in parentheses). It can be seen that $\tau_{a,\text{int}}$ is virtually not dependent on the choice of n, which, strictly speaking, does not follow from formula (1).

However, in a linear approximation it is easy to derive from (1)

[ИНТ = int] $$\tau_{a,\ инт} = \cos\zeta\left(1 - \frac{I}{I_0}\right) - \tau_{R,\ инт} - \tau_{v,\ инт} = \text{const} \qquad (12)$$

independently of the choice of n.

Table 2 indicates the broad range of applicability of the assumption $\tau_{a,int}$ = const. In this case there is a considerable simplification of the procedure for determining the aerosol attenuation spectrum on the basis of measurements of I. Table 1 with n = 0 or formulas (5), (6) are used in determining $\tau_{a,\ int}$. Then, with stipulated n, using formula (10) we compute $\tau_{a,\ \lambda_0}$ and using formula (7) we restore the $\tau_{a,\lambda}$ spectrum.

Now we will examine the error in the approximation (4).

In Table 3 we give a comparison of the $\tau_{a,\ \lambda_0}$ values, computed directly using Table 1 (numerator) and with use of the simplification (4) (denominator). It can be seen that the error of this approximation almost does not exceed the limits 5%.

We also compared the methods published by different authors. In all cases use was made of the functions P_R and P_V which we computed and identical $I_{0,\lambda}$ values in order to avoid differences unrelated to the fundamental peculiarities of the considered methods. Individual examples of the comparisons are given in Table 3, from which it can be seen that the greatest errors arise as a result of linearization of formula (1) (see [4]) and reduction to the mass 2. The empirical expressions used in [10] also lead to substantial errors. The separation of variables in formula (1) and its reduction to the form (6) is most justified.

BIBLIOGRAPHY

1. Averkiyev, M. S., Yevnevich, T. V., "Determination of Aerosol and Moist Turbidity in the Real Atmosphere," METEOROLOGIYA I GIDROLOGIYA (Meteorology and Hydrology), No 12, 1973.

2. Kargin, V. A., Krasnokutskaya, L. D., Feygel'son, Ye. M., "Reflection and Absorption of Solar Radiant Energy by Cloud Layers," IZV. AN SSSR, FIZIKA ATMOSFERY I OKEANA (News of the USSR Academy of Sciences, Physics of the Atmosphere and Ocean), Vol 8, No 5, 1972.

3. Livshits, G. Sh., RASSEYANNYY SVET DNEVNOGO NEBA (Scattered Light of the Daytime Sky), Alma-Ata, Nauka, 1973.

4. Pivovarova, Z. I., "Distribution of the Coefficient of Atmospheric Transparency (for the Integral Flux Over the Territory of the USSR)," TRUDY GGO (Transactions of the Main Geophysical Observatory), No 213, 1968.

5. Rozenberg, G. V., Gorchakov, G. I., Georgiyevskiy, Yu. S., Lyubovtseva, Yu. S., "Optical Parameters of Atmospheric Aerosol," FIZIKA ATMOSFERY I PROBLEMY KLIMATA (Atmospheric Physics and Climatic Problems), Moscow, Nauka (in press).

6. RUKOVODSTVO GIDROMETEOROLOGICHESKIM STANTSIYAM PO AKTINOMETRICHESKIM NABLYUDENIYAM (Manual for Hydrometeorological Stations for Actinometric Observations), Moscow, Gidrometeoizdat, 1971.

7. Rusina, Ye. N., "Determination of the Characteristics of Aerosol Turbidity in the Atmosphere Using Data from Spectral Actinometric Observations," METEOROLOGIYA I GIDROLOGIYA (Meteorology and Hydrology), No 5, 1977.

8. Sivkov, S. I., "Solar Radiation and Atmospheric Transparency at Kursk," ZH. GEOFIZICH. (Geophysical Journal), Vol I, No 1-2, 1931.

9. Sivkov, S. I., METODY RASCHETA KHARAKTERISTIK SOLNECHNOY RADIATSII (Methods for Computing the Characteristics of Solar Radiation), Moscow, Gidrometeoizdat, 1968.

10. Timofeyev, N. A., ISSLEDOVANIYE RADIATSIONNOGO REZHIMA OKEANOV (Investigation of the Radiation Regime of the Oceans), Dissertation, Moscow, 1979.

11. Shifrin, K. S., Avaste, O., "Fluxes of Short-Wave Radiation in the Cloudless Atmosphere," ISSLEDOVANIYA PO FIZIKE ATMOSFERY (Investigations of Atmospheric Physics), No 2, 1960.

12. Yamamoto, G., Tanaka, M., Araa, K., "Hemispherical Distribution of Turbidity Coefficient as Estimated from Direct Solar Radiation Measurement," J. METEOROL. SOC. JAPAN, Ser 11, Vol 46, No 4, 1968.

UDC 551.(510.42+578.467)

INVESTIGATION OF AEROSOL FALLOUT DURING DISTANT TRANSPORT OF CONTAMINATING SUBSTANCES

Moscow METEOROLOGIYA I GIDROLOGIYA in Russian No 4, Apr 80 pp 47-51

[Article by Candidate of Physical and Mathematical Sciences T. N. Zhigalovskaya and Candidates of Technical Sciences I. M. Nazarov and Sh. D. Fridman and O. S. Renne, Institute of Applied Geophysics, submitted for publication 23 August 1979]

Abstract: A study was made of the possibility of detecting the distant transport of contaminating substances in the atmosphere on the basis of fallout. The snow cover is used as an accumulator of fallout. The methods for sampling and preliminary processing of samples are described. The dry residues of samples were analyzed for the content of six elements. It is shown that the concentrations of elements in the snow samples decrease exponentially with increasing distance from the source. It is shown that contaminations from industrial sources, using the described method, can be detected at distances up to 1,000 km or more.

[Text] The problem of distant transport of technogenic aerosols is of substantial interest in relation to regional and global contamination of the environment and the possibility of transport of contaminating substances across national boundaries into the territories of other countries [1-6, 8].

This study was carried out for the purpose of investigating the possibility of detecting distant transport on the basis of fallout and determination of the dependence of the quantity of fallout on distance to the source. The snow cover was used as the accumulator of the fallout [7].

Measurement method. The detection of fallout from an industrial source at distances of hundreds, and especially thousands of kilometers is a complex problem. This involves the necessity of discriminating low concentrations of contaminating substances from a distant source against the

background of arbitrarily changing levels from local sources. In order to solve this problem we selected a region with linear dimensions of about 2,000 km in which there were virtually no local sources. On the margin of the selected region there was a powerful source of aerosols, carriers of trace elements. The selected industrial source at a distance of more than 100 km can be considered a point source. In the sampling we used six meteorological stations at which standard network snow surveys are made. The meteorological stations are situated approximately along the prevailing direction according to the wind rose, with a mean monthly wind frequency of about 40% at the 850-mb level. In addition, sampling was carried out at three meteorological stations in the opposite direction, where the mean monthly wind frequency at the 850-mb level was about 5%. Each sample consisted of three samples taken at the beginning, middle and end of the line. The volume of the combined sample usually exceeded 2 liters of water. Such a volume, according to our estimates [7], ensured an adequate representativeness of the samples. The procedure of sampling, storage and transporting of samples to the laboratory was described in [7].

Each sample was filtered, thereby being divided into conditionally soluble and conditionally insoluble parts. The conditionally insoluble part, remaining in the filter, consisted for the most part of relatively coarsely disperse insoluble particles with some small quantity of subcolloidal and colloidal particles and possibly soluble compounds remaining in the filter as as a result of physical and chemical sorption processes in the filter material and insoluble precipitate particles. The conditionally soluble part consisted of truly dissolved substances and some quantity of highly disperse, colloidal and subcolloidal particles.

Table 1

Concentration of Elements (mg/kg) in Samples Taken at Different Times

Дата 1	Параметры 2	Никель 3	Свинец 4	Цинк 5	Серебро 6	Медь 7	Ванадий 8
10 I	q_{oc} 9	2000	350	890	43	1600	50
	q_p	300	50	60	3,6	160	3,5
25 III	q_{oc} 10	2100	190	220	38	1300	28
	q_p	10000	200	2700	20	5000	23

Note: q_{prec} is the concentration of the element in the precipitate in the filter, q_{dry} is the concentration in the dry residue of the part of the sample which has passed through the filter.

KEY:

1. Date
2. Parameters
3. Nickel
4. Lead
5. Zinc
6. Silver
7. Copper
8. Vanadium
9. qprec
10. qdry

In the preparation and processing of the samples (reduction to ash, evaporation) with microquantities of metals there can be considerable uncontrollable losses, as a result of which there is a distortion of the measurement results. We developed a method for the preliminary processing of samples which excludes such losses. The filters with the samples prior to reduction to ash were wetted with sulfuric acid of the OSCh grade and held in quartz crucibles at a temperature of 100°C to the point of carbonization and removal of traces of acid. Then the filters were reduced to ash in a muffle furnace at a temperature not greater than 450°C. The conditionally soluble part of the sample was evaporated with the addition of sulfuric acid of the OSCh grade at a temperature of 100°C in a quartz crucible with a volume of 5 ml, to which the sample was added in small portions as evaporation progressed. Upon attaining a hundredfold decrease in volume the sample was conveyed to the filter and after thorough drying under a lamp was reduced to ash. All the samples were weighed on microanalytical scales and analyzed for their content of nickel, cobalt, copper, zinc, lead, vanadium, tin and silver. The volume concentrations in μg/liter were computed on the basis of the weight of the ash and the volume of the sample to be analyzed.

As indicated by the experiments, in the samples taken near the source long before the melting of the snow, for example, in January, the ratio of the concentrations in the conditionally soluble and insoluble parts for all the elements which we studied usually does not exceed one or two tenths. As time passes this ratio increases and during the period before snow thawing can exceed unity. As an example we give Table 1, which gives the concentrations of elements in mg/kg (in the dry residue of the samples) selected at different times at one of the stations.

Table 1 shows that the concentrations of elements in the precipitate on the filter in samples taken prior to snow melting (25 March) are reduced or remain approximately constant in comparison with the concentrations in samples taken at an earlier time. The concentrations of elements in the part of the samples passing through the filter increased appreciably. This can be explained on the assumption that by the time of the second sampling there was a partial dispersion and dissolving of the solid precipitate. This effect may not be discovered if the concentrations of elements do not relate to dry residue, but to the entire liquid part of the sample in a case if the weight of the dry residue in the part of the sample passing through the filter is very small. Thus, the initial relationship between the conditionally soluble and insoluble parts in the snow can change with time as a result of physical and chemical processes in the solid and liquid phases. In order to study the possible changes in this relationship and to choose the most acceptable times for the taking of samples we compared the data obtained at several sampling times: in January, February, March and April. In order to obtain data undistorted by processes transpiring in the lying snow it is evidently better to take all the samples at earlier times.

Principal Patterns of Aerosol Fallout

An analysis of the collected data indicated that the concentrations of metals in the snow cover decrease with the distance x from the source and quantitatively are satisfactorily approximated by the dependence $q(x) = q_0 \exp(-kx)$, where q_0 is the concentration at the station used as the initial point separated from the studied point at the distance x km. The k coefficient is a constant value for the direction, mean velocity and element.

Table 2

Values of Aerosol Transport Parameters

Параметр 1	Свинец 2	Цинк, медь, никель, ванадий, олово 3	Серебро, кобальт 4
5 $K_{пр} \cdot 10^3$ км$^{-1}$	3,0±0,3	6,0±0,5	1,7±0,2
6 $K_{обр} \cdot 10^3$ км$^{-1}$	26±8	25±2	14±1
$L_{пр}$ км	300	170	600
$L_{обр}$ км	40	40	70
$T_{пр}$ ч	15	8,5	30
$T_{обр}$ ч	2,0	2,0	3,5

KEY:
1. Parameter
2. Lead
3. Zinc, copper, nickel, vanadium, tin
4. Silver, cobalt
5. $K_{prevailing}$
6. $K_{reverse}$

With a change in wind direction the k value changes. For example, in our case $k_{prevailing} = (6.0 \pm 0.5) \cdot 10^{-3}$ km^{-1} in the direction of the prevailing winds and $k_{reverse} = (25 \pm 2) \cdot 10^{-3}$ km^{-1} in the reverse direction.

The elements which we studied can be divided into three groups differing with respect to the value of the coefficient k, as shown in the figure, which gives the dependence of the logarithm of the ratio of concentrations on distance to the source. In order to construct the graph we carried out normalization to the values of the concentrations at a point situated approximately 100 km from the source. A similar dependence is observed for all fallout in the opposite direction, but the concentrations are reduced more rapidly. On the average the ratio of the coefficients k for these two directions $k_{prevailing}/k_{reverse} = 0.15$. The k values are given in Table 2, where the subscripts "prevailing" and "reverse" characterize the forward and reverse directions.

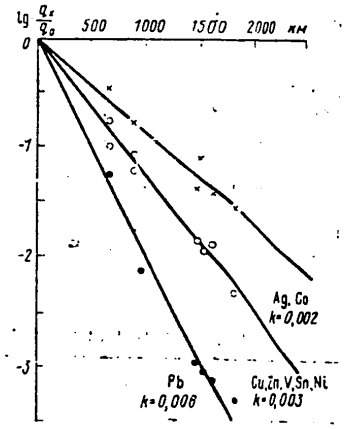

In addition, Table 2 gives the values L = 1/k and T = L/v -- the distance and time in which the concentration decreases by a factor of e. In order to obtain the mean values of these parameters, given in the table, we made 150 measurements. The mean wind velocity was assumed equal to 20 and 2 km/hour for $v_{prevailing}$ and $v_{reverse}$. The k value is evidently influenced not only by wind velocity and direction, but also by the mean lifetime of aerosols in the atmosphere. It is usually assumed that the mean lifetime of industrial aerosols in the atmosphere τ in the case of transport for great distances is a value of about two days. The T value which we computed should be less than the τ value since the concentration of aerosols in the air with increasing distance from the source decreases as a result of two factors: aerosol fallout and atmospheric diffusion, so that the relationship $T<\tau$ will be correct. In this sense the data which we obtained are in satisfactory agreement with the generally accepted value.

Table 3

Contribution of Conditionally Soluble Part to Total Concentration, %

Расстояние, км (1)	Никель (2)	Свинец (3)	Цинк (4)	Серебро (5)	Медь (6)	Ванадий (7)	Кобальт (8)
100	6±4	5±3	2±1	9±6	7±5	7±5	6±3
2000	200±80	70±30	220±40	45±20	210±100	80±60	110±50

KEY:

1. Distance, km
2. Nickel
3. Lead
4. Zinc
5. Silver
6. Copper
7. Vanadium
8. Cobalt

Thus, the empirical dependences which we obtained are in satisfactory agreement with existing concepts concerning atmospheric transport over great distances and can serve for approximate quantitative estimates.

It also follows from the collected data that the contribution of the conditionally soluble part to the total concentration near the source of effluent is not more than several percent, whereas at great distances it can increase to tens and hundreds of percent. Table 3 contains figures giving some idea concerning the magnitude of the contribution of the conditionally soluble part in samples taken at distances of 100 and 2,000 km. The samples whose measurements were used in preparing Table 3 were taken in January, that is, at the time when the distribution of concentrations between the conditionally soluble and insoluble parts still could not change significantly.

With time the contribution of the conditionally soluble part at a particular point increases as a result of the physicochemical processes transpiring in the snow cover; therefore, as noted above, the initial composition of the fallout must be characterized by samples taken soon after the formation of a stable snow cover.

An analysis of the data indicated that in the first approximation the decrease in the concentrations of the insoluble and conditionally soluble parts separately at distances 100-2,000 km can also be described by an exponential dependence. Such an approximation is satisfactory within the limits of the accuracy of the experimental data due to the small contribution of the conditionally soluble part to the initial composition of the aerosol. The principal difference in the behavior of the conditionally soluble and insoluble parts is that the k value for the conditionally soluble part on the average is approximately 1 1/2-2 times less than for the conditionally insoluble part and accordingly the aerosols associated with the conditionally soluble part of the sample are propagated over great distances and probably can be the main reason for the change in the global background. The derived dependences made it possible to discriminate the influence of weak local sources in a study of transport from powerful remote sources.

Conclusions

1. It was demonstrated that a study of distant transport can be made by investigating the concentrations of contaminating substances in the snow cover.

2. It is shown that contaminations are discovered at distances of 1,000 km or more, which agrees with the data published by other authors; the concentrations of contaminating substances decrease exponentially with increasing distance from the source; the exponent is dependent on wind velocity and direction.

3. It was established that the ratio of concentrations in the insoluble and conditionally soluble parts of the sample in the lying snow at a given point increases with time.

BIBLIOGRAPHY

1. Aleksandrov, E. L., Kireyeva, N. M., Mashkova, G. B., Yasevich, N. P., "Concentration of Natural Atmospheric Aerosols in Air Masses of Different Direction of Transfer," TRUDY IEM (Transactions of the Institute of Experimental Meteorology), No 12(31), 1976.

2. Andryukov, V. P., Ryaboshapko, A. G., Shopauskene, D. A., Erdman, L. K., "Atmospheric Transport of Contaminating Substances Over a Distance of About Hundreds of Kilometers," TRUDY IPG (Transactions of the Institute of Applied Geophysics), No 39, 1978.

3. Garger, Ye. K., Zhigalovskaya, T. N., et al., "Estimating the Background Content of Trace Elements in Frontal Regions," TRUDY IEM, No 2(36), 1972.

4. Grigor'yev, A., Kondrat'yev, K., "Atmospheric Dust. Observations from Space," NAUKA I ZHIZN' (Science and Life), No 6, 1979.

5. Zhigalovskaya, T. N., Kireyeva, N. M., "The Content of Some Trace Elements in a Frontal Zone Determined from Measurements on a High Meteorological Mast," TRUDY IEM, No 2(36), 1972.

6. Kireyeva, N. M., Mashkova, G. B., Yasevich, N. P., "Change in the Concentrations of Atmospheric Aerosols During the Passage of Fronts," TRUDY IEM, No 12(31), 1976.

7. Nazarov, I. M., Fridman, Sh. D., Renne, O. S., "Use of Network Snow Surveys for Study of Contamination of the Snow Cover," METEOROLOGIYA I GIDROLOGIYA (Meteorology and Hydrology), No 7, 1978.

8. Bigg, E. K., Ayers, G. P., Turkey, D. E., "Measurement of the Dispersion of a Smoke Plume at Large Distances from the Source," ATMOS. ENVIRON., Vol 12, No 8, 1978.

UDC 551.576.1:519.24

STATISTICAL CHARACTERISTICS OF THE VERTICAL STRUCTURE OF THE LIQUID WATER CONTENT AND TEMPERATURE FIELDS IN CUMULUS CLOUDS

Moscow METEOROLOGIYA I GIDROLOGIYA in Russian No 4, Apr 80 pp 52-59

[Article by V. S. Kosolapov, All-Union Machine-Building Correspondence Institute, submitted for publication 5 May 1979]

Abstract: Using data on the profiles of liquid water content and temperature obtained as a result of repeated aircraft penetrations of individual cumulus and well-developed cumulus clouds the author has computed their mean profiles and correlation matrices. The results indicate a relatively high correlation between deviations of liquid water content and temperature from their mean values at all levels. The eigenvalues and eigenvectors were computed for the correlation matrices of the four groups of clouds which differed with respect to degree of development. It is shown that depending on the required accuracy there can be an optimum approximation of any random profile of liquid water content and temperature by the first two or three eigenvectors.

[Text] Systems of so-called statistical orthogonal functions or vectors are important characteristics of the statistical structure of the fields of meteorological elements. Systems of eigenvectors of the corresponding correlation matrix [1, 4, 5] constitute an optimum system of base vectors (in the case of discrete stipulation of random functions). These vectors most completely and economically (that is, using a small number of vectors) describe the vertical structure of the meteorological elements for solving a number of problems in atmospheric physics, such as for restoration of their vertical profiles [4, 6, 7].

We will examine the vertical structure of the liquid water content and temperature fields in cumulus clouds.

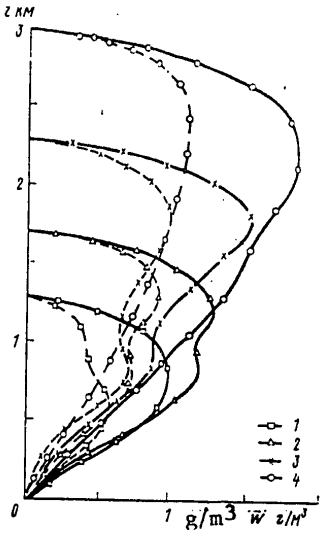

Fig. 1. Mean vertical profiles of liquid water content (solid curves) and standard deviations (dashed curve) for different groups of cumulus clouds. 1) first group; 2) second group; 3) third group; 4) fourth group

Due to the lack of systematic measurements of the spatial distribution of liquid water content in individual cumulus clouds the available quantitative data constituted a relatively small mass of records of vertical profiles of liquid water content and temperature (approximately 120). The empirical data were classified on the basis of concepts concerning the uniformity of the sample and were combined into four groups (with approximately 30 cases each). Processing was carried out separately for each of the four groups of clouds differing in vertical development ΔH (from 1.3 to 3 km). These probably can be identified with Cu hum. (first group, $\Delta H \approx$ 1.3 km), Cu med. (second group, $\Delta H \approx 1.7$ km) and Cu cong. (third and fourth groups, $\Delta H \approx 2.3$ km and $\Delta H \approx 3.0$ km).

Figure 1 shows the mean profiles of liquid water content of the mentioned groups of clouds and their standard deviations. Figure 1 shows that the mean profile of the first group of clouds has one maximum approximately at an altitude of $2/3\Delta H$ from the lower cloud base. The mean profiles for clouds of the second, third and fourth groups have two maxima: the main maximum in the upper part of the cloud and the second, more or less expressed in the lower or middle part (this maximum was obtained due to cases with a maximum in the lower part of the cloud and as a result of cases with two maxima). The maximum liquid water content increases from the first to fourth groups.

This is in qualitative agreement with the results obtained by a number of authors [2, 3, 8]. The standard deviations from the means for the most part duplicate the main features of their mean profiles, evidence of the possibility of considerable variations of liquid water content in the middle and upper parts of the cloud (constituting 60-80% of their mean values).

As an example, Tables 1-4 give the normalized correlation matrices of deviations of liquid water content and temperature from their mean values for some groups. Table 1 gives a correlation matrix computed for the random vectors, in which, in addition to the profile of liquid water content, we have also formally included the integral liquid water content, altitudes of the lower and upper cloud boundaries and the temperature of the lower and upper boundaries. Therefore, in the upper left corner we give the usual matrix of liquid water content (separated by a dashed line), whereas the bordering elements represent the coefficients of correlation between liquid water content and the above-mentioned parameters and also the cross-correlation coefficients between these parameters. Tables 1 and 2 show that there is a rather high degree of correlation between the deviations of liquid water content from the means at all levels, although there are regions of a rapid decrease in the correlation moments with altitude, for example, in the first group of clouds between the levels 600 and 900 m, and in the third -- between 800 and 1,100 m. This reflects the frequently observed process of a redistribution of liquid moisture from the lower part of the cloud into the middle part. In actuality, Fig. 1 shows that in this region there is a local or absolute maximum of liquid water content.

Tables 3 and 4 reflect the very high correlation between the deviations of temperature at all levels, especially for clouds in the first group. In the upper part of clouds in the fourth group there is a dropoff of the correlation coefficients. This can occur, first of all, due to the upward movement of warm masses here. Locally there can also be a descent of colder atmospheric air masses into the warmer cloud mass.

A similar picture in the behavior of the correlation coefficients also occurs in two other groups of clouds, differing only quantitatively: with an increase in cloud thickness the correlation moments of the matrices decrease more strongly and at the upper boundaries have lesser values.

Now we will examine the "bordering" in the matrix for the first group $\Delta H \cong$ 1,300 m (Table 1). The considerable correlation of integral liquid water content with the liquid water contents at all levels is completely understandable. There is also a high correlation (0.5-0.8) between the temperature deviations at the lower and upper boundaries of the cloud and the deviations of liquid water content at all levels. This is related to the fact that the increase in the condensation (dew) point (it can be assumed that the lower cloud boundary is close to the condensation level) occurs due to an increase in the absolute and relative air humidity under the cloud and since convective clouds receive liquid moisture for the most part from

below, this is reflected in an increase in the liquid water content of the cloud (that is, a positive correlation with the temperature of the lower boundary). However, a temperature decrease at the upper cloud boundary leads to an intensification of the condensation process and accordingly, an increase in the liquid water content of the cloud (negative correlation with the temperature of the upper boundary).

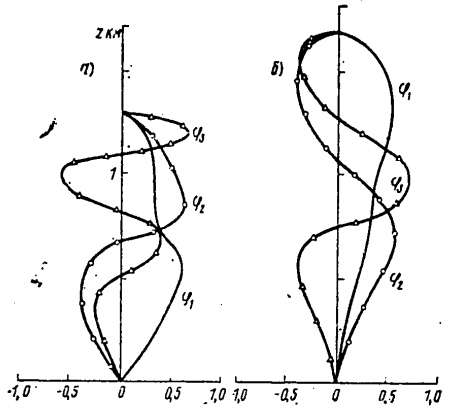

Fig. 2. Vertical variation of first (φ_1), second (φ_2) and third (φ_3) eigenvectors of non-normalized correlation matrix of profile of liquid water content of clouds of the first (a) and second (b) groups.

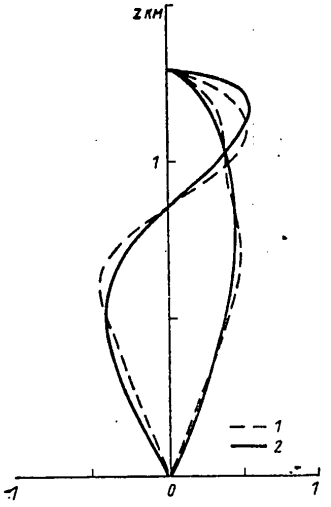

Fig. 3. Optimum approximation (1) of two types of deviation from mean of profile (2) with use of three first eigenvectors.

It was found that the deviations of the altitudes of the lower and upper boundaries correlate with the deviations of liquid water content at all levels to a somewhat lesser extent than the temperature deviations at these boundaries (in this case, understandably, the correlation signs are opposite the correlation signs of temperature and liquid water content).

Now we will examine the eigenvalues μ_i and the eigenvectors $\varphi_i(z_j)$ of clouds in all groups (Table 5, Fig. 2).

As demonstrated in [1, 5], using empirical orthogonal functions it is possible to approximate any random function or vector with a stipulated error by a minimum (among all orthogonal systems) number of base functions or vectors (k). The accuracy of this approximation is determined by the ratio

Table 1

Correlation Matrix for $\Delta H \approx 1{,}300$ m (With "Bordering") (Normalized)

	200	400	600	800	1000	1200	W	$H_{нг}$ lower	$H_{вг}$ upper	$t_{нг}$	$t_{вг}$	1 Среднеквадратичные значения: абсол.2	в % к сред.3	Среднее значение 4
200	1	0,992	0,948	0,319	0,402	0,491	0,823	—0,288	0,703	0,715	—0,842	0,277	83	0,33
400		1	0,972	0,386	0,465	0,535	0,865	—0,309	0,721	0,729	—0,866	0,494	76	0,65
600			1	0,542	0,546	0,565	0,917	—0,276	0,787	0,680	—0,897	0,584	62	0,93
800				1	0,670	0,608	0,737	—0,188	0,628	0,232	—0,479	0,451	45	1,00
1000					1	0,719	0,652	—0,489	0,441	0,518	—0,389	0,360	40	0,90
1200						1	0,762	—0,657	0,447	0,611	—0,401	0,284	56	0,50
W							1	—0,403	0,776	0,684	—0,784	0,4038	48	0,836
$H_{нг}$	lower							1	0,035	—0,764	0,015	88,192	5,2	1700
$H_{вг}$	upper								1	0,326	—0,794	120,95	4	3050
$t_{нг}$										1	—0,570	0,994	0,4	279,76
$t_{вг}$											1	1,4075	0,5	270,16

Table 2

Correlation Matrix of Liquid Water Content Profile for Clouds with $\Delta H \approx 2{,}300$ m (Normalized)

	200	400	600	800	1000	1200	1400	1600	1800	2000	2200	1 Среднеквадратичные значения: абсол.2	в % к сред.3	Среднее значение 4
200	1	0,960	0,849	0,815	0,743	0,755	0,818	0,659	0,519	0,468	0,447	0,0945	59	0,16
400		1	0,955	0,939	0,794	0,760	0,845	0,723	0,606	0,553	0,513	0,238	68	0,35
600			1	0,992	0,769	0,689	0,808	0,732	0,650	0,593	0,542	0,506	84	0,60
800				1	0,787	0,709	0,823	0,757	0,683	0,633	0,582	0,711	85	0,83
1000					1	0,964	0,899	0,865	0,796	0,736	0,664	0,645	72	0,87
1200						1	0,943	0,879	0,787	0,733	0,677	0,674	68	0,99
1400							1	0,914	0,812	0,765	0,721	0,760	64	1,18
1600								1	0,972	0,920	0,822	0,912	65	1,41
1800									1	0,970	0,861	0,992	65	1,51
2000										1	0,942	0,866	65	1,33
2200											1	0,50	74	0,68

KEY:

1. Mean square values
2. Absolute
3. In % of mean
4. Mean value
5. Lower boundary
6. Upper boundary

Table 3

Correlation Matrix of Vertical Temperature Profile in Clouds With Thickness $\Delta H \approx 1{,}300$ m (Normalized)

	200	400	600	800	1000	1200	Среднеквадратичные значения 1: абсол. 2	в % от сред. 3	Среднее значение 4
200	1	0,973	0,978	0,979	0,990	0,997	1,08	0,4	278,3
400		1	0,998	0,994	0,987	0,976	1,19	0,4	276,7
600			1	0,996	0,991	0,980	1,474	0,5	275,3
800				1	0,996	0,982	1,53	0,5	274
1000					1	0,994	1,54	0,5	272,6
1200						1	1,57	0,6	271,1

Table 4

Correlation Matrix of Vertical Temperature Profile in Clouds $\Delta H \approx 3{,}000$ m (Normalized)

	200	500	800	1100	1400	1700	2000	2300	2600	2900	Среднеквадратические значения 1: абсол. 2	в % от сред. 3	Среднее значение 4
200	1	0,997	0,985	0,967	0,950	0,955	0,977	0,939	0,808	0,782	0,907	0,3	279,5
500		1	0,994	0,982	0,967	0,971	0,983	0,918	0,772	0,744	1,09	0,4	277,6
800			1	0,995	0,988	0,984	0,975	0,879	0,717	0,691	1,23	0,4	275,5
1100				1	0,997	0,993	0,970	0,844	0,666	0,647	1,35	0,5	273,5
1400					1	0,995	0,963	0,819	0,633	0,615	1,46	0,5	271,6
1700						1	0,979	0,840	0,661	0,660	1,46	0,5	269,6
2000							1	0,915	0,768	0,766	1,20	0,4	267,9
2300								1	0,959	0,936	0,99	0,4	266
2600									1	0,976	1,16	0,4	263,8
2900										1	1,21	0,5	261,1

KEY:

1. Standard deviations
2. Absolute
3. In % of mean
4. Mean value

Table 5

Eigenvalues of Correlation Matrices of Profiles of Liquid Water Content and Temperature and Values of Dispersions ε_i(%)

i	Group Группа											
	1		2		3		4		1		4	
	μ_i^w	ε_i^w	μ_i^w	ε_i^w	μ_i^w	ε_i^w	μ_i^w	ε_i^w	μ_i^T	ε_i^T	μ_i^T	ε_i^T
	Liquid water content Водность								Temperature Температура			
1	0,8125	73,6	2,498	69,5	4,2887	84,2	4,9944	80,9	11,681	99	13,275	89
2	0,2261	94	0,8577	93,3	0,4591	93,2	0,75523	93,2	0,0872	99,9	1,435	98,7
3	0,0551	99	0,1662	98	0,2015	97,2	0,3177	98,3	0,0158		0,1136	99,5
4	0,0059	99,7	0,0634	99,7	0,0697	98,6	0,05856	99,3	0,005		0,0571	
5	0,0035	99,9	0,0083	99,95	0,0533	99,6	0,02474		10^{-5}		0,0289	
6	0,00044	100	0,0013		0,0071	99,8	0,01282		10^{-6}		0,0130	
7	—		0,0004		0,0065		0,00374				0,00113	
8			0,0001		0,0027		0,00204				0,00082	
9					0,0013		0,00086				0,00038	
10					0,00057		0,00023				0,00002	
11					0,00005							

FOR OFFICIAL USE ONLY

APPROVED FOR RELEASE: 2007/02/08: CIA-RDP82-00850R000200100010-7

of the corresponding eigenvalues to the spur of the matrix (n is the order of the matrix), that is

$$\varepsilon_k = \frac{\sum_{i=1}^{k} \mu_i}{\sum_{i=1}^{n} \mu_i},$$

ε_k is the so-called total dispersion of the expansion coefficients $w'(z_j)$ into a series for $\varphi_i(z_j)$.

Table 5 gives the eigenvalues for four groups of clouds and the values of the dispersions ε_i, whereas Fig. 2 gives the vertical variation of the first three eigenvectors of clouds of the first and second groups. We note that the first eigenvectors of all groups of clouds do not pass through zero. The vertical variation of the first vectors resembles the vertical profile of its standard deviations.

It is known that as a rule the first eigenvector describes the most characteristic vertical distribution of deviations of meteorological elements from their mean profile. Physical allowance for only the first eigenvector for the liquid water content profile can be interpreted in the following way: if a deviation of the liquid water content profile from the mean developed, it will be everywhere of the same sign, changing only in value with altitude. The second and subsequent vectors characterize the finer structure in liquid water content variations. The second and third vectors of all groups of clouds accordingly once and twice pass through zero. Physically their presence in the expansion of variations means that in the cloud there are regions of an excess or deficit of liquid moisture relative to the mean profile. Thus, each eigenvector is indicative of localization of liqu'd water content in definite parts of a cloud.

It is evident that if for any group of clouds the correlation coefficients more or less smoothly decrease with altitude, for this group allowance for the eigenvectors, beginning already with the second or third, is unimportant. Mathematically this is also expressed in a more rapid decrease in the eigenvectors with an increase in the number. And this makes it possible to accomplish an optimum approximation of the random functions (or vectors) by one, two or a maximum of three of the first eigenvectors.

Figure 3 gives an example of optimum approximation of the arbitrary functions $f'(z_j)$:

$$f'(z_j) = \sum_{i=1}^{n} c_i \varphi_i(z_j), \quad c_i = \sum_{j=1}^{n} f'(z_j)\, \varphi_i(z_j),$$

with n = 3, $\varepsilon_3 \cong 99\%$.

It can therefore be seen that already the first three eigenvectors approximate quite well random vectors of different types.

In conclusion we will briefly formulate the principal results.

In order to investigate the vertical structure of liquid water content and temperature of cumulus clouds all the experimental material was collected into four groups in dependence on cloud thickness. The mean profiles of liquid water content and temperature of these groups indicate a number of differences of both a quantitative character (for example, an increase in the maximum liquid water content of clouds from the first to the fourth groups) and a qualitative character (different number of liquid water content maxima with altitude in the groups).

For all these groups we computed the correlation matrices of the profiles of liquid water content and temperature and for these matrices -- their eigenvalues and vectors. It was found that on the whole there is a rather high correlation between the deviations of liquid water content at all levels. There are also regions (for different groups at different altitudes) of rapid decrease in the correlation moments, indicative of local or absolute maxima and deficits of liquid water content and temperature.

The eigenvalues and eigenvectors of different groups of clouds indicated the possibility of an optimum approximation of the profiles of liquid water content and temperature in dependence on the required accuracy (Table 5) by two or three eigenvectors, which have a deep physical sense: the first eigenvector indicates the most characteristic universal increase or decrease in liquid water content or temperature relative to their mean value, whereas the second, third and other vectors emphasize a finer structure in variations of liquid water content.

The expansion of the unknown random profiles of liquid water content into a series of eigenvectors can be used in radiometric methods in restoring these profiles [7].

In conclusion I regard it as my pleasant duty to express deep appreciation to N. I. Vul'fson and V. I. Skatskiy for the furnishing of factual material from aircraft measurements of liquid water content and temperature of clouds and to M. S. Malkevich for valuable consultations and discussion of the results.

BIBLIOGRAPHY

1. Bagrov, N. A., "Analytical Representation of a Series of Meteorological Fields by Natural Orthogonal Representations," TRUDY TsIP (Transactions of the Central Institute of Forecasts), No 74, 1959.

2. Voyt, F. Ya., Mazin, I. P., "Liquid Water Content of Cumulus Clouds," IZV. AN SSSR, FIZIKA ATMOSFERY I OKEANA (News of the USSR Academy of Sciences, Physics of the Atmosphere and Ocean), Vol VIII, No 11, 1972.

3. Gavrilenko, N. M., Yashovskaya, Z. M., "Liquid Water Content and Thickness of Convective Clouds in Different Synoptic Processes," TRUDY UkrNIGMI (Transactions of the Ukrainian Scientific Research Hydrometeorological Institute), No 61, 1966.

4. Malkevich, M. S., OPTICHESKIYE ISSLEDOVANIYA ATMOSFERY SO SPUTNIKOV (Optical Investigations of the Atmosphere from Satellites), Moscow, Nauka, 1973.

5. Obukhov, A. M., "Statistical Orthogonal Expansions of Empirical Functions," IZV. AN SSSR, SERIYA GEOFIZ. (News of the USSR Academy of Sciences, Geophysical Series), No 3, 1960.

6. Popova, N. D., "Parameterization of the Vertical Distribution of Liquid Water Content of Clouds Using Natural Components," TRUDY GGO (Transactions of the Main Geophysical Observatory), No 395, 1977.

7. Popova, N. D., "Determination of the Vertical Distribution of Liquid Water Content in Clouds Using Natural Components," TRUDY GGO, No 411, 1978.

8. Skatskiy, V.I., "Investigation of the Liquid Water Content of Cumulus Clouds," TRUDY IPG (Transactions of the Institute of Applied Geophysics), No 13, 1969.

UDC 551.551.8

INFLUENCE OF ABSORBING PROPERTIES OF THE SURFACE ON THE DIFFUSION OF AN IMPURITY IN THE ATMOSPHERIC BOUNDARY LAYER

Moscow METEOROLOGIYA I GIDROLOGIYA in Russian No 4, Apr 80 pp 60-65

[Article by Candidate of Physical and Mathematical Sciences M. A. Novitskiy, Institute of Experimental Meteorology, submitted for publication 20 June 1979]

Abstract: The article gives the results of an analysis of the absorbing properties of the surface on the diffusion characteristics of a cloud of impurity in the atmospheric boundary layer. The scattering of the impurity from an instantaneous point source was computed by numerical solution of a system of equations for the concentration moments and equations describing the stationary horizontally homogeneous boundary layer of the atmosphere. It is shown that the trajectory of the center of gravity of the cloud and the longitudinal integral dispersion are essentially dependent on the absorption of the impurity by the surface.

[Text] A quantitative analysis of the diffusion of contaminating substances in the atmosphere is becoming more and more important with an increasing contamination of the environment. In computations of propagation of impurities a complex problem is determination of their interaction with the underlying surface. Difficulties in determining the absorbing properties of the surface more and more make it necessary to assume that the underlying surface completely reflects the impurity falling on it. It is evident that the results of computations of the scattering of an impurity obtained using such an assumption cannot be adequately correct. In addition, it must be remembered that the absorbing properties of the surface are not constant but are dependent on the season, the falling of precipitation and other factors. Accordingly, it is of unquestionable interest to ascertain to what extent the diffusion characteristics of the scattered impurity are dependent on the absorbing properties of the underlying surface.

The interaction between the impurity and the earth's surface is usually described by the following boundary condition with z = 0:

$$k(z)\frac{\partial C}{\partial z} + wC = \beta C, \tag{1}$$

where C is the concentration of the impurity, k(z) is the coefficient of turbulent diffusion, w is the rate of gravitational precipitation of the impurity, β is the coefficient of absorption of the impurity by the underlying surface [1].

The process of turbulent scattering will be described by the semi-empirical equation of diffusion in a parabolic form

$$\frac{\partial C}{\partial \tau} + U\frac{\partial C}{\partial \xi} + V\frac{\partial C}{\partial \zeta} = \varkappa^2\left\{\frac{\partial}{\partial \eta}\left(K_\eta \frac{\partial C}{\partial \eta}\right) + K_\xi \frac{\partial^2 C}{\partial \xi^2} + K_\zeta \frac{\partial^2 C}{\partial \zeta^2}\right\}, \tag{2}$$

where

$$\tau = tf/\varkappa^2,\ \xi = xf/\varkappa u_*,\ \zeta = yf/\varkappa u_*,\ \eta = zf/\varkappa u_*,$$

f is the Coriolis parameter, $\varkappa$ is the Karman constant, u_* is dynamic velocity, U, V are the dimensionless components of wind velocity, K_η, K_ξ, K_ζ are the dimensionless coefficients of diffusion in the corresponding directions.

In solving the formulated problem it is desirable to limit ourselves to an analysis of the behavior of the several first moments of the concentration. This is justified because in practical applications we are most frequently interested precisely in the integral characteristics of the cloud of impurity, such as the coordinates of the center of gravity and dispersion. In addition, the problem is substantially simplified because it is possible to transform from a three-dimensional diffusion equation to a system of one-dimensional equations for the concentration moments. We will multiply equation (2) by ξ in a corresponding power and integrate for ξ and ζ. Then we obtain [4] the following system of equations:

$$\frac{\partial q}{\partial \tau} = \varkappa^2 \frac{\partial}{\partial \eta}\left(K \frac{\partial q}{\partial \eta}\right), \tag{3}$$

$$\frac{\partial m_1}{\partial \tau} = \varkappa^2 \frac{\partial}{\partial \eta}\left(K_\eta \frac{\partial m_1}{\partial \eta}\right) + qU, \tag{4}$$

$$\frac{\partial s_1}{\partial \tau} = \varkappa^2\left\{\frac{\partial}{\partial \eta}\left(K_\eta \frac{\partial s_1}{\partial \eta}\right) + 2K_\xi q\right\} + 2m_1 U, \tag{5}$$

where q, m_1, s_1 are the concentration moments

$$q = \int C d\xi d\zeta, \tag{6}$$

$$m_1 = \int \xi C d\xi d\zeta, \tag{7}$$

$$s_1 = \int \xi^2 C d\xi d\zeta. \tag{8}$$

Equations similar to equations (7) and (8) can also be written for the ζ - components of m_2 and s_2. By means of the concentration moments the dispersions are computed in the following way:

$$\Sigma_\xi^2 = \frac{\int s_1 d\eta}{\int q d\tau_1} - C_\xi^2, \quad \Sigma_\zeta^2 = \frac{\int s_2 d\eta}{\int q d\tau_1} - C_\zeta^2, \tag{9}$$

where C_ξ and C_ζ are the coordinates of the center of gravity of the cloud,

$$C_\xi = \frac{\int m_1 d\tau_1}{\int q d\tau_1}, \quad C_\zeta = \frac{\int m_2 d\eta}{\int q d\eta}. \tag{10}$$

In order to determine the wind velocity profiles entering into equations (4)-(5) we used a model of a stationary horizontally homogeneous boundary layer [6]. The system of equations for the model has the following form:

$$\frac{d^2 X}{d\tau_1^2} + \frac{Y}{K_m} = 0,$$

$$\frac{d^2 Y}{d\tau_1^2} - \frac{X}{K_m} = 0, \tag{11}$$

where

$$X = K_m \frac{dP}{d\tau_1}, \quad Y = K_m \frac{dQ}{d\tau_1}, \quad P = \varkappa \frac{u - u_g}{u_*},$$

$$Q = \varkappa \frac{v - v_g}{u_*}, \quad K_m = \frac{fk_m}{\varkappa^2 u_*^2},$$

u_g, v_g are the components of geostrophic wind velocity, k_m is the eddy viscosity coefficient.

The x-axis of the coordinate system is directed along the surface friction vector.

For closing the system of equations (11) we used the hypothesis of the Prandtl displacement length

$$K_m = \frac{L}{\varkappa} (X^2 + Y^2)^{1/4}, \tag{12}$$

where $L = L(\eta, L_\infty)$ is the displacement length, L_∞ is a parameter making it possible to stipulate the thermal stratification. In the computations the displacement length was determined by an expression from [6]

$$L = \frac{\varkappa \eta}{1 + \varkappa \frac{(\eta - \eta_0)^{5/4}}{L_\infty}}, \tag{13}$$

where η_0 is the dimensionless roughness of the underlying surface.

The boundary conditions for equations (11)-(13) were as follows:

$$\eta = \eta_0 \quad X = 1, \quad Y = 0;$$
$$\eta \to \infty, \quad X \to 0, \quad Y \to 0.$$

In solving the system of equations (3)-(5), describing the scattering of the impurity, the coefficient of vertical diffusion K_η was assumed to be equal to the coefficient of eddy viscosity Km; the coefficients of horizontal diffusion K_ξ and K_ζ were proportional to Km,

$$K_\xi = aK_m, \quad K_\zeta = bK_m, \tag{14}$$

where a and b are some constants (possibly dependent on stratification). Unfortunately, the presently available data on the values of these constants and their dependence on stratification are contradictory. The computations were made with a = 4.5 and b = 13, which corresponds to the estimates cited in [3].

It is understandable that the use of the constants obtained for the surface layer is not entirely correct for the entire boundary layer. However, the computations made indicated that beginning with some moment in time shear diffusion introduces a definite contribution to the horizontal scattering of the impurity and the horizontal dispersions cease to be dependent on the values of the constants a and b. (In this case the center of gravity of the cloud is still in the lower part of the boundary layer). Therefore, the use of the values of these constants cited above does not lead to the appearance of appreciable errors in the entire boundary layer.

The components of geostrophic wind velocity U_g and V_g were computed using the functions X and Y by use of the expression $U(\eta_0) = V(\eta_0) = 0$; then we determined the $U(\eta)$ and $V(\eta)$ profiles. Since we examined the diffusion of a weightless impurity from an instantaneous point source, the initial condition for equation (3) was stipulated in the form

$$q(\eta, 0) = q_0\delta(\eta - h), \tag{15}$$

where h is the height of the impurity source.

The initial conditions for equations (4) and (5) were zero conditions. The boundary conditions are easily obtained from expression (1). Since a weightless impurity was considered, then w = 0. Integrating (1) for ξ and ζ 1, for equation (3) we obtain the condition

$$K_\eta \frac{\partial q}{\partial \eta} = \frac{\beta}{\varkappa u_*} q. \tag{16}$$

The boundary conditions for equations (4) and (5) have a similar form.

The cited equations (3)-(5) and (11)-(13) were solved numerically: the boundary layer equations were solved by the iteration method proposed in [5]; the equations for the concentration moments were solved by an implicit second-order method [2].

Figure 1 shows the trajectories of the center of gravity of the cloud of impurity for cases of ideal reflection of an impurity by the surface (1) and complete absorption (2) with different stratification. Variant a -- slight instability, L_∞= 0.1, Ro = $6.7 \cdot 10^6$, variant b -- neutral

stratification, $L_\infty = 0.015$, $Re = 7.5 \cdot 10^6$, c -- weak stability, $L_\infty = 10^{-3}$, $Re = 1.2 \cdot 10^7$. The impurity source was at the height $h = 10^{-4}$, the roughness of the underlying surface was $\eta_0 = 10^{-5}$. It can be seen that in the case of total absorption of the impurity by the surface the deviation of the trajectory from the direction of the surface wind is greater than in the case of total reflection of the impurity. With an increase in atmospheric stability the trajectories become increasingly more distant from one another. This is attributable to the fact that in the case of instability the intensity of mixing is greater, the impurity is more rapidly raised upward and the influence of the lower boundary condition is less. We will proceed in the following way in order to explain the large angle of deviation of the trajectory in the case of total absorption of the impurity at the boundary. We will integrate equations (4) for η. Then, taking (3) into account, we obtain the following equations for the total moments M_1 and M_2:

$$\frac{\partial M_1}{\partial \tau} = -\varkappa^2 \beta m_1(\eta_0) + \int qU d\eta,$$

$$\frac{\partial M_2}{\partial \tau} = -\varkappa^2 \beta m_2(\eta_0) + \int qV d\eta, \qquad (17)$$

where

$$M_1 = \int m_1 d\eta, \quad M_2 = \int m_2 d\eta.$$

The second terms on the right-hand side of these equations have the sense of the mean velocities of transfer of the impurity in the corresponding directions. It can be seen that in the case of total absorption of the impurity the contribution of the lower layers leads to a relative increase in the contribution of the V-component of velocity to the total transport of the impurity, as a result of which there is a greater angle of deviation of the trajectory of the center of gravity of the cloud in the case of total absorption of the impurity at the boundary.

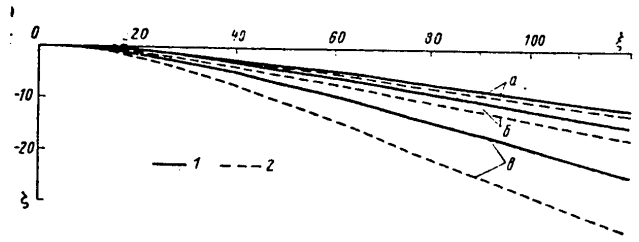

Fig. 1.

Figure 2 shows the dependence of height of the center of gravity of the cloud of impurity on time. These variants correspond to the same values of the parameters as the similarly denoted curves in Fig. 1. In the case of total absorption of the impurity by the surface there is a more rapid rise of the center of gravity. This is attributable to the fact that the absorbing surface eliminates the impurity from the lower part of the boundary layer. The rate of ascent of the center of gravity increases with

an increase in instability due to an increase in the intensity of mixing.

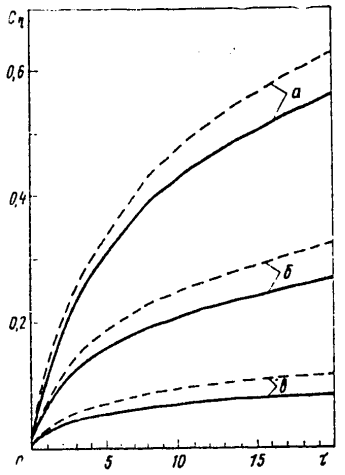

Fig. 2

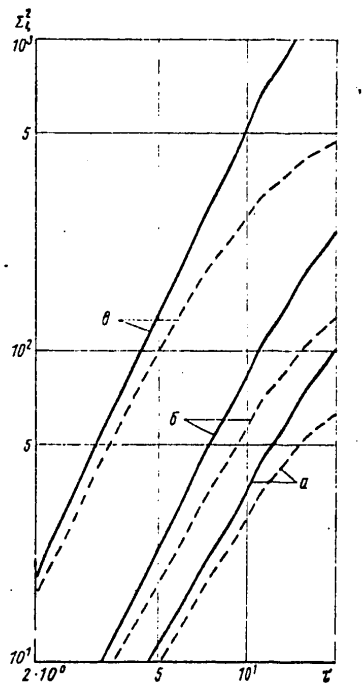

Fig. 3

An analysis of the behavior of the vertical dispersion $\sum_\eta^2$ indicated that the change in the boundary condition exerts a very weak influence on its value.

Figure 3 shows the integral dispersions of concentration of the impurity $\sum_\xi^2$ also for cases of total reflection of the impurity at the boundary (solid curves) and total absorption (dashed curves). The variants a, b, c correspond to the same boundary layer characteristics as in Fig. 1. A comparison of the illustrated curves reveals that absorption of the impurity at the boundary leads to a decrease in the longitudinal dispersion. With an increase in stability the influence of the boundary condition becomes stronger. In contrast to this, it follows from computation of the behavior of the transverse dispersions $\sum_\zeta^2$ that in the considered time interval with a change in the lower boundary condition they virtually do not change. Such a behavior of the dispersions can be explained in the following way. The longitudinal scattering of the impurity is determined to a considerable degree by the wind shear. Since the shear is greatest at the surface,

the absorption of the impurity by the surface leads to a decrease in the contribution of the lower layers to longitudinal scattering. However, transverse scattering of the impurity at the surface is determined by eddy diffusion and therefore the change in the lower boundary condition exerts no appreciable influence on $\sum_5^2$.

Thus, our analysis reveals that in computations of transverse dispersion the nature of the interaction of the impurity with the underlying surface plays no significant role. At the same time, a knowledge of the absorption coefficient is entirely necessary in computations of longitudinal dispersion and the trajectories of movement of the center of gravity of the cloud of impurity. The cited graphs in actuality determine the corridor in which the curves describing the behavior of the corresponding parameters fall in the case of a real underlying surface.

BIBLIOGRAPHY

1. Krotova, I. A., Natanzon, G. A., "Influence of an Underlying Surface on the Propagation of a Weightless Impurity in the Atmospheric Surface Layer," TRUDY IEM (Transactions of the Institute of Experimental Meteorology), No 21(80), 1978.

2. Samarskiy, A. A., VVEDENIYE V TEORIYU RAZNOSTNYKH SKHEM (Introduction to the Theory of Difference Schemes), Moscow, Nauka, 1971.

3. Yaglom, A. M., DIFFUZIYA PRIMESI OT MGNOVENNOGO TOCHECHNOGO ISTOCHNIKA V TURBULENTNOM POGRANICHNOM SLOYE. TURBULENTNYYE TECHENIYA (Diffusion of an Impurity from an Instantaneous Point Source in a Turbulent Boundary Layer. Turbulent Currents), Moscow, Nauka, 1974.

4. Saffman, P. G., "The Effect of Wind Shear on Horizontal Spread from an Instantaneous Ground Source," QUART. J. ROY. METEOROL. SOC., Vol 88, No 378, 1962.

5. Wipperman, F. K., "The Planetary Boundary Layer of the Atmosphere," DEUTSCHER WETTERDIENST. OFFENBACH a. M., 1973.

6. Wipperman, F. K., "Eddy Diffusion Coefficients in the Planetary Boundary Layer," ADVANCES IN GEOPHYSICS, Vol 18a, Academic Press, 1974.

UDC 614.71:551.510.42(261/264)

CONTAMINATION OF THE ATMOSPHERIC SURFACE LAYER OVER THE ATLANTIC OCEAN BY BENZ(A)PYRENE

Moscow METEOROLOGIYA I GIDROLOGIYA in Russian No 4, Apr 80 pp 66-72

[Article by Candidate of Geographical Sciences A. I. Osadchiy, Candidates of Physical and Mathematical Sciences A. I. Shilina and S. G. Malakhov, Institute of Experimental Meteorology, submitted for publication 1 August 1979]

Abstract: An experimental evaluation of the latitudinal distribution of benz(a)pyrene is presented. A decrease in the concentration of benz(a)pyrene in atmospheric air toward the equator to 10^{-3}-10^{-4} ng/m^3 was discovered. In the region of the temperate and subtropical latitudes the relative coefficient of enrichment of lead and the relative concentration of benz(a)pyrene (relative to the value near the ICZ) were close in value, which can be evidence of the presence of a common source of their emission.

[Text] Benz(a)pyrene (BP) is of particular interest among the anthropogenic atmospheric pollutants. It is a by-product of many types of human activity. BP enters both into the lower layers of the atmosphere (surface layer) and into the higher layers (middle and upper troposphere, lower stratosphere). As a result of persistence the BP in the form of passive aerosols can be transported for many thousands of kilometers from the site of entry into the atmosphere. Facts concerning the transport of BP over great distances are given in [5]. There is every basis for assuming that BP is propagated globally.

In this connection it is of considerable interest to estimate the BP concentration in the atmosphere of the least contaminated regions on the earth -- over the ocean in the northern and southern hemispheres and also in the Antarctic region, where the BP sources are considerably less than in the northern hemisphere. The levels of concentration of BP obtained

in this way could characterize the present-day global background of contamination in the atmospheric surface layer. The paper gives the results of measurement of the aerosol component of BP in the near-water air layer over the Atlantic Ocean in the latitude range 57°N-74°S, and also in the region of the Antarctic coast between 52°W and 46°E. The observations were made during the work of the 22d Soviet Antarctic Expedition from aboard the steamer "Estoniya" during the period from 25 January through 7 April 1977.

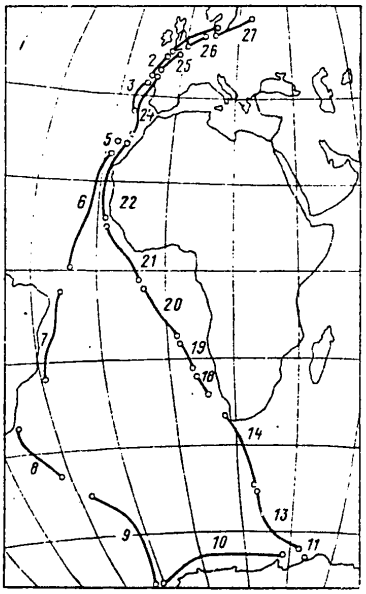

Fig. 1. Sketch map of sampling sites.

The sampling was carried out from the deck of the steamer at a height of about 15 m above the sea level using a FVU apparatus of the centrifugal type using FPP-15 filters with a rate of air throughput of about 200 m^3/hour. The duration of the sampling varied from 10 hours to several days [2]. The air sampling was accomplished under conditions precluding the possibility of their contamination by shipboard effluent. During the sampling, on the basis of an analysis of synoptic weather charts and the pressure pattern charts, regularly received aboard the ship, an allowance was made for the synoptic situation and the nature of the transport of air masses for the purpose of obtaining samples representative for definite circulatory conditions in this region of the ocean. A quantitative determination of BP was made by the method of quasilinear luminescence spectra

using the Shpol'skiy effect [4]. The filters with the samples were subjected to extraction using purified n-hexane in air-flow columns with a rate of outflow of the extract 0.2 ml/min. The extract was frozen at the temperature of the liquid nitrogen (-196°C) and irradiated by a flux of UV radiation with a wavelength of 365 nm. The intensity of the analytical BP quasiline with a wavelength λ = 402.4 nm was measured using an FEP-1 photoelectric attachment for an ISP-51 spectrograph.

Table 1

Benz(a)pyrene Concentration in Different Regions of Atlantic Ocean

Проба 1	Дата 2	3 Координаты участка отбора проб: 4 начало — широта 5	4 начало — долгота 6	конец 7 — широта 5	конец 7 — долгота 6	Концентрация бенз(а)пирена, нг/м³ 8
1	27 I	57°46′ с 9	40°45′ в 10	51°42′ с	02°22′ в	0,12
2	28	51 42	02 22	43 02	09°23′ в	0,15
3	30	41 34	10 15	37 40	12 04	0,01
4	02 II	13 Санта-Крус де Тенериф				0,01
5	02	27°44′ с	16°37′ з	27°44′ с	16°37′ в	0,003
6	03	27 40	16 35 12	01 10	28 30	0,0004
7	08	05 10	31 00	23°00′ ю	39 00	0,0003
8	14	34 05	52 30	47 02	42 16	0,0003
9	20	51 30	36 00	74 46	26 50	0,0002
10	26	74 00	25 00	67 37	36°18′ в	0,0003
11	04 III	67 00	45°30′ в	67 40	45 50	0,0006
13	07	67 00	44 00	50 00	26 00	0,0005
14	10	50 00	26 00	34 30	18 10	0,0004
18	16	28°30′ ю	13 24	26 10	11 40	0,005
19	17	26 10 11	11 40	18 30	05 10	0,003
20	18	18 30	05 10	06 35	04°42′ з	0,001
21	21	04 45	06°15′ з	11°00′ с	11 30	0,0005
22	24	11°10′ с	17 30	27 44	16 30	0,002
23	28	13 Санта-Крус де Тенериф				0,17
24	29	28°30′ с	16°00′ з	44°00′ с	09°00′ з	0,002
25	01 IV	46 15	07 00	51 30	00°03′ в	0,001
26	03	51 30	00 05	57 15	08 30	0,15
27	04	57 15	08 30	57 50	22 40	0,04

KEY:

1. Sample
2. Date
3. Coordinates of sampling sector
4. Beginning
5. Latitude
6. Longitude
7. End
8. BP concentration, ng/m^3
9. N
10. E
11. S
12. W
13. Santa Cruz de Tenerife

The limit of BP detection is $1 \cdot 10^{-9}$ mol/liter and the reproducibility of the analytical results was ±15%.

Figure 1 shows the track of the steamer "Estoniya" during the voyage as part of the 22d Soviet Antarctic Expedition. Data on atmospheric contamination by BP along the ship's track and in some ports are given in Table 1. The atmospheric contamination by BP is maximum in ports -- 0.06-0.6 ng/m^3 (Table 1). Fluctuations of the BP concentrations in the near-water air layer in ports are very great and evidently are determined primarily by the wind direction and weather conditions. The data in Table 1 make it possible to estimate the BP concentration in the principal climatic zones of the Atlantic Ocean (except for the polar regions of the northern hemisphere).

Table 2 gives the mean and extremal BP concentrations in the principal climatic zones of the Atlantic Ocean. Table 2 indicates that the highest BP concentrations are observed in the temperate latitudes of the northern hemisphere, in the English Channel, Strait of Dover, in the Baltic and North Seas. The lowest BP concentrations are observed in the western regions of the Atlantic Ocean in the temperate latitudes of the southern hemisphere.

Figure 2 shows the latitudinal variation of the concentrations of benz(a)-pyrene in the near-water air layer over the Atlantic Ocean. The solid curve represents measurements on the route to Antarctica; the dashed curve represents measurements during the return of the ship. The gaps correspond to measurements made in ports (see Table 1) or sectors of the track on which samples were not taken. Figure 2 shows that in the northern hemisphere the general variation of change in the concentrations of BP in the near-water layer of the atmosphere over the Atlantic Ocean was retained during movement of the steamer to Antarctica and back. In the northern hemisphere the BP concentrations decrease relatively rapidly from north to south to the meteorological equator (ICZ).

In the southern hemisphere in the western regions of the Atlantic Ocean the BP concentrations decrease with an increase in latitude. In the eastern regions of the Atlantic Ocean the BP concentrations are substantially higher than in the western regions, evidently due to the stronger influence of the continent, caused by the peculiarities of atmospheric circulation in these regions and the heavier shipping than in the western regions. In the latitude region 0-30° in the eastern regions of the Atlantic Ocean in the southern hemisphere the BP concentrations are equal to or are somewhat greater than the BP concentrations in the northern hemisphere in this same latitude range. Along the shores of Antarctica there is an increase in the BP concentrations in comparison with the BP concentrations in the temperate and subantarctic latitudes of the southern hemisphere.

An interesting peculiarity of the distribution of BP concentrations over the Atlantic Ocean is that within the limits of one and the same regions in the temperate and subtropical latitudes of the northern hemisphere

Table 2

Mean and Extremal Benz(a)pyrene Concentration in Near-Water Atmospheric Layer Over Atlantic Ocean in Principal Climatic Regions, ng/m^3

Полушарие	Район наблюдений	3 Районы Атлантического океана						6 В среднем в обоих районах		
		4 Западный			5 Восточный					
		среднее значение	число измерений	диапазон изменений	среднее значение	число измерений	диапазон изменений	значение	число измерений	диапазон изменений
1	2	7	8	9	7	8	9	10	8	9
11 Северное	12 Северное, Балтийское моря и проливы				0,12	4	$(4 \div 15) \cdot 10^{-2}$	0,12	4	$(4 \div 15) \cdot 10^{-2}$
	13 Умеренные и субтропические широты				$4{,}5 \cdot 10^{-3}$	3	$(2 \div 10) \cdot 10^{-3}$	$4{,}5 \cdot 10^{-3}$	3	$(2 \div 10) \cdot 10^{-3}$
	14 Пассатная зона				$1{,}8 \cdot 10^{-3}$	3	$(4 \div 30) \cdot 10^{-4}$	$1{,}8 \cdot 10^{-3}$	3	$(4 \div 30) \cdot 10^{-4}$
	15 Внутритропическая зона конвергенции и экваториальная зона				$5 \cdot 10^{-4}$	1	—	$5 \cdot 10^{-4}$	1	—
16 Южное	14 Пассатная зона	$3 \cdot 10^{-4}$	1	—	$1 \cdot 10^{-3}$	1	—	$6{,}5 \cdot 10^{-4}$	2	$(3 \div 10) \cdot 10^{-4}$
	13 Умеренные и субтропические широты	$2{,}5 \cdot 10^{-4}$	2	$(2 \div 3) \cdot 10^{-4}$	$4{,}5 \cdot 10^{-4}$	2	$(4 \div 5) \cdot 10^{-4}$	$3{,}5 \cdot 10^{-4}$	4	$(2 \div 5) \cdot 10^{-4}$
	17 Субантарктические и антарктические широты	$3 \cdot 10^{-4}$	1	—	$6 \cdot 10^{-4}$	1	—	$4{,}5 \cdot 10^{-4}$	2	$(3 \div 6) \cdot 10^{-4}$
	18 р-н Африканского побережья (субтропические широты)				$4 \cdot 10^{-3}$		$(3 \div 5) \cdot 10^{-3}$	$4 \cdot 10^{-3}$	2	$(3 \div 5) \cdot 10^{-3}$

KEY TO TABLE 2

1. Hemisphere
2. Observation region
3. Atlantic Ocean region
4. Western
5. Eastern
6. Average in both regions
7. Mean value
8. Number of measurements
9. Range of changes
10. Value
11. Northern
12. North Sea, Baltic Sea, straits
13. Temperate and subtropical latitudes
14. Trades zone
15. ICZ and equatorial zone
16. Southern
17. Subantarctic and Antarctic latitudes
18. African coast region (subtropical latitudes)

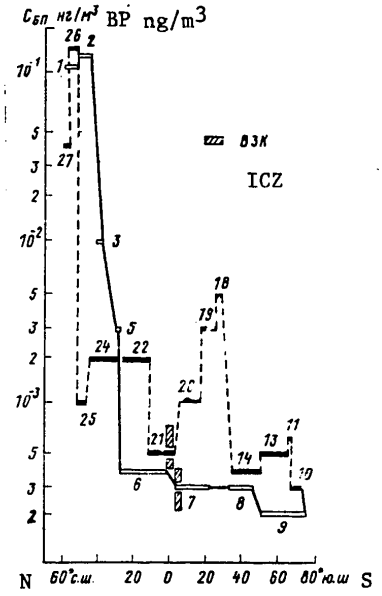

Fig. 2. Distribution of concentrations of benz(a)pyrene (BP) over Atlantic Ocean by latitude. The figures on the graph correspond to the numbers of samples.

the BP concentrations can vary substantially (the differences between the minimum and maximum values attain two orders of magnitude). In the tropical and equatorial regions the changes in BP concentration are considerably less. For the purpose of clarifying the reasons for such considerable variations in BP concentrations in the temperate and subtropical latitudes of the northern hemisphere in these regions of the Atlantic Ocean we analyzed the conditions for the transport of air masses at the level of the 700-mb isobaric surface, describing the distant transport of a passive atmospheric impurity in the lower troposphere.

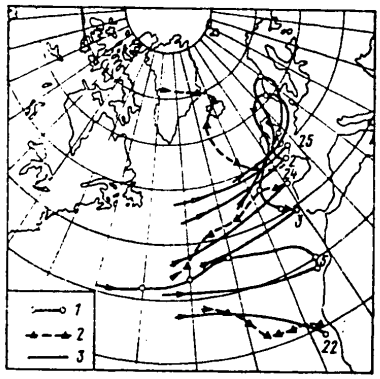

Fig. 3. Reverse trajectories of air masses, drawn from sampling sites. 1) on route to Antarctica, 2) with movement in opposite direction, 3) long-term mean monthly trajectories of transport of air masses. The figures correspond to the numbers of the samples in Table 1.

Figure 3 gives the trajectories of movement of air masses at the 700-mb level corresponding to the middle of the period of sampling (due to the fact that when taking samples an allowance was made for the synoptic situation and the nature of the transport of air masses the trajectory is representative for the entire sampling period) and also the long-term mean trajectories of movement of air masses within the limits of this region, constructed on the basis of the data in [1]. An analysis of the nature of the transport of air masses makes it possible to note that the maximum BP concentrations in air samples were observed during the transport of air masses from the territory of Europe (samples Nos 2, 3). These concentrations were close to the BP concentrations in cities [5]. The relatively low BP concentrations were observed in the case of transport of air masses from the subtropical and temperate latitudes of the western and arctic regions of the Atlantic Ocean (samples Nos 5, 22, 24, 25).

An analysis of the trajectories of air masses during the sampling period and the mean long-term (climatic) trajectories of transport of air masses make it possible without a great volume of observational statistics to

obtain some idea concerning the background BP concentrations in these regions of the Atlantic Ocean under typical conditions of atmospheric circulation by means of exclusion of the data obtained under anomalous conditions of transport of air masses. Figure 3 shows that samples Nos 5, 22 and 24 are representative samples, reflecting the background concentrations of BP in the near-water air layer over the Atlantic Ocean in the temperate and subtropical latitudes of the northern hemisphere. Thus, the background concentration of BP in the eastern regions of the Atlantic Ocean in the region of the temperate and subtropical latitudes of the northern hemisphere can be assumed equal to 0.002 ng/m^3.

Also of considerable interest is the increase in BP concentrations along the shores of Antarctica in comparison with its concentrations in the temperate and subantarctic latitudes of the southern hemisphere. A similar effect was registered earlier along the shores of Antarctica in an investigation of the concentrations of global radioactive products of nuclear explosions in the surface air layer. The increase in the concentrations of global radioactive products of nuclear explosions in the region of the coast of Antarctica is attributable to the presence in this region of intensive vertical transport of air masses from the upper troposphere (lower stratosphere) into the lower layers [3]. This makes it possible to postulate that in the process of transport of global aerosols of benz(a)pyrene into the Antarctic region a factor which can be of substantial importance is the transport of air masses containing BP in the upper layers of the troposphere (possibly also in the stratosphere) and their subsequent subsidence into the lower layers in the region of the Antarctic coast. Observational data on the concentration of BP in the interior regions of Antarctica and an increase in statistics of measurements of the BP concentration in the temperate and subantarctic latitudes of the southern hemisphere will assist in the final solution of this problem.

Table 3

Distribution of the Relative Concentrations of BP and the Coefficient of Lead Enrichment in the Near-Water Layers of the Atmosphere in the Eastern Regions of the Atlantic Ocean in the Principal Climatic Zones of the Northern and Southern Hemispheres

Hemisphere	Observation region	BP	Lead
Northern	North Sea, Baltic Sea and straits	230.0	--
	Temperate and subtropical latitudes	8.0	7.9
	Trades zone	3.6	1.2
	Equatorial zone and ICZ	1	1
Southern	Trades zone	2.0	2.3
	Region of African coast (subtropical latitudes)	8.0	5.6

In connection with the increased BP concentrations in the near-water layer of the atmosphere in the neighborhood of the African coast of the Atlantic Ocean it is of interest to compare them with measurement data for lead in this region, cited in [6]. It is desirable to examine the relative (for example, in relation to the content in the air masses of the ICZ) BP concentrations and coefficients of lead enrichment which we computed on the basis of the data in [6] in different climatic regions of the Eastern Atlantic (Table 3).

Table 3 gives the relative (in relation to the concentration in the ICZ) BP concentrations and the lead enrichment coefficients in the regions of the temperate and subtropical latitudes (regions of westerly transport) and the Northeast Trades of the northern hemisphere, and also the Trades zone of the southern hemisphere.

Table 3 shows that the relationships between the BP concentrations and the coefficients of enrichment of atmospheric aerosols with lead in these regions are rather close, as a result of which it can be postulated that the BP and the lead in the near-water layer of the atmosphere in these regions have a common source of origin.

Conclusions

1. In the Atlantic Ocean it is the near-water layers of the atmosphere in the temperate and subtropical latitudes of the northern hemisphere and the eastern regions of the southern hemisphere which are most contaminated with BP.

2. The BP concentration in the near-water layer of the atmosphere in the northern hemisphere in the Atlantic Ocean region increases with an increase in latitude, whereas in the southern hemisphere there is a decrease. Along the shores of Antarctica the BP concentration is higher than in the temperate and subantarctic latitudes of the southern hemisphere.

3. The BP concentration in the near-water air layer in aerosol form in the most remote clean regions of the Atlantic Ocean is 10^{-3}-10^{-4} ng/m^3.

BIBLIOGRAPHY

1. ATLAS KLIMATICHESKIKH KHARAKTERISTIK TEMPERATURY, PLOTNOSTI I DAVLENIYA VOZDUKHA I GEOPOTENTSIALA V TROPOSFERE I NIZHNEY STRATOSFERE SEVERNOGO POLUSHARIYA (Atlas of Climatic Characteristics of Air Temperature, Density and Pressure and Geopotential in the Troposphere and Lower Stratosphere of the Northern Hemisphere), No 4, Moscow, Gidrometeoizdat, 1974.

2. Davydov, Ye. M., Malakhov, S. G., Makhon'ko, K. P., Mashkov, F. T., "Filtering Apparatus for Determining the Concentration of Radioactive Dust in the Atmospheric Surface Layer," TRUDY IEM (Transactions of the Institute of Experimental Meteorology), No 2, 1970.

3. Zhukov, V. A., "Radioactive Contamination of Surface Air Over the Antarctic Continent," METEOROLOGIYA I GIDROLOGIYA (Meteorology and Hydrology), No 11, 1976.

4. Teplitskaya, T. A., KVAZILINEYCHATYYE SPEKTRY LYUMINESTSENTSII KAK METOD ISSLEDOVANIYA SLOZHNYKH PRIRODNYKH ORGANICHESKIKH SMESEY (Quasilinear Luminescence Spectra as a Method for Investigating Complex Natural Organic Mixtures), Moscow, Izd-vo MGU, 1971.

5. Shabad, L. M., O TSIRKULYATSII KANTSEROGENOV V OKRUZHAYUSHCHEY SREDE (Circulation of Carcinogens in the Environment), Moscow, Meditsina, 1973.

6. Chester, R., Stoner, Y. H., "Pb in Particulates from the Lower Atmosphere of the Eastern Atlantic," NATURE, Vol 2815, 1973.

UDC 551.464(260)(100)

COMPUTATION OF CONTAMINATION OF SURFACE WATERS OF SOME REGIONS IN THE WORLD OCEAN BY THE ATMOSPHERIC FALLOUT OF STRONTIUM-90

Moscow METEOROLOGIYA I GIDROLOGIYA in Russian No 4, Apr 80 pp 73-78

[Article by Candidate of Physical and Mathematical Sciences K. P. Makhon'-ko, Institute of Experimental Meteorology, submitted for publication 3 July 1979]

Abstract: The author examines anticyclonic subtropical macrocirculatory systems in the South Atlantic, southern part of the Indian Ocean and northern part of the Pacific Ocean, within which the advection of water masses is difficult and in the first approximation can be neglected. The concentration of Sr^{90} in the surface waters is computed for the period 1954-1978 in its temporal variation on the basis of the fallout of this isotope from the atmosphere onto the underlying surface and with allowance for its penetration into the deeper layers of the ocean. A satisfactory agreement of the results of computations and observational data is observed.

[Text] The author of [9] computed the contamination of the surface waters of the North Atlantic by Sr^{90} in the region of an anticyclonic subtropical macrocirculatory system within which the convection of water masses is difficult and in the first approximation can be neglected. In the computations this made it possible to take into account only the fallout of Sr^{90} from the atmosphere onto the ocean surface.

Computations of the concentration of the isotope in the quasihomogeneous surface layer of the ocean with the thickness h were made in [9] by a numerical method using the formula

$$C = e^{-\Lambda' t} \int_0^t \frac{P(\theta)}{h} e^{\Lambda' \theta} d\theta, \quad (1)$$

where P(t) is the fallout of the isotope from the atmosphere, t is time, $\Lambda' = \Lambda + \lambda$ is the sum of the constant of removal of the isotope from the quasihomogeneous layer into the depths of the ocean and the constant of radioactive decay.

It is interesting to attempt to carry out similar computations of contamination of the surface waters with Sr^{90} for other similar regions in the oceans. As is well known, in the world ocean there are a whole series of macrocirculatory systems, the most powerful of which are five anticyclonic subtropical circulations in the North and South Atlantic, in the northern part of the Pacific Ocean and in the southern parts of the Pacific and Indian Oceans [17]. In the Atlantic and Pacific Oceans the southerly anticyclonic systems are characterized by a lesser intensity of circulation of waters than in the northern hemisphere. In the southern part of the Pacific Ocean the general pattern of circulation is not expressed so clearly. In the northern part of the Indian Ocean the circulation of waters in general is characterized by a greater complexity and seasonal variability as a result of monsoonal shifting of the winds and the high degree of disruption of the ocean by land mass. Accordingly, we will limit ourselves to an examination of contamination of the surface waters only in the southern parts of the Atlantic and Indian Oceans and in the northern part of the Pacific Ocean, where it is possible to discriminate regions within which the advection of radioactive water masses in the first approximation can be neglected and it can be assumed that the contamination of waters was caused only by radioactive fallout from the atmosphere.

South Atlantic. A southerly subtropical anticyclonic circulation is formed by the Bengal Current on the northeastern periphery, the Brazilian Current on the west and the Circular Antarctic Current on the south. Despite the fact that it, in turn, is subdivided into quasistationary eddies having dimensions an order of magnitude less, the general macroscale circulation is expressed quite clearly. Its period is approximately three years, which is more than two times greater than the period of circulation in the North Atlantic; the exchange of surface waters across the equator is difficult. All this makes it possible to discriminate in the South Atlantic a region having a closed circulation of water masses approximately limited by the coordinates 5-40°S, 10°E-35°W, within which the advection of Sr^{90} with ocean waters from other regions with a certain degree of approximation can be neglected [1, 10, 11, 18].

Then the Sr^{90} concentration in the surface waters of this region in the ocean will be determined by the entry of the isotope from the atmosphere onto the ocean surface P(t) and the simultaneously transpiring process of its outflow into the deeper water layers [9]. The data in [24, 25] will be used in determining the P(t) values in the considered latitude zone necessary for computations using formula (1). Figure 1a shows the pattern of temporal change of fallout of Sr^{90} from the atmosphere; Fig. 1b shows the concentration of this isotope in the surface waters of this region of the Atlantic, computed using formula (1), for a mean thickness of the quasihomogeneous layer h = 40 m and $\lambda' = 0.3\ g^{-1}$, which corresponds to a residence time of Sr^{90} in the quasihomogeneous layer $\tau = 1/\lambda$ = 3.6 years. The dots represent measurements of the Sr^{90} concentration in the surface waters of this region of the ocean, cited in systematized

form in monograph [10] and supplemented by the results in [5]. The vertical lines represent the values of the mean square scatter of data and the figures over the dots correspond to the number of observations entering into the averaging. The λ' value was selected in such a way as to obtain the best correspondence between the experimental data and the computed curve.

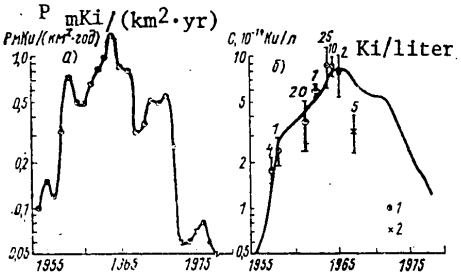

Fig. 1. Temporal change in the fallout of Sr^{90} from the atmosphere in the latitude zone 5-40°S (a) and its concentration in the surface layer of the ocean within the zone of the subtropical anticyclonic circulation of the South Atlantic (b). 1) [10]; 2) [5].

Unfortunately, the number of observations of the Sr^{90} concentration in the waters of the South Atlantic is substantially less than in the northern hemisphere, which makes the estimate of residence time of Sr^{90} in the quasihomogeneous layer τ = 3.6 years less reliable. Nevertheless, we can note the satisfactory agreement of the shape of the computed curve with observational data and draw a qualitative conclusion concerning the lesser intensity of the vertical exchange of water masses in the southern part of the Atlantic than in the northern part.

Indian Ocean. The southerly subtropical anticyclonic circulation is formed in the north by the Southern Equatorial Current which passes along 10°S from the Sunda Archipelago to the shores of Africa, on the west by the Madagascar Current, on the south by the South Indian Ocean Current; the eastern boundary of the circulation is the West Australian Current. Within the limits of this macrocirculatory system there is a series of anticyclonic circulations formed by the southern periphery of the South Equatorial Current. The surface homogeneous layer in the entire central part of the ocean is about 30 m. The transport of waters from the Pacific Ocean into the Indian Ocean through the Indonesian seas is $2.12 \cdot 10^3$ m^3/sec, which is negligible. The existence of a closed circulation makes it possible to discriminate a region of the ocean approximately bounded by the coordinates 20-40°S, 50-110°E within which in the first approximation it is possible to neglect the advection of water masses [8, 22].

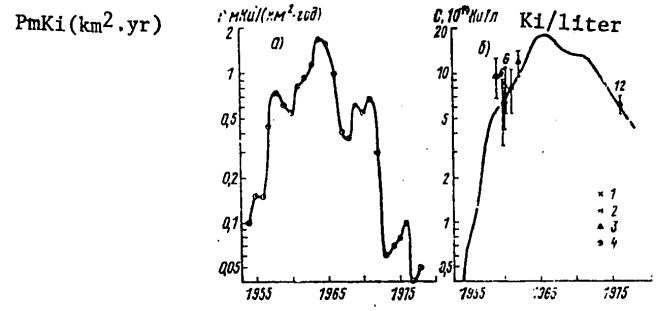

Fig. 2. Temporal change in fallout of Sr^{90} from atmosphere in latitude zone 20-40°S (a) and its concentration in the surface layer of the ocean within the zone of the southerly subtropical anticyclonic circulation of the Indian Ocean (b). 1) [13, 14], 2) [26], 3) [30], 4) [16].

With respect to radiation conditions, the southern part of the Indian Ocean is one of the least investigated regions of the world ocean. The extreme scantiness of observational data on the concentrations of long-lived isotopes in the waters of this ocean makes it possible to draw only qualitative conclusions concerning the patterns of their behavior. Earlier, on the basis of measurements of the Sr^{90} concentrations in the equatorial part of the Indian Ocean the conclusion was drawn that there is an anomalously high reserve of this isotope. It was postulated that the rate of self-purification of the surface waters does not differ from that in other regions of the world ocean. The transport of more radioactive waters from the Pacific Ocean is too small to change the general pattern of contamination in the Indian Ocean [12]. It was therefore postulated that this effect was caused by the maximum of annual precipitation in the equatorial zone [14] or the fallout of the products of nuclear explosions transported in the troposphere from the Pacific Ocean region [12]. However, the trajectories of radioactive masses propagating from explosions in the Pacific Ocean over the Indian Ocean lie for the most part to the north of the equator with a deflection onto the Arabian Peninsula [29], that is, in the direction away from the region of interest to us.

We will demonstrate that the radioactive contamination of the surface waters in the considered region of the Indian Ocean can be attributed only to the radioactive fallout onto its surface.

For the computations we will use data [24, 25] on the fallout of Sr^{90} from the atmosphere in 1954-1978. Figure 2a shows the pattern of temporal change in the fallout of this isotope in the latitude zone 20-40°S, and in Fig. 2b, the concentration of Sr^{90} in the surface waters of the considered region of the Indian Ocean, computed using formula (1), with $\lambda' = 0.2$ year^{-1} -- corresponding to $\tau = 1/\lambda = 5.7$ years. The determined residence time for

Sr^{90} in the surface waters of the southerly subtropical anticyclonic circulation in the Indian Ocean is entirely realistic with respect to order of magnitude. It is true that the extremely limited number of observations of the Sr^{90} concentration in this region of the ocean forces us to use the results with great caution and regard the conclusion about a lesser rate of vertical exchange in comparison with similar regions in the Atlantic as only purely qualitative. Data from observations of the Sr^{90} concentration in the waters of the considered region are cited in [13, 14, 16]; reference [26] gives data on the concentration of Cs^{137} which we recomputed into the Sr^{90} concentration taking into account the Cs^{137}/Sr^{90} = 1.6 ratio obtained in [26] on the basis of a great volume of statistical data for the Pacific Ocean. This exhausts the observational data for the particular region and therefore for orientation Fig. 2b also gives observational data on the Sr^{90} concentrations in the entire latitude zone 20-40° S in the Indian Ocean. Figure 2b shows that these data do not contradict the determined general picture of contamination of surface waters in the considered region of the ocean by Sr^{90}. It follows from this that the role of advection of Sr^{90} in this latitude zone of the Indian Ocean in general is small.

Pacific Ocean. In the northern part of the Pacific Ocean the surface circulation of waters in general does not change from season to season and from year to year. The subtropical anticyclonic circulation is formed in the southern part by the North Trades Current, in the west — by the Kuroshio Current, a continuation of a branch of which is the North Pacific Ocean Current, running to the east and on its path sending branches to the south. The most continuous is the circulation zone bounded approximately by the coordinates 20-35°N and 140-180°E (without the northwestern corner) [2, 3, 32]. The depth of the upper quasihomogeneous layer of the ocean in this region averages 60 m [23].

A peculiarity of the Pacific Ocean is the presence of intensive local sources of radioactive contamination of waters: for the most part polygons for the testing of nuclear weapons and also the dumping of the wastes of atomic industry, the sites of their burial, etc. [6, 7, 27]. As indicated by estimates [6], about 70% of the reserve of Sr^{90} in the waters of the Pacific Ocean as of 1961 must be attributed to the direct introduction of this isotope into ocean waters directly at the site of nuclear shots and in the form of local fallout from the atmosphere. However, the slowness and the spatial nonuniformity of processes of mixing and circulation of waters in the ocean do not make it possible to evaluate the contribution of local contaminations to the total contamination of waters in individual regions of the Pacific Ocean. Accordingly, it is already impossible to apply the computation scheme employed above to the region which we investigated: on the basis of data from observations of the Sr^{90} concentration in the surface waters using formula (1) find Λ', and then, on the basis of the fallout P(t), restore the pattern of changes in concentration during the years when there were no observations.

In such a situation it remains only to attempt to estimate the λ' value, proceeding on the basis of indirect data.

We will assume that vertical water exchange in the considered region of the Pacific Ocean is similar to the water exchange in the similarly situated region of the Atlantic. Then in the region as the exchange constant we use the value found in [9] for the anticyclonic circulation in the North Atlantic $\lambda' = 0.5$ yr^{-1}. Since the water exchange in the subtropical anticyclonic circulation must evidently be somewhat more intensive than in the tropical zone, this value does not contradict the value $\lambda' = 0.4$ yr^{-1} ($\tau = 1/\lambda = 2.7$ yr), found in [31] for the equatorial abyssal region near Bikini atoll on the basis of measurements of the Pb^{210} concentration.

Figure 3a shows the fallout of Sr^{90} from the atmosphere in the region 20-35°N [24, 25], whereas Fig. 3b, with a solid curve, shows the temporal change in the concentration of Sr^{90} in the surface waters of the considered region of the Pacific Ocean, computed using formula (1) for the value $\lambda' = 0.5$ yr^{-1}, corresponding to $\tau = 2.1$ years. The dashed curves in this same figure represent the concentrations computed for values $\lambda' = 0.3$ and 0.7 yr^{-1} ($\tau = 3.6$ and 1.5 years), which we feel are still realistic, but less probable. This same figure shows data from observations [5, 15, 19-21] of the concentration of Sr^{90} in the surface waters of the considered region and data [26, 28] which we computed on the basis of the observed Cs^{137} concentrations. Unfortunately, all the observational results relate only to two short time intervals: 1961-1962 and 1965-1968, and therefore the data have been supplemented by information for 1974 on the Sr^{90} concentration in another region of the ocean situated nearby with the coordinates 20-28°N and 150°E-160°W [4].

Figure 3b shows that the solid curve ($\lambda' = 0.5$ yr^{-1}) coincides with the minimum values of the Sr^{90} concentration observed in the described region. Most of the points on the graph fall above this computed curve. This may be related to the presence of a slow exchange of water masses between the inner part of the anticyclonic circulation and the outer part of the ocean area, whose waters were subjected to the effect of local contamination sources. The upper dashed curve ($\lambda' = 0.3$ yr^{-1}) in general coincides quite well with the experimental points. Thus, within the framework of available observational data with a residence time of Sr^{90} in the surface waters of $\tau = 3.6$ years there is no need for using the hypothesis of the existence of an appreciable water exchange between the inner part of the ring of circulation of waters and the outer ocean area for explaining the real picture of ocean contamination.

However, as time passes, the gradual quasidiffusional evening-out of the Sr^{90} concentrations in the entire ocean should nevertheless come about, which in subsequent years leads to a deflection of the computed curve downward from the observational data. In this case the curve computed using data on the global fallout of Sr^{90} can be regarded as the lower limit of the possible concentrations of this isotope in the surface waters of the ocean.

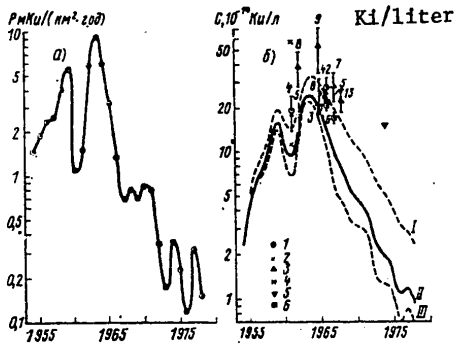

Fig. 3. Temporal change of fallout of Sr^{90} from atmosphere in the latitude zone 20-35°N (a) and its concentration in the surface layer of the ocean within a northerly subtropical anticyclonic circulation in the Pacific Ocean (b). I) $\lambda' = 0.3$ year^{-1}, II) $\lambda' = 0.5$ year^{-1}, III) $\lambda' = 0.7$ year^{-1}; 1) [28], 2) [15], 3) [19-21], 4) [5], 5) [4], 6) [28].

What has been said applies to an equal degree to the other oceans as well. The difference between observational data and the computed curve in principle will make it possible to evaluate the role of such quasi-diffusion in the dynamics of contamination of waters in the considered regions of the world ocean.

BIBLIOGRAPHY

1. Bulatov, R. P., Barash, M. S., Ivanenkov, V. N., Marti, Yu. Yu., ATLANTICHESKIY OKEAN (Atlantic Ocean), Moscow, Mysl', 1977.

2. Burkov, V. A., OBSHCHAYA TSIRKULYATSIYA VOD TIKHOGO OKEANA (General Circulation of Waters in the Pacific Ocean), Moscow, Nauka, 1972.

3. Burkov, V. A., "Structure of Currents in the Pacific Ocean and Their Nomenclature," OKEANOLOGIYA (Oceanology), Vol 4, No 1, 1966.

4. Vakulovskiy, S. M., Vorontsov, A. I., Katrich, I. Yu., Koloskov, I. A., Roslyy, Ye. I., Chumichev, V. V., "Sr^{90} and Tritium in the Surface Waters of the Northern Part of the Pacific Ocean in 1974," OKEANOLOGIYA, Vol 18, No 2, 1978.

5. Vdovenko, V. M., Kolesnikov, A. G., Spitsyn, V. I., Vernovskaya, R. N., Gedeonov, L. I., Gromov, V. V., Ivanova, L. M., Nelepo, B. A., Tikhomirov, V. N., Trusov, A. G., "Radioactivity of Waters of the World Ocean and Behavior of Some Fission Products in the Ocean," ATOMNAYA ENERGIYA (Atomic Energy), Vol 31, No 4, 1971.

6. Zudin, O. S., Nelepo, B. A., STATISTICHESKIY ANALIZ INFORMATSII O RADIOAKTIVNOM ZAGRYAZNENII OKEANA (Statistical Analysis of Information on Radioactive Contamination of the Ocean), Leningrad, Gidrometeoizdat, 1975.

7. Zudin, O. S., Nelepo, B. A., Spiring, A. N., Trusov, A. G., "Distribution of the Cs Concentration in the Surface Waters of the Pacific Ocean," ATOMNAYA ENERGIYA, Vol 32, No 4, 1972.

8. Kort, V. G., "Water Exchange Between the Oceans," OKEANOLOGIYA, Vol 2, No 4, 1962.

9. Makhon'ko, K. P., "Computation of the Contamination of Surface Waters in the Central Region of the North Atlantic by Atmospheric Fallout of Sr^{90}," METEOROLOGIYA I GIDROLOGIYA, No 3, 1979.

10. Nelepo, B. A., YADERNAYA GIDROFIZIKA (Nuclear Hydrophysics), Moscow, Atomizdat, 1970.

11. Ozmidov, R. V., Popov, N. I., "Some Data on the Propagation of Soluble Impurities in the Ocean" (Disposal of Radioactive Wastes into Seas, Oceans and Surface Waters) PROC. SYMP. IAEA, Vienna, 16-20 May 1966, IAEA, Vienna, 1966.

12. Patin, S. A., "Regional Distribution of Sr^{90} at the Surface of the World Ocean," OKEANOLOGIYA, Vol 5, No 3, 1965.

13. Popov, N. I., Orlov, V. M., Patin, S. A., "Sr^{90} in the Deep Waters of the Indian Ocean," TRUDY INSTITUTA OKEANOLOGIYA (Transactions of the Institute of Oceanology), Vol 82, 1966.

14. Popov, N. I., Orlov, V. M., Patin, S. A., Ushakova, N. P., "Sr^{90} in the Surface Waters of the Indian Ocean in 1960-1961," OKEANOLOGIYA, Vol 4, No 3, 1964.

15. Popov, N. I., Patin, S. A., Polevoy, R. I., Konnov, V. A., "Sr^{90} in the Waters of the Pacific Ocean. Communication 2: Surface Waters of the Central Region, 1961," OKEANOLOGIYA, Vol 4, No 6, 1964.

16. Petrov, A. A., Ovchinnikova, S. S., Komagurov, V. Ye., "Present-Day Radioactive Contamination of Sea Waters by Sr^{90} and Cs^{137}," TRUDY VNIRO (Transactions of the All-Union Scientific Research Institute of Fishing and Oceanography), Vol 117, 1978.

17. Stepanov, V. N., MIROVOY OKEAN. DINAMIKA I SVOYSTVA VOD (The World Ocean. Dynamics and Properties of Waters), Moscow, Znaniye, 1974.

18. FIZIKA OKEANA. T. 1. GIDROFIZIKA OKEANA (Physics of the Ocean. Vol 1. Hydrophysics of the Ocean), edited by V. M. Kamenkovich, A. S. Monin, Moscow, Nauka, 1978.

19. Chumichev, V. B., "Sr^{90} Content in the Waters of the Pacific Ocean in 1962 and 1964," TRUDY INSTITUTA OKEANOLOGII, Vol 82, 1966.

20. Chumichev, V. B., "Sr^{90} in Waters of the Northwestern Part of the Pacific Ocean During 1966-1978," TRUDY IEM (Transactions of the Institute of Experimental Meteorology), No 1(32), 1972.

21. Chumichev, V. V., "Sr^{90} in Pacific Ocean Waters During 1964-1966," TRUDY IEM, No 3(42), 1974.

22. Shcherbinin, A. D., STRUKTURA I TSIRKULYATSIYA VOD INDIYSKOGO OKEANA (Structure and Circulation of Waters in the Indian Ocean), Leningrad, Gidrometeoizdat, 1976.

23. Bathen, K. H., "On the Seasonal Changes in the Depth of the Mixed Layer in the North Pacific Ocean," JGR, Vol 77, No 36, 1972.

24. ENVIRONMENTAL QUARTERLY, Appendix, EML-353, 1979.

25. FALLOUT PROGRAM, Appendix, HASL-329, 1977.

26. Folsom, T. R., Mohanrao, G. J., Pillai, K. C., Sreekumaran, C., "Distributions of Cs^{137} in the Pacific," HASL-197, 1968.

27. Folsom, T. R., Mohanrao, G. J., Winchell, P., "Fallout of Cesium in Surface Sea Water Off the California Coast (1959-1960) by Gamma-Ray Measurements," NATURE, Vol 187, No 4736, 1960.

28. Folsom, T. R., Sreekumaran, D., Hansen, N., Moore, J. M., Crismore, R., "Some Concentrations of Cs^{137} at Moderate Depths in the Pacific 1965-1968," HASL-217, 1970.

29. Machta, L., List, R. Y., Hubert, L., "World-Wide Travel of Atomic Debris," SCIENCE, Vol 124, No 3220, 1956.

30. RADIOACTIVITY IN THE MARINE ENVIRONMENT, Nat. Acad. Sci., Washington, 1971.

31. Schell, W. R., "Concentration, Physicochemical States and Mean Residence Times of Ph^{210} and Po^{210} in Marine and Estuarine Waters," GEOCHIM. AND COSMOCHIM. ACTA, Vol 41, No 8, 1977.

32. Tully, J. P., "Oceanographic Regions and Processes in the Seasonal Zone of the N. Pacific Ocean," STUDIES ON OCEANOGRAPHY, Seattle, 1965.

UDC 551.465.7(261)

CALCULATION OF THE PROPAGATION OF AN IMPURITY IN THE NORTHEASTERN ATLANTIC AND IN ADJACENT SEAS

Moscow METEOROLOGIYA I GIDROLOGIYA in Russian No 4, Apr 80 pp 79-83

[Article by B. R. Zaripov and Candidate of Physical and Mathematical Sciences D. G. Rzheplinskiy, All-Union Scientific Research Institute of Fisheries and Oceanography and Institute of Oceanology USSR Academy of Sciences, submitted for publication 5 March 1979]

Abstract: A study was made of the propagation of impurities in the boundary regions of the Atlantic and Arctic Oceans. In the computations use was made of the characteristics of currents obtained by the diagnostic method. The authors give prognostic mean long-term maps of the contamination level, taking into account the location of the principal sources of dumping of wastes and the processes of decay of the impurity.

[Text] The present-day level of contamination of the world ocean is quite high and this can lead to a considerable decrease in its bioproductivity [6, 9, 12, 13]. There is a special danger for bioproductivity from petroleum contaminations [6, 9, 12]. According to available data [7], the world ocean annually receives from 5 to 10 million tons of petroleum. In the North Sea alone there are more than 1,000 wells which yield more than 50 million tons of petroleum annually [9]. The contamination of the investigated region, which includes the Northeast Atlantic, and also the highly productive Norwegian, Greenland and North Seas, is extremely great [8, 12-14].

The amount of observational data on contamination of the ocean is constantly increasing, but for the time being they are inadequate for evaluating the contamination of large-scale ocean areas over long periods of time. For this purpose it is promising to make use of numerical modeling methods. In this case the well-known semi-empirical turbulent diffusion equation is used for computing the propagation of an impurity. We examined some theoretical and practical aspects of use of this equation for such purposes in earlier studies [3, 4].

In order to compute the propagation of an impurity it is necessary to have data on currents. But there have been virtually no measurements of currents at the spatial-temporal scales investigated here and therefore the authors first carried out computations of the mean long-term horizontal and vertical circulation of waters with the use of the diagnostic method described in [10]. This method takes into account the principal factors involved in the formation of currents -- the water density field, bottom relief and wind -- and gives reliable results [11]. The stationary mean long-term winter circulation of waters is stipulated in computations of propagation of the impurity [5].

The turbulent diffusion coefficients were assumed to be constant in time and space and were determined from the well-known "four-thirds" laws formulated by Richardson and Obukhov. For horizontal and vertical diffusion these values were $0.2 \cdot 10^8$ and $0.2 \cdot 10^1$ (in cgs) respectively. As the boundary conditions we stipulated the impurity flux through the boundary surface.

The available data on the quantity of contaminating substances entering the ocean and their physicochemical transformation are extremely scanty. Accordingly, the magnitude and direction of the impurity flux at the boundaries was stipulated on the basis of the following qualitative considerations. The runoff of the rivers of Western Europe and Great Britain is highly contaminated; in addition, along the shores there is a great number of large cities with a considerable volume of runoff of industrial and household wastes. Accordingly, the time-constant impurity flux directed into the ocean through the "solid" boundary -- the shores of Europe and Great Britain -- is stipulated. Since the volume of contaminated water entering the ocean from the shores of Iceland and Greenland is small, in these sectors of the "solid" boundary the impurity flux was assumed equal to zero.

Observational data [9, 12] show that the Gulf Stream, and then the North Atlantic Current, carry contaminated waters and therefore in the southern and western sectors of the "fluid" boundary the flux of impurity directed into the computation region is stipulated (see Fig. 1a). South of Greenland, in the region of transport of waters by the East Greenland Current, the impurity flux is directed from the computation region. The flux in the northern sector of the "fluid" boundary is directed from the computation region since in the eastern part there is transport of contaminated waters by the Norwegian Current, whereas in the western part there is "dilution" by the purer waters of the East Greenland Current. At the ocean surface there is stipulation of a small impurity flux, uniform over the entire ocean area, directed from the ocean into the atmosphere; such transport, according to data in [7], occurs due to evaporation and spray accompanying waves. A settling of the impurity occurs at the bottom [7]; this is also taken into account in the computations.

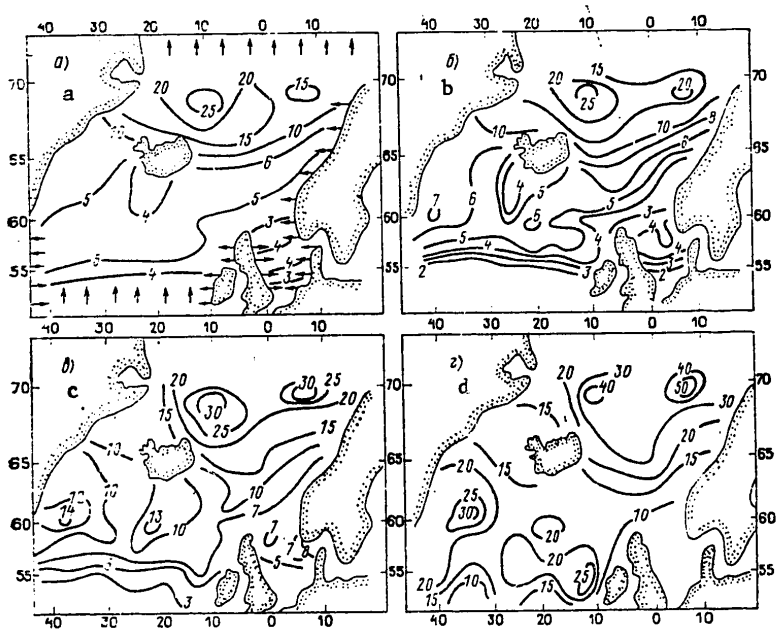

Fig. 1. Distribution of impurity six months after onset of computations in arbitrary units (the arrows indicate a stipulated direction of transport of the impurity through the boundaries). a) at surface; b) at 50-m horizon; c) at 100-m horizon; d) at 200-m horizon.

The rate of decay of contaminating substances in the ocean is extremely different, and in particular, decreases with a decrease in water temperature. Here we assumed a uniform absorption of impurity with a rate of 0.3% per day. As the initial conditions it was assumed that the investigated ocean area is free of the impurity. The correctness of such initial conditions was examined in [2] for computing the distribution of a nonconservative impurity. The turbulent diffusion equation was there numerically using the "directed differences" method (for example, see [10]). The interval of the computation grid was 1° in latitude and 2° in longitude; in the North Sea the interval was reduced to 0.5° and 1° respectively. The time interval was 3 days. The computations were made for a period of six months and indicated that the distribution of the impurity three months after the onset of the computations assumes a "quasistationary" character and thereafter remains virtually constant.

The results of the computations were used in constructing maps of the distribution of impurity at the horizons 0, 50, 100, 200 and 500 m. The entire layer 0-500 m (see Fig. 1) is characterized by a higher content of the impurity in the Norwegian-Greenland basin. This is determined by the peculiarities of circulation of these waters. In the layer 0-50 m the

impurity, entering through the southern boundary of the computation region, is transported quite rapidly into the Norwegian Sea together with the waters of the North Atlantic Current, whose velocity is high. At the 50-m horizon the isolines of concentration of the impurity were directed approximately along the main flow of the North Atlantic and Norwegian Currents. In the central part of the Northeast Atlantic a local zone of increased concentration (up to 6 arbitrary units) is formed, associated with reduced current velocities. In the western part of the Northeast Atlantic the increase in the concentration of the impurity is associated with the cyclonic circulation of waters, which in turn is determined by the Icelandic Low. In the Norwegian-Greenland basin there is an accumulation of the impurity and it is possible to discriminate two zones of increased concentration (up to 20-25 arbitrary units) -- to the northeast of Iceland and in the eastern part of the Norwegian Sea on the periphery of the cyclonic circulation of waters. There is an increased concentration in the central part of the North Sea, associated with the cyclonic movement of waters and ascending movements in this region.

Zones of increased concentration of the impurity -- in the western part and to the south of Iceland -- begin to be formed at the 100-m horizon (Fig. 1,c,d) in the Northeast Atlantic. An increase in the concentration is observed in the eastern part of the North Sea. In the southern part of the Northeast Atlantic the isolines have a zonal direction. At the 200-m horizon there is an appreciable increase in the level of contamination of the Northeast Atlantic, which especially in the west and southeast becomes comparable with the level of contamination of the Norwegian-Greenland basin. The reason for this is evidently that the current velocity at this horizon is lower than at the surface and as a result the impurity is not so rapidly transported into the Norwegian Sea. A zone of increased concentration up to 30 arbitrary units is formed in the western part of the Northeastern Atlantic; its center coincides with the region of water upwelling. In the southeast, in the region of an increase in the concentration of the impurity, the directions of the currents are unstable [5]. There is a high level of contamination in the Norwegian-Greenland basin. To the northwest of Iceland, in the region of the East Greenland Current, the waters are purer.

On the basis of the results of these computations we will examine the principal peculiarities of distribution of the impurity in the investigated water area. In the considered layer the contamination level increases with depth. The horizontal distribution of the impurity is essentially nonuniform and for the most part is determined (with stipulated boundary conditions) by the peculiarities of water circulation. In general, the level of contamination in the Norwegian and Greenland Seas is greater than in the Northeast Atlantic. The North Atlantic Current transports impurities into the Norwegian-Greenland basin, characterized by a cyclonic movement of waters. Zones of less mobile waters ("stagnant" zones) are formed in which there is an accumulation of impurity. The impurity concentration is increased in the central part of the North Sea, but in general it is

lower than in the Norwegian Sea. This can be associated with the stipulated settling of the impurity on the bottom (the North Sea is a shallow-water basin) and with a quite intensive water exchange between the sea and the Atlantic. The impurity concentration in the zone of the Norwegian Current is increased; this current carries contaminated waters which enter from the North Sea and which are transported by the North Atlantic Current. In the Norwegian-Greenland basin there are two zones of increased concentration: in the eastern part and toward the northeast of Iceland. To the west of Iceland the waters are purer because this region is remote from the principal sources of contamination.

The maps of the distribution of impurity cited here are prognostic maps of the mean long-term (winter) level of contamination of the investigated water area. They can be used for different purposes precisely in this way. We note that in many cases the zones of increased concentration of the impurity coincide with the regions of increased bioproductivity. The contamination level of the Norwegian-Greenland basin is increased -- and this is one of the most productive regions in the world ocean. Computations indicated that the system of water circulation in this region, in combination with delayed processes of decay of contaminants favors the accumulation of the impurity, which can lead to a decrease in its bioproductivity. The coincidence of regions of increased contamination and high productivity is not random. As is well known, the basis of primary bioproductivity is the supply with biogenous substances and the water circulation favors the accumulation in one and the same regions of both biogenous and contaminating substances. We also note that these maps can be used as the background level in computing mesoscale processes of transport of the impurity (for example, in determining the consequences of tanker accidents or damage to oil wells).

As noted above, observational data on contamination, averaged for the spatial-temporal scales considered here, are virtually unavailable. A comparison of the computed maps with data from individual surveys is not entirely correct. However, comparison of our maps with data from some surveys [1, 9] in general indicated their fair qualitative correspondence. We note in conclusion that the development of the theory of sea currents in the near future should lead to the possibility of preparation of quite precise forecasts of currents with different times in advance [11], which in turn will make it possible to prepare prognostic maps of the contamination level both for the entire world ocean and for its individual regions.

BIBLIOGRAPHY

1. Buyanov, N. I., "Sr^{90} and Cs^{137} in the North and Norwegian Seas," MATERIALY RYBOKHOZYAYSTVENNYKH ISSLEDOVANIY SEVERNOGO BASSEYNA (Materials of Fishery Investigations in the Northern Basin), No 21, Murmansk, 1974.

2. Galkin, L. M., RESHENIYE DIFFUZIONNYKH ZADACH METODOM MONTE-KARLO (Solution of Diffusion Problems by the Monte Carlo Method), Moscow, Nauka, 1975.

3. Zaripov, B. R., "Modeling of the Distribution of Matter in Water Bodies Using the Turbulent Diffusion Equation," EKSPRESS-INFORMATSIYA TsNIITEIRKh (expansion unknown), Series 9, No 9, 1977.

4. Zaripov, B. R., Rzheplinskiy, D. G., "Use of the Diffusion Equation for Computing the Distribution of Oceanological Characteristics," EKSPRESS-INFORMATSIYA TsNIITEIRKh, Series 9, No 10, 1977.

5. Zaripov, B. R., Rzheplinskiy, D. G., "Mean Long-term Seasonal Circulation of Waters of the Northeast Atlantic, Norwegian, Greenland and North Seas (Diagnostic Computations)," OKEANOLOGIYA (Oceanology), Vol XVII, No 5, 1977.

6. Mironov, O. G., "Biological Aspects of Contamination of Seas by Petroleum and Petroleum Products," IZV. AN SSSR, GEOGRAFIYA (News of the USSR Academy of Sciences, Geography), No 2, 1972.

7. Mironov, O. G., "Concise Description of the Physical Factors Exerting an Influence on the Fate of Petroleum in the Sea," TRANSPORT I KHRANENIYE NEFTI I NEFTEPRODUKTOV (Transport and Storage of Petroleum and Petroleum Products), No 10, 1975.

8. Oradovskiy, S. G., Simonov, A. I., Yushak, A. A., "Investigation of the Nature of the Distribution of Chemical Contaminants in the Gulf Stream Zone and Their Influence on the Primary Productivity of Ocean Waters," METEOROLOGIYA I GIDROLOGIYA (Meteorology and Hydrology), No 2, 1975.

9. Ryabchikov, A. M., "Environmental Contamination by Petroleum," VESTNIK MGU (Herald of Moscow State University), GEOGRAFIYA (Geography), 1974.

10. Sarkisyan, A. S., OSNOVY TEORII I RASCHET OKEANICHESKIKH TECHENIY (Principles of the Theory and Computation of Ocean Currents), Leningrad, Gidrometeoizdat, 1966.

11. Sarkisyan, A. S., CHISLENNYY ANALIZ I PROGNOZ MORSKIKH TECHENIY (Numerical Analysis and Prediction of Sea Currents), Leningrad, Gidrometeoizdat.

12. Simonov, A. I., Oradovskiy, S. G., Yushak, A. A., "Present Status of Chemical Contamination of Waters of the North Atlantic," METEOROLOGIYA I GIDROLOGIYA, No 3, 1974.

13. Terziyev, F. S., Norina, A. M., "Scientific and Practical Aspects of the Problem of Contamination of the Northern Seas," PROBLEMY ARKTIKI I ANTARKTIKI (Problems of the Arctic and Antarctic), No 25, 1977.

14. Roll, H. V., "Die heutige Verunreinigung der Meere," UNIVERSITAS, Vol 26, No 7, 1971.

UDC 551.464.38(260)(100)

SALT BALANCE IN THE WORLD OCEAN

Moscow METEOROLOGIYA I GIDROLOGIYA in Russian No 4, Apr 80 pp 84-89

[Article by A. M. Gritsenko and Professor V. N. Stepanov, Institute of Oceanology USSR Academy of Sciences, submitted for publication 3 July 1979]

Abstract: A study was made of the principal components of exchange of the total content of salts, including exchange between the oceans, the ocean and the atmosphere and land. For the first time an attempt has been made to determine the balance of salts in the world ocean. Available data and indirect computation methods are used for evaluating the components.

[Text] Significant concepts in this field are extremely limited. The most thorough investigations have been made on the exchange of salts between the ocean and the atmosphere and the land. Relatively recently a very valuable study was published by V. N. Ivanenkov and A. N. Gusarova [8], devoted to the exchange of dissolved oxygen, silicic acid and inorganic phosphorus. With respect to the transfer of salts in the waters of the ocean an article has been published by Yu. A. Grigor'yev [6], which examines exchange between the Atlantic and Indian Oceans, and also the Indian and Pacific Oceans. In addition, computations have been made of the transfer of salts in individual small regions.

Our objective was to estimate the receipt and loss components of the salt balance in the world ocean. The intensity of exchange of salts, like individual chemical elements (judging from data published by V. N. Ivanenkov and A. N. Gusarova), are determined primarily by water exchange between the oceans. Their concentration in ocean waters plays a secondary role. The exchange of salts between the ocean and the atmosphere is three orders of magnitude less than in the waters of the ocean.

Exchange of salts between the oceans. According to the computations in [10] the total content of salts in the world ocean is about $46.5 \cdot 10^{15}$ tons. Almost $7 \cdot 10^{14}$ tons (Table 1) or 1.5% of their quantity is drawn into

the exchange between the oceans. Accordingly, the total exchange of salts in the world ocean can occur in approximately 70 years.

Table 1

Exchange of Salts Between Oceans

Океан (1)	Приход (2) 10^{12} т/год (5)	%	Расход (3) 10^{12} т/год	%	Разность (4) 10^{12} т/год	%
(6) Атлантический	232,7	33	235,3	34	—2,6	1,1
(7) Индийский	249,9	36	249,2	36	+0,7	0,3
(8) Тихий	199,9	29	197,5	28	+2,4	1,2
(9) Северный Ледовитый	13,0	2	13,1	2	—0,1	0,8
(10) Всего:	695,5	100	695,1	100	+0,4	0,06

KEY:

1. Ocean
2. Receipt
3. Loss
4. Difference
5. tons/year
6. Atlantic
7. Indian
8. Pacific
9. Arctic
10. Total

Most of the salts are transported into the Antarctic part of the oceans (Table 4), where the water exchange is particularly significant. Its volume in the Atlantic and Indian Oceans differs little -- 33-36% relative to the global exchange; here total exchange can occur in 40-45 years. In the Pacific Ocean it is substantially less; the reason is the barrier created by the narrow Drake Passage and this is also reflected in the Atlantic Ocean. Constituting about 1/3 of the salt exchange in the entire world ocean, the total exchange in the Pacific Ocean with its enormous water mass can take place in approximately 125 years. The smallest role in the planetary exchange of salts is played by the Arctic Ocean -- only 2% of their total mass transported in the world ocean. The rate of exchange of waters in the oceans is virtually the same [11].

It should be emphasized that the cited estimates can be regarded as extremely approximate. They were made without allowance for the different intensity of movement of waters, determined by the peculiarities of stratification and the related nonuniformity in the rate of transfer of energy and matter. And nevertheless the determined values are as small as those given by other authors (in particular, as given by Ivanenkov and Gusarova [8]). At the same time, estimates of a completely different order of magnitude are also known; for example, A. Poldervart [9] points out that during the last billion years of existence of the world ocean the sodium chloride, constituting 77% of all the dissolved salts, has been exchanged roughly only 9-10 times.

Estimates of components of exchange of salts through ocean surface. Particularly thorough investigations in this field have been made by S. V. Bruyevich and Ye. Z. Kulik [5], then by S. V. Bruyevich and V. D. Korzh [4], and finally S. V. Bruyevich and V. N. Ivanenkov [3]. Among the studies of foreign authors we should note a study by E. Eriksson [12]. The mentioned studies give a review of the main literature, which makes it possible to limit ourselves here only to those highly important conclusions which were drawn with respect to the considered problem.

The transfer of salts from the ocean into the atmosphere occurs in the process of evaporation and as a result of the spraying of water during wind waves, constantly occurring in the ocean with greater or lesser force. N. N. Zubov has proposed that the loss of salts in the presence of waves be called "mechanical evaporation," whereas L. I. Belyayev has proposed that it be called "mechanical loss of salts." The appearance of salts in the air as a result of evaporation is called "physical evaporation," and only for it is there a quantitative estimate based on field and laboratory experiments. According to S. V. Bruyevich and his colleagues, 0.5 g of salts is lost from 1 m^2 of ocean surface.

In the literature we were unable to find data on how much salt can enter the atmosphere as a result of the spraying of water when waves are present. It is very difficult to obtain such estimates, primarily due to the extremely great variability of the wind waves and the complexity of the process of salt ejection. S. V. Bruyevich and V. D. Korzh [4] examine a considerable number of Soviet and foreign studies devoted to the mechanism of formation and destruction of air bubbles and water droplets arising when waves are present. When the bubbles burst a small streamlet is ejected from their surface and this gives rise to individual tiny droplets so that the larger of them enter the ocean, whereas the tiniest ones become condensation nuclei.

Indirect computation methods were employed in order to ascertain the possible volume of the salts entering the atmosphere. For example, E. Eriksson [12], on the basis of the quantity of salts transferred across 1 km of shore per day (5.4 tons) and a total length of the shore line of the world ocean (250,000 km), determined that during a year $0.5 \cdot 10^9$ tons is carried onto the land from the ocean in a year. Estimating the magnitude of transfer of salts onto the land at 10% of their total quantity entering into the air, E. Eriksson obtained a total value for the entire mass of salts in the atmosphere equal to $5 \cdot 10^9$ tons/year. These computations were confirmed by S. V. Bruyevich on the basis of the fact that the salts transported onto the land are then returned to the ocean with river runoff; he determined the magnitude of chemical runoff at $0.5 \cdot 10^9$ tons/year. Assuming that river runoff is about 10% of the entire evaporation from the surface of the world ocean, the transfer of salts into the atmosphere was found to be the same as found by E. Eriksson, equal to $5 \cdot 10^9$ tons/year.

Proceeding on the basis of available estimates of individual components of the exchange of salts through the ocean surface, we made an attempt to determine their budget for individual oceans and the world ocean as a whole (Table 2). In order to ascertain the quantity of salts which is released to the atmosphere by each ocean we used the earlier-computed evaporation; for the world ocean it was $496 \cdot 10^3$ km^3 annually [11].

Table 2

Exchange of Salts Through Ocean Surface in 10^9 tons/year

	Составляющие обмена 1	Океан 2				
		Мировой 3	Атлантический 4	Индийский 5	Тихий 6	Северный Ледовитый 7
8	Разбрызгивание ветровым волнением	—4,752	—1,140	—1,044	—2,471	—0,097
9	Физическое испарение	—0,248	—0,060	—0,056	—0,129	—0,003
10	Выпадение солей с осадками	4,500	0,980	1,057	2,440	0,043
11	Химический сток рек	0,500	0,220	0,063	0,160	0,057
12	Общее количество солей, участвующих в обмене через поверхность океана:					
	10^9 т/год	5,0	1,2	1,1	2,6	0,1
13	%	100	24	22	52	2

KEY:

1. Exchange components
2. Ocean
3. World
4. Atlantic
5. Indian
6. Pacific
7. Arctic
8. Spraying by wind waves
9. Physical evaporation
10. Salts falling in precipitation
11. Chemical runoff in rivers
12. Total quantity of salts participating in exchange through ocean surface
13. Tons/year

Physical evaporation was computed, taking into account that according to the estimates made by S. V. Bruyevich, et al. during this process 0.5 g of salts enters the air from 1 m^2 of water. It is therefore found that $0.248 \cdot 10^9$ tons of salts annually are carried from the surface of the world ocean into the atmosphere. Since this is 5% of the total transfer of salts, their total quantity participating in exchange through the surface of the world ocean is the same as given by the authors mentioned earlier, equal to $5 \cdot 10^9$ tons/year. The relationship of the salts released by each ocean will naturally be proportional to the evaporation value (Table 2).

The quantity of salts sprayed by wind waves in the first approximation evidently can be obtained from the difference between the total mass of salts entering the air and their transport in the course of physical evaporation. Accordingly, this is 95% of all the salts carried into the atmosphere or $4.752 \cdot 10^9$ tons/year for the entire world ocean. Somewhat more than $1 \cdot 10^9$ tons/year can come from the Atlantic and Indian Oceans and almost $2.5 \cdot 10^9$ tons/year from the Pacific Ocean.

The "receipts" part of the balance of salts drawn into the exchange between the world ocean and the atmosphere consists of the quantity of salts falling with precipitation and the chemical runoff of rivers. On the basis of determinations of the content of chlorine made by S. V. Bruyevich and a number of other specialists, O. A. Alekin [1] estimated its magnitude with an annual river runoff at that time assumed to be $36 \cdot 10^3$ km^3. Since according to present-day data [2] it is $44.7 \cdot 10^3$ km^3/year, the quantity of chlorine transported into the world ocean is $2.83 \cdot 10^8$ tons. With a chlorine coefficient for the ocean assumed to be 1.8, the total mass of salts carried into the world ocean is $0.5 \cdot 10^9$ tons/year. For the individual oceans the chemical runoff was assumed to be proportional to the river runoff (Table 2). Thus, it was found that not even half of all the salts are carried into the Atlantic Ocean (44% of its total quantity), 32% are carried into the Pacific Ocean, 13% into the Indian Ocean and 11% into the Arctic Ocean.

Table 3

Estimate of Exchange of Salts Between Ocean and Land

1 Составляющие обмена	2 Океан									
	Мировой 3		Атлантический 4		Индийский 5		Тихий 6		Северный Ледовитый 7	
	10^9 т/год	%	10^9 т/год	%	10^9 т/год	%	10^9 т/год	%	10^9 т/год	%
	8									
9 Перенос солей на сушу	−0,5	100	−0,12	24	−0,11	22	−0,26	52	−0,01	2
10 Химический сток рек	0,5	100	0,22	44	0.063	13	0,16	32	0,057	11
11 Разность	0		0,1		−0,047		−0,10		0,047	

KEY:

1. Exchange component
2. Ocean
3. World
4. Atlantic
5. Indian
6. Pacific
7. Arctic Ocean
8. tons/year
9. Transport of salts onto land
10. Chemical runoff of rivers
11. Difference

Salts, returning to the oceans with precipitation, will correspond to their total mass carried into the air, except for what is returned with river runoff, since in the first approximation a balance should exist.

We should note a specific peculiarity of the salt balance in the Arctic Ocean. In contrast to the other oceans, where the chemical runoff of rivers is much less than the fallout of salts with precipitation, in the Arctic it is substantially higher (Table 2). This is attributable to the great river runoff but a particularly small amount of precipitation. It would seem that thereby there should be an accumulation of sulfates, predominating in river waters and precipitation. However, the constancy of the salt composition in the Arctic Ocean, it must be assumed, is maintained by the inflow of a considerable mass of chlorides with Atlantic and Pacific Ocean waters.

Exchange of salts between the ocean and the land. In particular, it must be noted that the balance between the transport of salts from the ocean to the land and their return with chemical runoff occurs only with respect to the world ocean as a whole. The budget is different for the individual oceans (Table 3). For example, in the Atlantic and Arctic Oceans the chemical runoff of rivers exceeds the transport onto the land, whereas in the other two oceans the picture is the reverse.

The most interesting peculiarity of exchange of salts between the oceans and the land is, as demonstrated by the investigations of S. V. Bruyevich, et al., that during the spraying of salts when wind waves are present the chlorides for the most part remain in the ocean, whereas the sulfates for the most part pass into aerosols determining the salt composition of precipitation. This takes place at the moment of direct detachment of microdroplets of ocean water. There is a redistribution of ions of saline composition [5]. This evidently thereby determines the difference in the chemical composition of ocean and river water. The latter, flowing into the ocean, compensates that shortage of sulfates which is formed in the process of salt exchange with the atmosphere.

Balance of salts in the world ocean. It has already been stated above that the transport of waters in Antarctica is of fundamental importance. Since exchange through the ocean surface is three orders of magnitude less than the quantity which is propagated in the water layer, in the balance of salts in the world ocean it is possible to limit ourselves to determination of their transport between the oceans (Table 4). In this respect the salt balance differs considerably from the balance of water and heat. For example, the fraction of moisture exchange between the ocean and the atmosphere is 2-4% of the total circulation of water [7]. However, in the heat balance exchange with the atmosphere plays a leading role, on the average for the world ocean attaining 77% [11].

Table 4

Balance of Salts in the Oceans

	Составляющие обмена 1	Приход 2 10^{12} т/год 4	Расход 3 10^{12} т/год 4	Приход 2 %	Расход 3 %
	5 Атлантический океан				
10	Обмен с Индийским океаном	52,7	218,4	23	93
11	Обмен с Тихим океаном	164,9	3,4	70	1
12	Обмен с Северным Ледовитым океаном	13,1	11,9	6	5
13	Обмен со Средиземным морем	2,0	2,0	1	1
14	Итого:	232,7	235,3	100	100
15	Разность между приходом и расходом	—2,6		1,1	
	6 Индийский океан				
16	Обмен с Атлантическим океаном	218,4	52,7	88	21
11	Обмен с Тихим океаном:				
17	а) проливы Зондского архипелага и Бассов пролив	28,1	—	11	—
18	б) о. Тасмания — Антарктида	3,4	196,5	1	79
14	Итого:	249,9	249,2	100	100
15	Разность между приходом и расходом	—0,7		0,3	
	7 Тихий океан				
10	Обмен с Индийским океаном:				
17	а) проливы Зондского архипелага и Бассов пролив	—	28,1	—	14
18	б) о. Тасмания — Антарктида	196,5	3,4	99	2
16	Обмен с Атлантическим океаном	3,4	164,9	1	83
12	Обмен с Северным Ледовитым океаном	—	1,1	—	1
14	Итого:	199,9	197,5	100	100
15	Разность между приходом и расходом	2,4		1,2	
	8 Северный Ледовитый океан				
16	Обмен с Атлантическим океаном	11,9	13,1	92	100
11	Обмен с Тихим океаном	1,1	—	8	—
14	Итого:	13,0	13,1	100	100
15	Разность между приходом и расходом	—0,1		0,8	
	9 Мировой океан				
19	Количество солей, участвующих в обмене между океанами	695,5	695,1	100	100
15	Разность между приходом и расходом	0,4		0,06	

KEY TO TABLE 4:

1. Exchange components
2. Receipts
3. Expenditures
4. Tons/year
5. Atlantic Ocean
6. Indian Ocean
7. Pacific Ocean
8. Arctic Ocean
9. World Ocean
10. Exchange with Indian Ocean
11. Exchange with Pacific Ocean
12. Exchange with Arctic Ocean
13. Exchange with Mediterranean Sea
14. Total
15. Difference between receipts and expenditures
16. Exchange with Atlantic Ocean
17. Straits of Sunda Archipelago and Bass Strait
18. Tasmania-Antarctica
19. Quantity of salts participating in exchange between oceans

---

In the case of the Atlantic Ocean exchange with the Arctic Ocean is of considerable importance (5-6% of the receipts and expenditures). For the Arctic Ocean this exchange is decisive not only in the balance, but also in its entire nature. In the Pacific and Indian Oceans the salt exchange through the Sunda straits exerts a considerable influence. The "nonclosures" of the salt balance were very small.

The attempt made here to evaluate the principal components of the balance of the total content of salts in the world ocean and the contribution of exchange with the atmosphere and land, despite their small role, is of unquestionable interest for understanding the peculiarities of the planetary redistribution of salts.

BIBLIOGRAPHY

1. Alekin, O. A., KHIMIYA OKEANA (Ocean Chemistry), Leningrad, Gidrometeoizdat, 1966.

2. Alyushinskaya, N. M., Ivanov, V. V., "Water Inflow from the Land," MIROVOY VODNYY BALANS I VODNYYE RESURSY ZEMLI (World Water Balance and the Earth's Water Resources), 1974.

3. Bruyevich, S. V., Ivanenkov, V. N., "Problems in the Chemical Balance of the World Ocean," OKEANOLOGIYA (Oceanology), Vol XI, No 5, 1971.

4. Bruyevich, S. V., Korzh, V. D., "Salt Exchange Between the Ocean and the Atmosphere," OKEANOLOGIYA, Vol IX, No 4, 1969.

5. Bruyevich, S. V., Kulik, Ye. Z., "Chemical Interaction Between the Ocean and the Atmosphere," OKEANOLOGIYA, Vol VII, No 3, 1967.

6. Grigor'yev, Yu. A., "Study of Water, Heat and Salt Flows on the Profiles Africa-Antarctica and New Zealand-Antarctica," BYULLETEN' SAE (Bulletin of the Soviet Antarctic Expedition), No 59, 1966.

7. Gritsenko, A. M., Stepanov, V. N., "Water Balance of the World Ocean and its Role in Planetary Processes," IZV. AN SSSR, SERIYA GEOGRAF. (News of the USSR Academy of Sciences, Geographical Series), 1979 (in press).

8. Ivanenkov, V. N., Gusarova, A. N., "Annual Exchange of Dissolved Oxygen, Silicic Acid and Inorganic Dissolved Phosphorus Between the Oceans," KHIMIYA MOREY I OKEANOV (Chemistry of the Seas and Oceans), Moscow, Nauka, 1973.

9. Poldervart, A., "Chemistry of the Earth's Crust," ZEMNAYA KORA (The Earth's Crust), Moscow, IL, 1957.

10. Stepanov, V. N., Burenin, V. V., Galerkin, L. I., Gritsenko, A. M., Moiseyev, L. K., "Heat Content of Waters of the World Ocean," OKEANOLOGIYA, Vol XVIII, No 3, 1978.

11. Stepanov, V. N., Gritsenko, A. M., "Heat Balance of the World Ocean," OKEANOLOGIYA, 1979 (in press).

12. Eriksson, E., "The Yearly Circulation of Chloride and Sulfur in Nature," Pt 2, TELLUS, Vol 12, No 1, 1959.

UDC 556.535.5.06(282.247.41+470.46)

SHORT-RANGE PREDICTION OF AUTUMN AND WINTER ICE JAM LEVELS ON THE LOWER VOLGA AT CHERNYY YAR STATION

Moscow METEOROLOGIYA I GIDROLOGIYA in Russian No 4, Apr 80 pp 90-95

[Article by P. I. Bukharitsin, Astrakhan Zonal Hydrometeorological Observatory, submitted for publication 3 September 1979]

Abstract: The article briefly examines the hydrometeorological and ice conditions on the Lower Volga during the autumn-winter period of 1978-1979. The author describes the largest and most unusual ice jams observed during this period in the neighborhood of Kamennyy Yar, Chernyy Yar and the mouth of the Yenotayevka channel. A prognostic dependence is proposed for use in the preparation of short-range forecasts of autumn and winter ice jam levels at Chernyy Yar station.

[Text] Autumn and winter ice jams and the accumulation of water under snow on the Lower Volga under conditions of regulated runoff (beginning in 1959) have been observed annually. They are associated with a change in the ice and thermal regime of the Volga and also the regime of water discharges and levels following the construction of the Volga Hydroelectric Power Station imeni XXII Congress CPSU and the formation of the Volgogradskoye Reservoir.

The studies of many researchers have been devoted to investigation of autumn and winter ice jams on USSR rivers. Extremely important studies with a description of the hydrometeorological conditions for the development of ice jams and processes preceding and accompanying the formation of ice jams, the geomorphological features of river reaches with ice jams and also an examination of the state of study of the processes of ice jam formation and making recommendations on preventing and contending with ice jams and the accumulation of water under ice have been made by R. A. Nezhikhovskiy [15], A. M. Filippov [23], R. V. Donchenko [6, 9], A. V. Shcherbak [25], P. M. Lur'ye [12], G. N. Ustinov [22], Z. A. Genkin [4], V. V. Lebedova and P. L. Medres [11], P. P. Angelopulo [1] and other authors.

Great attention has been devoted to the development of methods for predicting ice jams and computing the maximum ice-jam levels. These include the studies of R. A. Nezhikhovskiy, G. V. Ardesheva, N. P. Sakovskaya [13, 14, 16-19], R. V. Donchenko, A. M. Filippov [8], V. N. Karnovich [10], A. N. Chizhov and A. G. Deryugin [24].

The studies of V. V. Perzhinskiy [5, 20, 21], R. V. Donchenko, M. I. Bayusova [7] and A. K. Barabash [2, 3] were devoted to study of ice jams and the accumulation of water under snow on the Lower Volga.

The article by A. K. Barabash [2] is one of the first investigations devoted to study of maximum ice-jam induced levels during the autumn-winter period on the Lower Volga and in the delta. This study gives an analysis of the process of formation of ice jams under natural conditions and under conditions of regulation on the Volga River below the Hydroelectric Power Station imeni XXII Congress CPSU and a dependence is proposed for the short-range forecasting of the height of autumn ice-jam induced levels at Chernyy Yar station.

Recently, in connection with the problem of lengthening the navigation season on the internal water bodies of the USSR during winter the interest of scientists in study of the ice-thermal regime on the Lower Volga has considerably increased.

The unusually high water volume in the Volga River basin in the autumn of 1978 and the related great discharges from the Volgogradskoye Reservoir, about 9-11 thousand m^3/sec or more, caused a considerable increase in the level on the Lower Volga and in the delta. The mean 10-day levels at Astrakhan' at the end of October and November were 130 cm higher than the corresponding mean long-term levels under regulated conditions and 150-160 cm higher than in 1977. Such high autumn levels were observed for the first time during the entire period of observations since 1881.

Sharp temperature drops during the period of ice formation in December 1978 from +6 to -20°C, together with a high water level held back the time when an ice cover was formed. The prolonged going-out of the ice in individual river reaches resulted in major winter ice jams such as had not been observed earlier on the Volga.

An unusual ice jam was formed in late December at the mouth of Yenotayevka channel. The packed ice cover in the main channel of the Volga created a backwater and some of the Volga water bypassed it, going through the channel. A level rise and also a thaw at the very end of December favored the freeing of the channel of ice. The initiated going-out of the ice continued for more than half a day. The floating ice was concentrated at the channel mouth, since its further advance was impeded by the ice cover in the main channel. An ice jam was formed. The considerable level rise in the channel led to inundation of the floodplain between the channel and the main river channel. After 3 or 4 days the ice jam in the Yenotayevka channel was destroyed.

Table 1

Extremal Values of Winter Ice Jam and High Water Levels at Stations on the Lower Volga

1 Пункт и период наблюдений	Максимальный заторный уровень набл. зимой 1978—79 гг., *см* 2	Многолетние значения заторных зимних уровней, *см* 3		Многолетние значения половодных уровней, *см* 4	
		минимальный 5	максимальный 6	минимальный 5	максимальный 6
7 Каменный Яр (1974—78 гг.)	842	547	764	736	864
8 Черный Яр (1959—78 гг.)	605	380	641	700	860
9 Енотаевск (1959—78 гг.)	589	260	484	556	744

KEY:

1. Station and observation period
2. Maximum ice-jam induced level observed in winter of 1978-1979, cm
3. Long-term ice-jam induced winter levels, cm
4. Long-term high-water levels, cm
5. Minimum
6. Maximum
7. Kamennyy Yar
8. Chernyy Yar
9. Yenotayevsk

A large winter ice jam was formed during the first 10-day period of January 1979 below Kamennyy Yar. It caused a sharp (more than 3 m) level increase and movement of water into the Volga-Aktubinsk floodplain (Table 1).

At the same time, but more smoothly, a level rise began which was caused by a second ice jam forming below Chernyy Yar. Here the level increased by 1.5 m and almost attained the maximum winter ice-jam induced level during the entire period of regulated runoff which was observed in 1977 -- 641 cm (Fig. 1).

The formation of such large winter ice jams at Kamennyy Yar and Chernyy Yar was preceded by the going-out of the ice on the Volga River, continuing for 23 days. After it had poured into the floodplain the water found a roundabout course, bypassing the ice jams; the ice jam levels were stabilized and remained without significant changes until opening-up of the river.

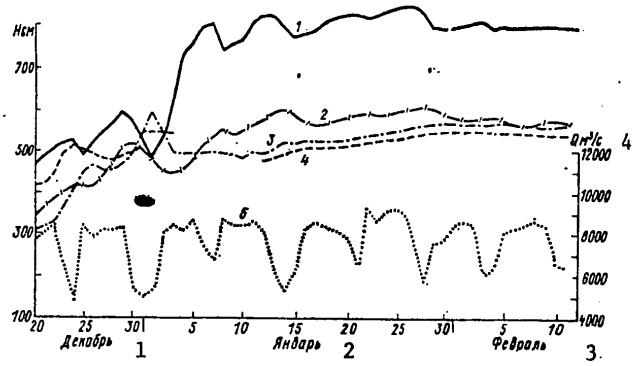

Fig. 1. Curves of level changes at stations on the Lower Volga and the mean daily discharges from the Volgogradskoye Reservoir during the winter of 1978-1979. 1) level variation at Kamennyy Yar, 2) level variation at Chernyy Yar, 3) level variation at Yenotayevsk, 4) level variation at Seroglazovka, 5) discharge from Volgogradskoye Reservoir.

KEY:

1. December
2. January
3. February
4. Q m^3/sec

Table 2

Change in Travel Time from Volgograd to Chernyy Yar in Dependence on Mean Daily Discharges in Lower Pool of the Volgograd Hydroelectric Power Station

Mean daily discharges at Volgograd Hydroelectric Power Station, thousands m^3/sec	Travel time, sec
5	3
5.5-6.5	3-4
6.5-7.5	4-5
7.5-8.5	5-6
9	6

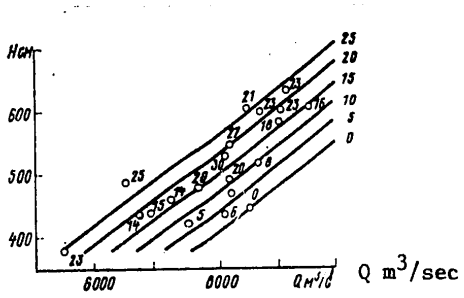

Fig. 2. Dependence of maximum levels at Chernyy Yar on water discharges in lower pool of Hydroelectric Power Station imeni XXII Congress CPSU and duration of going-out of the ice in days.

The formation of winter ice jams in the reach Kamennyy Yar - Yenotayevsk was confirmed by the results of aerial reconnaissance carried out in January-February by the Astrakhan Zonal and Volgograd Hydrometeorological Observatories and observations from the icebreaker "Kapitan Krutov," made

during an experimental voyage of the icebreaker along the reach Astrakhan'-Volgograd during February 1979. The thickness in the ice jams was 85-90 cm, locally attaining 140 cm. At the sites where the ice jams were formed there was much frazil ice in the channel. The layer of frazil ice beneath the main ice cover was 3.0-4.0 m; the hummocks were 1.5 m high.

During the period preceding and accompanying the formation of winter ice jams the mean daily discharges of the Volograd Reservoir on work days were about 8-9 thousand m^3/sec; on days off -- 5-6 thousand m^3/sec, which corresponds to the level at Chernyy Yar, equal in the case of an open channel to 280-300 cm. The high water volume and also the marked fluctuations of air temperature were responsible for the prolonged period of going-out of the ice on the Lower Volga and created the prerequisites for the formation of major ice jams.

The dependence between the maximum autumn-winter ice-jam induced levels at Chernyy Yar on the water discharges in the lower pool of the Volgogradskoye Reservoir

$$H_{\max \text{ ice jam}} = f(Q)$$

examined in a study by A. K. Barabash [2] unfortunately cannot be employed in routine work in the represented form for a number of reasons:
-- an inadequate series of observations;
-- no allowance is made for such an important factor as the influence of ice conditions (for example, the duration of going-out of the ice);
-- travel time from Volgograd to Chernyy Yar, taken from [2], equal to 4 days, is not a constant value; it is dependent on the water discharges and on ice conditions in a particular river reach.

Proceeding on the basis of these considerations, the author has proposed that a third variable be introduced into the dependence, namely the duration of going-out of the ice, and that the 8-year series of observations be extended to 20 years (1959-1979):

$$H_{\text{ice jam}} = f(Q;\ T_{\text{ice}}),$$

where Q is the mean daily water discharge in the lower pool of the Hydroelectric Power Station imeni XXII Congress CPSU, T_{ice} is the duration of going-out of the ice at Chernyy Yar from the date of the level rise, associated with formation of the ice jam, to the date of onset of a solid ice cover.

In constructing this dependence it was possible to establish a correlation between travel time and water discharge (Table 2).

Thus, it was now possible to use the actual travel time, corresponding to the the volume of the discharge and dependent on ice conditions, not the mean travel time, adopted in [2], equal to four days.

The regression equation for computing ice-jam induced levels at Chernyy Yar has the form

$$H_{\text{ice jam}} = 0{,}058x + 4{,}636\ y - 29, \qquad (1)$$

where x is the mean daily water discharge in the lower pool of the Hydroelectric Power Station imeni XXII Congress CPSU on the day of the forecast in m^3/sec, y is the duration of going-out of the ice at Chernyy Yar from the date of the level rise associated with formation of the ice jam to the date of preparation of the forecast in days.

The correlation coefficient of the derived dependence (Fig. 2) is equal to 0.85. The guaranteed probability of the method was 100% with an admissible error $\delta_{adm} = 0.674\sigma_\Delta = 53$ cm. The ratio of the mean square error to the standard deviation is $S/\sigma_\Delta = 0.37$. The condition of applicability of the dependence (1) in operational practice

$$15 < n < 25\ \frac{S}{\sigma_\Delta} \leq 0{,}75$$

is satisfied, where n is the number of terms in the series, equal to 20.

Thus, the quality indices of the method, which include the correlation coefficient, the guaranteed probability of the method and the condition of applicability of the dependence, computed in accordance with the "Instructions for the Hydrological Forecasts Service," make it possible to classify the dependence (1) in the "good" category.

The values of the maximum autumn-winter ice jam levels at Chernyy Yar from year to year vary in a great range. The long-term amplitude is 261 cm, which explains the high δ_{adm} value. However, the guaranteed probability of the method remains rather high (75%) even in a case when δ_{adm} is assumed equal to 30 cm, that is, considerably less than $0.674\sigma_\Delta$.

The derived dependence can be used in preparing short-range forecasts of autumn-winter ice jam levels at Chernyy Yar station for a period of 2-5 days in advance.

Computations of autumn-winter ice jam levels using equation (1) must begin with the date of a sharp rise in level at Chernyy Yar caused by the formation of an ice jam below the level post. For this purpose the "x" in equation (1) is replaced by the value of the mean daily water discharge at the Volgogradskaya Hydroelectric Power Station on the day of the forecast in m^3/sec and the "y" must be replaced by the duration of going-out of the ice at Chernyy Yar in days. The number of days with going-out of the ice is reckoned from the date of onset of the level rise associated with formation of the ice jam to the day of preparation of the forecast. The advance time of the forecast is determined by the travel time, which is 3-5 days (Table 2), but it must be taken into account that by the time of preparation of the forecast the mean daily discharge at the Volgogradskaya Hydroelectric Power Station is available only for the past day. Accordingly,

the actual advance time of forecasts is from 2 to 5 days.

The date of onset of setting-in of the ice is determined at Chernyy Yar station. With the setting-in of the ice the second term in equation (1) becomes a constant value and thereafter does not change. Equation (1) assumes the form

$$H_{\text{ice jam}} = 0.058\ x + 4.636\ y_{max} - 29 \qquad (2)$$

where y_{max} is the maximum duration of going-out of the ice at Chernyy Yar from the date of the level rise caused by the formation of an ice jam below Chernyy Yar to the date of setting-in of the ice at Chenyy Yar in days.

Computations using equation (2) are made from the date of setting-in of the ice cover to the onset of the maximum ice jam level at Chernyy Yar.

BIBLIOGRAPHY

1. Angelopulo, P. P., "Status of Study of Ice Jam Formation Processes," TRUDY LGMI (Transactions of the Leningrad Hydrometeorological Institute), No 36, 1969.

2. Barabash, A. K., "Autumn Ice Jams on the Lower Volga and in its Delta," TRUDY GIDROMETTSENTRA SSSR (Transactions of the USSR Hydrometeorological Center), No 117, 1974.

3. Barabash, A. K., "Influence of the Volgogradskoye Reservoir on the Times of Appearance of Ice and the Duration of Going-Out of the Ice on the Volga River Below Volgograd and in its Delta," TRUDY IV VSES. GIDROL. S"YEZDA (Transactions of the Fourth Hydrological Congress), Vol 7, Leningrad, Gidrometeoizdat, 1976.

4. Genkin, Z. A., Shmeleva, L. A., "Formulation of Recommendations on Preventing and Contending With Ice Jams and Water Accumulation Under Snow on the Amudar'ya River," NAUCHNYYE ISSLED. PO GIDROTEKHN. V 1969 (Scientific Investigations in Hydroengineering in 1969), Vol 2, Energiya, 1971.

5. Goryunov, I. V., Perzhinskiy, V. V., "Ice-Thermal Regime of the Lower Volga After Construction of the Volga Hydroelectric Power Station imeni XXII Congress CPSU and Formation of the Volgograd Reservoir," METEOROLOGIYA I GIDROLOGIYA (Meteorology and Hydrology), No 7, 1967.

6. Donchenko, R. V., "Regularities in Formation of Ice Jams in the Lower Pools at Hydroelectric Power Stations," TRUDY GGI (Transactions of the State Hydrological Institute), No 219, 1974.

7. Donchenko, R. V., Bayusova, M. I., "Evaluation of Change in the Conditions for Formation of Ice Jams in the Lower Pool at the Volga Hydroelectric Power Station imeni XXII Congress CPSU," TRUDY GGI, No 201, 1973.

8. Donchenko, R. V., Filippov, A. M., Bayusova, M. I., Chachina, N. S., "Investigations and Computations of the Intensity of Formation of Frazil Ice and Ice Jams on Regulated River Reaches," TRUDY IV VSES. GIDROLOG. S"YEZDA, Vol 6, Leningrad, Gidrometeoizdat, 1976.

9. Donchenko, R. V., "Conditions for the Formation of Ice Jams in Lower Pools," TRUDY GGI, No 227, 1975.

10. Karnovich, V. N., "Prediction of the Maximum Water Levels During Ice Jams on the Dnestr River and at Mogilev-Podol'skiy and Soroki Cities," TRUDY GIDROMETTSENTRA SSSR, No 140, 1975.

11. Lebedev, V. V., Medres, P. L., "Ice Jams on the Neva," SBORNIK RABOT LENINGR. GIDROMETEOROL. OBSERV. (Collection of Papers of the Leningrad Hydrometeorological Observatory), No 3, 1966.

12. Lur'ye, P. M., "Ice Jams on the Amudar'ya River and the Resulting Unprecedented Water Level Rise in January 1969," SB. RABOT ASHKHABAD. GIDROMETEOROL. OBSERV., No 6, 1971.

13. Nezhikhovskiy, R. A., Ardasheva, G. V., "Computation of the Maximum Ice-Jam Induced Levels on the Neva River," TRUDY GGI, 1970.

14. Nezhikhovskiy, R. A., Ardasheva, G. V., Sakovskaya, N. P., "Predictions of the Maximum Ice-Jam Induced Water Levels on the Dnestr River in the Reach Mogilev-Podol'skiy - Durbossary," TRUDY GGI, No 218, 1974.

15. Nezhikovskiy, R. A., "Types of River Freezing and Types of Ice Jams," METEOROLOGIYA I GIDROLOGIYA, No 2, 1974.

16. Nezhikhovskiy, R. A., Sakovskaya, N. P., "Prediction of the Maximum Ice-Jam Induced Water Level on the Severnaya Dvina River at Arkhangel'sk," TRUDY GGI, No 197, 1972.

17. Nezhikhovskiy, R. A., Sakovskaya, N. P., Ardasheva, G. V., "Predictions of Maximum Ice-Jam Induced Water Levels at Sites of Annual Formation of Ice Jams," TRUDY IV VSES. GIDROLOG. S"YEZDA, Vol 7, Leningrad, Gidrometeoizdat, 1976.

18. Nezhikhovskiy, R. A., Sakovskaya, N. P., "Predictions of Maximum Ice-Jam Induced Water Levels on the Severnaya Dvina and Neman Rivers," TRUDY GGI, No 227, 1975.

19. Nezhikhovskiy, R.A., Buzin, V. A., "Conditions for the Formation and Prediction of Ice Jams in Rivers," METEOROLOGIYA I GIDROLOGIYA, No 5, 1977.

20. Perzhinskiy, V. V., "Ice Jam Phenomena on the Volga at Chernyy Yar," METEOROLOGIYA I GIDROLOGIYA, No 8, 1970.

21. Perzhinskiy, V. V., "Ice Jam at Volgograd During the Winter of 1966-1967," SB. RABOT VOLGOGR. GIDROMETEOROL. OBSERV. (Collection of Papers of the Volgograd Hydrometeorological Observatory), No 1, 1970.

22. Ustinov, G. N., "Ice Jams on the Lower Vyg in the Belomorsk Neighborhood," TRUDY KOORDINATS. SOVESHCHANIY PO GIDROTEKHN. (Transactions of Coordination Conferences on Hydroengineering), No 56, 1970.

23. Filippov, A. M., "Experimental Investigations of the Dynamics of Formation of Ice Jams in the Lower Pools at Hydroelectric Power Stations," TRUDY GGI, No 227, 1975.

24. Chizhov, A. N., Deryugin, A. G., Lazarevskaya, V. I., Ponomareva, O. F., Al'tshuler, N. V., "Conditions for the Formation of Ice Jams on the Dnestr River," TRUDY GGI, No 201, 1975.

25. Shcherbak, A. V., Solonenko, L. I., "Conditions for Formation of Ice Jams and Accumulation of Water Under Snow in the Lower Reaches of the Danube River," TRUDY UkrNIGMI (Transactions of the Ukrainian Scientific Research Hydrometeorological Institute), No 116, 1972.

UDC 532.517.4

APPLICATION OF THE COHERENCE FUNCTION IN ANALYZING THE TURBULENT STRUCTURE OF A RIVER FLOW

Moscow METEOROLOGIYA I GIDROLOGIYA in Russian No 4, Apr 80 pp 96-100

[Article by Professor D. I. Grinval'd and M. P. Yekhnich, Odessa Hydrometeorological Institute, submitted for publication 7 September 1979]

Abstract: The paper gives the results of field investigations of the structure of turbulent river flow. The coherence function of two random processes was used as the mathematical approach. An analysis of the curves revealed the peculiarities of the coherence function in reaches with different bottom relief. This made it possible to ascertain the role of eddies of different scales in the formation of different channel forms.

[Text] Already in 1948 M. A. Velikanov, introducing the concept of a channel process as a process characterizing the interaction between the flow and channel, postulated that channel turbulence determines the entire mechanism of movement of sediments and channel deformations, being the principal factor in the channel process. However, until recently the mechanism of the effect of turbulent formations on the channel process was simply not understood.

During recent years we have carried out experimental investigations of the energy spectrum of river flow turbulence and its relationship to the peculiarities of bottom relief structure. As the criterion we used the ratio of the contribution of energy from eddies of different scales to the total kinetic energy of the flow [1, 2]. In developing these investigations in 1978 we carried out a number of experiments in reaches with different bottom relief in the Turunchuk River. The new experimental data were used in confirming the hypothesis expressed earlier that in the case of an equal relationship of the contribution of energy of small and medium eddies, on the one hand, and the energy of large eddies, on the other, the river channel will be relatively stable [1]. This was demonstrated for a

sector of the main hydrological reach on the Turunchuk River (Table 1). In sectors with sand ridges in the Rioni River (experiment of 1 August 1975) and in the Turunchuk River (experiment of 6 August 1978) we obtained an approximately equal relationship of the contributions of energy of eddies of three types to the total kinetic energy of the flow (Table 1).

Table 1

Contribution of Eddies of Different Scales (%) to Total Kinetic Energy of Flow

Eddies	Uneroded or slightly eroded bottom	Eroded bottom	Sector with sand ridges
Small	14.5	8.4	29.4
Medium	35.0	29.6	37.9
Large	50.5	62.0	32.7

Accordingly, it can be proposed that the formation of sand ridges is related to the effect of small- and medium-scale disturbances. Taking into account that the ridges in both sectors during a time interval up to 7 days change little in shape and size, that is, have a slightly transformed profile, the bottom relief in these sectors can be considered stable. According to K. V. Grishanin, the considered sectors are also stable because the channel stability coefficient

$$M = h(gB)^{1/4}/Q^{1/2} \tag{1}$$

falls in the range 0.70-1.05 [3]. Thus, according to the energy criterion the river channel is stable in two cases: with an equilibrium contribution of energy from eddies (in this case we can speak of an even uneroded or slightly eroded bottom), and also in the case of an equal ratio of the energy contributions of eddies of each of the three types (in this case it is possible to speak of a stable channel with a moving bottom).

Now we will examine the structure of turbulence of river flow using the cross-spectral analysis method. An analysis of the spatial-temporal "cross" spectra affords a possibility for ascertaining the interrelationship of stationary random processes in the frequency region and to determine what frequencies (high or low) are responsible for the linear correlation between these processes. The "cross" spectral density of two random stationary processes X(t) and Y(t), called the $S_{xy}(w)$ function, is determined by the Fourier transform of the "cross" correlation function

$$S_{xy}(w) = \frac{1}{2\pi} \int_{-\infty}^{\infty} R_{xy}(\tau)\, e^{-iw\tau}\, d\tau. \tag{2}$$

$$S_{xy}(w) = P_{xy}(w) - iQ_{xy}(w),$$

where $P_{xy}(\omega)$ is the cosine part of the "cross" spectrum or cospectrum, $Q_{xy}(w)$ is the sine part of the "cross" spectrum or the quadrature spectrum.

In a joint analysis of stationary random processes it is convenient to use a coherence function characterizing the degree of the relationship between the frequency components of these processes at different frequencies.

$$C_0^2 = \frac{P_{xy}^2(w) + Q_{xy}^2(w)}{S_{xx}(w)\ S_{yy}(w)}, \tag{4}$$

where $S_{xx}(w)$ and $S_{yy}(w)$ are autonomous spectra of the processes X(t) and Y(t).

The coherence function is a positively determined function and is interpreted similar to the correlation coefficient. The C_0^2 values vary in the range from 0 to 1. If the coherence coefficient at some frequency is equal to zero, it is assumed that at this frequency a linear correlation between the X(t) and Y(t) processes is absent; if $C_0^2 \cong 1$, a linear correlation exists. Using the coherence function it is possible to obtain a full idea concerning the correlation of the two stationary random processes and determine what frequencies (high or low) govern the presence or absence of a linear correlation between these processes

At the present time we have a very small volume of data from investigations of the structure of river turbulence by the "cross" spectral analysis method. It is worth noting a study by S. Yokosi [6] which was carried out using investigations of turbulence in the Uji River and the Sosui canal. He determined the coherence functions between velocity fluctuations at two points situated at distances 0.5, 1.0, 1.5, 2.0 and 3.0 m apart. The coherence function curves published by S. Yokosi indicate that C_0^2 for the distances Δl = 0.5 m and Δl = 1.0 m is equal to 0.75 (w = 0.07 rad/sec); with Δl = 1.5 m C_0^2 does not exceed 0.55 (w = 0.31 rad/sec). Then the values of the coherence function continue to decrease, approaching zero when Δl = 3.0 m. With respect to atmospheric turbulence we must note the studies of N. Z. Pinus [4, 5].

In this study, using the "cross" spectral analysis method, we describe an investigation of the structure of turbulent eddy formations in a river flow. Using the data from our special measurements of velocity fluctuations at different points in depth, along the length and also in the cross section of the flow, and also along a sand ridge, we ascertained the influence exerted on the degree of correlation between velocity fluctuations at different horizons by the distance between the horizons. It can be noted that the coherence function differs with respect to the maximum value and the position of the significant peaks (that is, peaks exceeding the level of nonzero coherence) in the frequency interval.

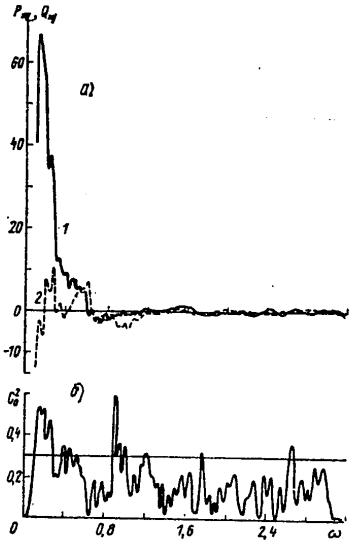

Fig. 1. Cospectrum P_{xy} (1), quadrature spectrum Q_{xy} (2) and coherence function C_0^2 of river flow velocity fluctuation (on the basis of data from experiment 8, 1971 -- horizons 0.6 H and 0.6 H + 1 m).

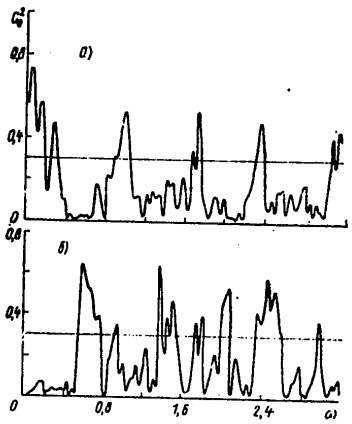

Fig. 2. Graph of coherence function. a) reach with even bottom (experiment 4, 1978, Turunchuk River, H = 6.78 m, horizons h = 3.70 and h = 3.20 m); b) reach with sand ridges (experiment 6, 1978, Turunchuk River, H = 2.0 m, horizons h = 1.35 m and h = 0.55 m).

Table 2

Maximum Coherence Values and Corresponding Frequency Values

По длине потока р. Турунчук 1			Основной гидроствор р. Турунчук 2			3 Участок с песчаными грядами					
						4 р. Турунчук			5 р. Рионн		
Δl м	C^2_{0max}	w_{max}	Δh м	C^2_{0max}	w_{max}	Δh м	C^2_{0max}	w_{max}	Δh м	C^2_{0max}	w_{max}
1,0	0,95	0,10	1,03	0,71	0,12	0,40	0,50	1,80	0,20	0,57	1,98
3,0	0,88	0,44	3,49	0,65	0,27	0,80	0,44	2,0	1,0	0,56	1,41
5,0	0,84	0,42	4,72	0,41	1,68	1,20	0,43	0,53	1,4	0,50	0,20
7,0	0,62	0,10	5,75	0,55	1,60	1,60	0,69	0,44	1,6	0,68	2,74
10,0	0,54	2,23									

KEY:

1. Along length of Turunchuk River
2. Main hydrological reach on Turunchuk
3. Reach with sand ridges
4. Turunchuk River
5. Rioni River

An analysis of the coherence curves shows that as a rule with an increase in the distance between the measurement points the coherence level decreases. For example, with a spacing of the points along the length of the flow $\Delta\ell$ = 1.0 m the coherence maximum is 0.95 at a frequency w = 2.23 rad/sec and with $\Delta\ell$ = 10 m C_0^2 = 0.54 at a frequency w = 1.23 rad/sec; in the depth of the flow the best correlation exists between near-lying layers, such as the surface and 0.2 H, 0.6 H and 0.8 H, 0.8 H and the bottom (Δ h = 0.90-1.30 m). The maximum value of the coherence coefficient decreases with increasing distance of the layer from the surface (Table 2). In the depth of the flow the coherence maximum is noted in the surface layer -- 0.2 H (Δ h = 1.03 m) and is 0.70-0.75. In most cases the lowest maximum coherence peak is observed in the surface layer -- 0.8 H (Δ h averaging 4.5 m), where C_0^2 = 0.40-0.45. We should note the rather high level of the correlation between the velocity fluctuations of the surface and bottom horizons with Δ h = 5.5-5.8 m C_0^2 = 0.55-0.65. This is indicative of the existence of stable eddy formations taking in the entire thickness of the flow. The regularities in change in $C_{0\ max}^2$ with depth in the flow are illustrated in Table 2 in the example of experiment 1, 7 August 1977, carried out at the main channel vertical of the main hydrological reach of the Turunchuk River. This is also correct for reaches with sand ridges in the Rioni and Turunchuk Rivers.

It was not possible to ascertain any regularities in change of the frequency corresponding to the maximum value of the coherence function. The values of the frequency corresponding to the first significant coherence peak were approximately the same as the frequencies of the maxima for the cospectrum and quadrature spectrum functions (Fig. 1).

These regularities are correct for all the considered reaches. A lessening of the correlation with an increase in the distance between measurement points is also noted over an even bottom and over sand ridges. However, the relationship between velocity fluctuations in reaches with different bottom relief is governed by the different frequency components. In a reach with sand ridges the presence of a correlation is usually governed by the high-frequency components, evidence of a predominance of medium and small eddies in the flow. This coincides with the result of determination of the predominating eddies in the flow by the dispersion analysis method [2]. In a reach with an even bottom (where, as indicated above, large eddies predominate) the highest correlation level in most cases is observed in the low-frequency region, corresponding to large-scale disturbances (Fig. 2).

On this basis it can be concluded that there is a difference in the mechanism of the effect of turbulent disturbances in reaches with different bottom relief and eddies of each of the three types play a definite role in the formation of bottom relief.

BIBLIOGRAPHY

1. Grinval'd, D. I., "Energy Characteristics of Turbulent Channel Flow," METEOROLOGIYA I GIDROLOGIYA (Meteorology and Hydrology), No 7, 1976.

2. Grinval'd, D. I., Yekhnich, M. P., "Influence of River Flow Turbulence on Bottom Relief," METEOROLOGIYA I GIDROLOGIYA, No 12, 1977.

3. Grishanin, K. V., USTOYCHIVOST' RSEL REK I KANALOV (Stability of River and Canal Channels), Leningrad, Gidrometeoizdat, 1974.

4. Pinus, N. Z., "Small-Scale Turbulent Heat Exchange in the Upper Troposphere and Lower Stratosphere," IZV. AN SSSR, FIZIKA ATMOSFERY I OKEANA (News of the USSR Academy of Sciences, Physics of the Atmosphere and Ocean), Vol 11, No 8, 1975.

5. Pinus, N. Z., "Experimental Investigations of Small-Scale Turbulence in the Upper Atmosphere," IZV. AN SSSR, FIZIKA ATMOSFERY I OKEANA, Vol 13, No 11, 1977.

6. Shoitiro Yokosi, "The Structure of River Turbulence," BULL. DISAS. PREV. INST. KYOTO UNIV., Vol 17, Part 2, 121, 1967.

UDC 551.5:633.14

METHOD FOR PREDICTING THE WINTERING OF WINTER RYE

Moscow METEOROLOGIYA I GIDROLOGIYA in Russian No 4, Apr 80 pp 101-106

[Article by V. A. Shavkunova, USSR Hydrometeorological Scientific Research Center, submitted for publication 15 October 1979]

Abstract: The author demonstrates the influence of agrometeorological conditions prevailing during the winter and the degree of development of winter rye plants in autumn on the thinning-out of plant density in winter and the area with dead plantings by the time of renewal of the growing season. Equations are proposed for describing these relationships. The possibility of using these equations in preparing a prediction of the wintering of winter rye is described.

[Text] Winter rye is one of the most important grain crops. It is more winter resistant and less demanding on the soil and moisture than is winter wheat. In our country the plantings of winter rye constitute 10-15 million hectares -- almost a third of the sown areas of all winter crops.

The greatest areas of winter rye in the USSR are occupied by the varieties Vyatka, Vyatka-2, Khar'kovskaya-55, Khar'kovskaya-60, Kazanskaya, Saratovskaya and Saratovskaya krupnozernaya. During recent years there has been considerable expansion of sowings of new, recently "regionalized" varieties of winter rye -- Gibridnaya, Belta, Leningradskaya tetra, Chulpan.

A common property for all the new varieties of winter rye is, as a rule, a greater resistance to unfavorable weather conditions and diseases than was true of the old varieties.

During the last 17 years winter rye in individual cases has completely perished during wintering in an area not greater than 30% of its sown area. The standard deviation of the extent of the area with dead plantings for Bryanskaya, Kalininskaya, Moskovskaya, Ryazanskaya, Tul'skaya and Yaroslavskaya Oblasts, Mariyskaya, Mordovskaya and Chuvashskaya ASSRs is 12-17%, but in most other oblasts -- 5-10% of their sown area.

In the nonchernozem zone of the European USSR, where the principal sown areas of winter rye are concentrated, the principal factors responsible for its death in winter are: in the northern and eastern parts of the zone -- wasting of plants as a result of their prolonged presence under a thick snow cover; in the west -- soaking of the plants in autumn and in the early spring due to overmoistening of the soil and flooding of the fields by melt water; in the south and southeast of the zone -- the freezing of the plants during the first half of the winter.

When there is an excess of moisture in the soil in autumn the plants have a lessened winter resistance. In these cases, with unfavorable wintering conditions, winter rye is damaged to a greater extent than is winter wheat [1]. Overmoistening leads to a decrease in the energy of germination and sprouting of seeds and also to a slowing of the subsequent growth of sprouts. Quantitative indices were established, as were methods for evaluating the conditions under which there is rotting of winter crops [4]. The degree of thinning of the fields as a result of soaking in depressed parts of the relief in fields is determined primarily by the duration of the period of flooding, water temperature and the condition of the plants.

The wasting away of rye plants occurs when a deep snow cover (more than 30 cm) remains on the ground for a long time, in combination with a soil temperature which is relatively high for winter at the depth of the tillering node (close to 0°C) and when there is shallow freezing of the soil (less than 50 cm). Under such conditions the plants expend a considerable quantity of the sugars accumulated from autumn on the respiration process and this leads to their exhaustion. Greatly weakened, they are attacked by fungi and perish [6].

The minimum temperature at the depth of the tillering node is an integral index of wintering conditions. It is dependent on the value of a complex of meteorological elements: minimum air temperature, depth of soil freezing, depth and density of the snow cover, etc.

The optimum conditions for the wintering of winter crops are created with a minimum soil temperature at the depth of the tillering node equal to -7, -8°C.

A regression analysis of the results of observations during the last ten years at the meteorological stations of the nonchernozem zone on the state of winter crops and the agrometeorological conditions of their wintering enabled us to refine the quantitative dependence of thinning-out of plant density with a wasting situation u% on the minimum temperature at the depth of the tillering node t_3. The correlation was quite close and has a nonlinear character:

$$M = \frac{h\,(gB)^{1/4}}{Q^{1/2}} \qquad (1)$$

$$u = 8{,}174\ t_3 + 0{,}130\ t_3^2 + 66{,}822,$$
$$R = 0{,}810 \pm 0{,}057, \quad S_u = \pm 14{,}32. \qquad (1)$$

The equation is valid with a t_3 value higher than -10°C and a snow cover depth over the course of five or more 10-day periods equal to 30 cm or more.

The dependence of thinning-out u% of winter rye in the case of such a damping (wasting) process on the minimum temperature at the depth of the tillering node t_3 and the degree of development of sown fields in autumn for the varieties most commonly used during recent years -- Vyatka, Vyatka-2, Gibrid-173, Gibrid-2, Khar'kovskaya-60 -- has the form

$$u = 7{,}039\ t_3 + 0{,}093\ t_3^2 - 27{,}514\ K_0 + 4{,}796\ K_0^2 + 93{,}106, \qquad (2)$$
$$R = 0{,}840 \pm 0{,}050, \quad S_u = \pm 13{,}225, \quad n = 53,$$

where n is the number of cases.

The minimum thinning-out of winter rye in individual fields was with K_0 = 3. Poorly thickening-out plantings and those which are overgrown thin out to a considerably greater degree under unfavorable wintering conditions (Table 1). A decrease in the minimum soil temperature at the depth of the tillering node to -7, -8°C also leads to a considerable decrease in the thinning-out of the plantings which are especially well developed in autumn (with K_0 equal to 2-3 shoots).

For example, the thinning-out of winter rye of the Gibrid-173 and Khar'kovskaya-60 varieties during 1977/1978 was the minimum with a minimum soil temperature at the depth of the tillering node -7°C (Table 2). A thick snow cover with a depth more than 30 cm was established in this year in late December-early January on poorly frozen soil. An increase in thinning-out was observed during the second half of winter. Its maximum value was for poorly developed crops, and also in fields with a minimum soil depth at the depth of the tillering node close to -1°C. The mean thinning-out in this case was 33-55%.

In Belorussia, where winter rye of the Belta variety for the most part is cultivated, the conditions for plant damping came about only in mid-February, when the snow cover depth attained 30 cm. Such a snow cover persisted for only three or four 10-day periods. Accordingly, there was no damage to winter crops from damping and thinning-out, according to the results of sprouting of plant samples, did not exceed 7% in February. The rye passed through the winter well.

We used the determined relationships of wintering conditions and the state of crops in winter in specific fields in regions of prolonged presence of a thick snow cover in ascertaining the dependence between the area with dead winter rye plants for the territory of an oblast and averaged by oblasts or republics and the values of the principal elements of the complex of agrometeorological conditions causing the death of plants from damping.

In the analysis we took the results of agrometeorological observations from 1968/69 through 1977/78 and data from an aerial reconnaissance of the state of plantings of winter rye in spring and autumn for all oblasts and republics within at least a part of whose territory a snow cover with a depth of more than 30 cm was formed on soil frozen to a shallow depth (less than 50 cm).

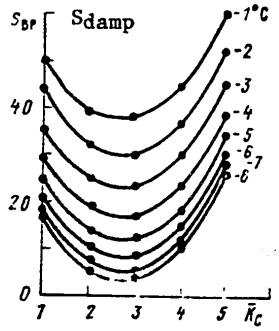

Fig. 1. Dependence of area with plantings of winter rye dead from damping S_{damp} % on bushiness K_0 and minimum soil temperature at depth of tillering node t_3.

As a result of carrying out correlation and regression analyses of long-term data on the area with dead plantings of winter rye due to damping and on the values of the principal meteorological factors determining the state of plantings after wintering, as in [4, 8] as the principal predictor we used the minimum soil temperature at the depth of the tillering node, averaged for an oblast. The dependence of the area with dead plantings of winter rye of the varieties cultivated in recent years on the minimum soil temperature at the depth of the tillering node, averaged for the territory of an oblast, is

$$S_{вр} = 10{,}945\,\bar{t}_3 + 0{,}582\,\bar{t}_3^2 + 54{,}712, \qquad (3)$$
$$R = 0{,}673 \pm 0{,}070, \quad S_{s_{вр}} = \pm 8{,}94, \quad n = 53,$$

[BP = damp(ing)] where S_{damp} is the area with dead plantings of winter rye; t_3 is the minimum soil temperature at the depth of the tillering node; n is the number of cases.

As already mentioned above, the state of the winter rye in spring after wintering is dependent to a considerable degree on the extent of development of winter crops after cessation of the growing season of plants in autumn. The bushiness of winter crops after cessation of the growing season is an indirect indicator of the degree of preparation of plants for wintering. Plantings which have thickened out have a higher winter resistance than those which have thickened out poorly or are overgrown.

Table 1

Thinning-out u % of Winter Rye in Individual Fields in Dependence on the Minimum Soil Temperature at the Depth of the Tillering Node t_3°C and Bushiness of Plants K_0 in Autumn in Regions of Damping (Wasting)

K_0	t_3							
	—1	—2	—3	—4	—5	—6	—7	—8
1	63,5	56,8	50,3	44,0	37,9	27,0	26,3	12,8
2	50,4	47,3	42,2	30,9	24,8	18,9	13,8	0,0
3	46,9	40,2	33,7	27,4	21,3	14,9	9,7	0,0
4	53,0	46,3	39,8	39,5	27,4	21,5	15,8	2,3
5	67,8	62,0	55,5	49,2	43,1	37,2	31,5	18,0

The mean oblast bushiness value also to some degree characterizes the supply of winter crops with heat and moisture, and indirectly the number of plantings in fallow and at the optimum times, since these plantings are also well developed and increase the average oblast bushiness value.

The dependence of the area with dead (due to damping) plantings of winter rye S_{damp} on the mean oblast bushiness value $\overline{K_0}$ and the minimum soil temperature at the depth of the tillering node t_3 for regionalized varieties has the form

$$S_{вр} = 9{,}708\,\overline{t_3} + 0{,}535\,\overline{t_3^2} - 23{,}709\,\overline{K_0} + 4{,}368\,\overline{K_0^2} + 78{,}853,$$
$$R = 0{,}700 \pm 0{,}070, \quad S_{s_{вр}} = \pm 8{,}64, \quad n = 53. \qquad (4)$$

[BP = damp(ing)]

The dependence of the area with dead (due to damping) plantings of winter rye S_{damp} on the minimum soil temperature at the depth of the tillering node t_3 and bushiness ($\overline{K_0}$) is represented in Fig. 1. It is easy to see that the area with dead plantings is the greater the higher the minimum soil temperature under a thick snow cover. For plantings with an average of three sprouts the percentage of death in spring is less than for poorly developed and highly bushing plantings.

The mean oblast minimum soil temperature at the depth of the tillering node is taken for the period from the first 10-day period in November to 20 February. It was established by V. A. Moiseychik in [8] that 20 February is the date before which in 97% of the years the minimum soil temperature for the entire winter is observed. An investigation of the seasonal variation of soil temperature at the depth of the tillering node indicated that when a thick snow cover is established (not less than 30 cm) on slightly frozen soil (less than 50 cm) the absolute minimum soil temperature at the depth of the tillering node in most cases is observed even during the second 10-day period in January. The further decrease in soil temperature is insignificant and can be ignored. Taking this into account, a long-range prediction of the state of winter rye in spring can be prepared already

Table 2

Thinning-Out u% as a Result of Damping of Winter Rye According to Data from Sprouting of Plant Samples Taken from Fields 1977/78

Станция (1)	Фаза развития K_0 (2)	Минимальная температура почвы на глубине узла кущения, °С (3)	Декада установления снежного покрова >30 см (4)	Глубина промерзания почвы, см (5)	Изреженность озимой ржи, % (6)			
					25 января (7)		23 февраля (8)	
					средняя (9)	максимальная (10)	средняя (9)	максимальная (10)
11 Гибрид-173								
14 Винница	всходы (23)	—5	1 декада января (25, 28)	24	13	40	18	44
15 Волхов	3-й лист (24)	—7	»	16	0	0	0	0
16 Максатиха	2,0	—1	3 декада декабря (27, 29)	13	29	36	30	37
17 Кашин	1,4	—4	»	24	9	15	11	13
12 Харьковская-60								
18 Йошкар-Ола	2,2	—4	3 декада декабря (27, 29)	50	5	11	5	6
19 Чухлома	3-й лист (24)	—7	»	50	2	6	0	0
13 Белта								
20 Барановичи	2,8	—5	2 декада января (26, 28)	50	0	0	0	0
21 Брест	1,2	—5	»	50	6	10	2	7
22 Ивацевичи	3,0	—6	1 декада января (25, 28)	50	1	3	2	4

KEY:

1. Station
2. Development phase K_0
3. Minimum soil temperature at depth of tillering node, °C
4. 10-day period of setting-in of snow cover $\geqslant$ 30 cm
5. Depth of soil freezing, cm
6. Thinning-out of winter rye, %
7. January
8. February
9. mean
10. maximum
11. Gibrid-173
12. Khar'kovskaya-60
13. Belta
14. Vinnitsa
15. Volkhov
16. Maksatikha
17. Kashin
18. Yoshkar-Ola
19. Chukhloma
20. Baranovichi
21. Brest
22. Ivatsevichi
23. sprouts
24. third leaf
25. 1st 10-day period
26. 2d 10-day period
27. 3d 10-day period
28. January
29. December

during the second ten-day period in January. Equations (3), (4) can be used for Bryanskaya, Kalininskaya, Moskovskaya, Ryazanskaya, Tul'skaya and Yaroslavskaya Oblasts and the Mariyskaya, Mordovskaya and Chuvashskaya ASSRs.

Table 3

Dependence of Area of Death of Winter Rye (S_{damp} % of Sown Area) on Mean Oblast Minimum Soil Temperature at Depth of Tillering Node ($\bar{t}_3$), Bushiness of Plants ($\bar{K}_0$) and Area With Poor State of Plantings (S_0% of Sown Area) in Regions of Winterkilling

№ п/п (1)	Вид уравнения (2)	Средняя квадратическая ошибка уравнения регрессии (3)	Коэффициент корреляции (4)
6	$S_{вр}$ (5) $=2{,}273\,\bar{t}_3+0{,}173\,\bar{t}_3^2+12{,}538$	6,48	0,847±0,038
7	$S_{вр}=0{,}555\,S_0+6{,}023\bar{t}_3+0{,}290\bar{t}_3^2+$ $+35{,}916$	3,50	0,848±0,056
8	$S_{вр}=4{,}033\,\bar{t}_3+0{,}215\,\bar{t}_3^2-4{,}211\,\bar{K}_0+$ $+0{,}521\,\bar{K}_0^2+31{,}451$	4,00	0,796±0,073
9	$S_{вр}=0{,}539\,S_0-0{,}189\,\bar{K}_0+6{,}005\,\bar{t}_3+$ $+0{,}283\,\bar{t}_3^2+35{,}152$	3,49	0,849±0,056

KEY:
1. No
2. Form of equation
3. Mean square error of regression equation
4. Correlation coefficient
5. BP = damp(ing)

During individual years the main reason for the death of winter rye in the investigated territory may be winterkilling.

The winterkilling of plantings occurs in years with an inadequate snow cover with a decrease in soil temperature at the depth of the tillering node below the critical temperature at which 50% of the plantings perish.

Regression and correlation analysis of long-term data on winter rye enabled us to derive a number of dependences for computing the area of the death of winter ryes in years when the main reason for death was winterkilling (Table 3).

The equations are valid at a soil temperature below -10°C.

The value of the mean error of these equations is less than the admissible forecasting error -- 0.67σ, where σ is the mean square area with plantings of winter crops killed in percent of the sown area in an oblast. Accordingly, these equations, especially (6) and (8), can be used in preparing a forecast of the wintering of winter rye in years with the winterkilling of plants. However, the best results are obtained when computing the expected area of death of winter rye using equation (8).

All the cited equations, both in regions with thick and in regions with an inadequate snow cover, make it possible to prepare forecasts of the state of winter rye in spring for 2 or 3 months in advance. Knowing in advance the reasons for the damage of winter crops and the extent of the area in which it is expected, by the application of a number of agricultural engineering measures, including the undersowing and resowing of dead winter crops in spring by spring crops, it is possible to reduce considerably the losses of grain yield. In the Nonchernozem zone the death of winter crops can be completely eliminated or considerably reduced far more successfully than in any other zone in the country when there is proper cultivation and good care for the plantings during the autumn and winter-spring periods.

***

BIBLIOGRAPHY

1. Beletskaya, Ye. K., "Comparative Resistance of Winter Crops to Inundation at Different Temperatures," USTOYCHIVOST' RASTENIY K NEBLAGOPRIYATNYM TEMPERATURNYM USLOVIYAM SREDY (Resistance of Plants to Unfavorable Environmental Temperature Conditions), Kiev, Naukova Dumka, 1976.

2. Beletskaya, Ye. K., Ostaplyuk, Ye. D., "Growth and Formation of Frost Resistance of Winter Crops in Dependence on Water Supply Conditions," USTOYCHIVOST' RASTENIY K NEBLAGOPRIYATNYM USLOVIYAM SREDY, Kiev, Naukova Dumka, 1976.

3. Kuperman, F. M., Moiseychik, V. A., VYPREVANIYE OZIMYKH KUL'TUR (Damping of Winter Crops), Leningrad, Gidrometeoizdat, 1977.

4. Moiseychik, V. A., AGROMETEOROLOGICHESKIYE USLOVIYA I PEREZIMOVKA OZIMYKH KUL'TUR (Agrometeorological Conditions and Wintering of Winter Crops), Leningrad, Gidrometeoizdat, 1975.

5. Moiseychik, V. A., "Agrometeorological Conditions for the Wintering of Crops and Methods for Preparing Long-Range Forecasts of the State of Winter Grain Crops in Spring," AGROMETEOROLOGICHESKIYE ASPEKTY PEREZIMOVKI RASTENIY (Agrometeorological Aspects of Wintering of Plants), Leningrad, Gidrometeoizdat, 1977.

6. Moiseychik, V. A., "Agrometeorological Conditions for the Wintering of Winter Crops," AGROMETEOROLOGICHESKIYE USLOVIYA I PRODUKTIVNOST' SEL'SKOGO KHOZYAYSTVA NECHERNOZEMNOY ZONY RSFSR (Agrometeorological Conditions and Productivity of Agriculture in the Nonchernozem Zone of the RSFSR), Leningrad, Gidrometeoizdat, 1978.

7. Moiseychik, V. A., SOSTAVLENIYE DOLGOSROCHNOGO PROGNOZA VYPREVANIYA OZIMYKH ZERNOVYKH KUL'TUR (Preparation of a Long-Range Forecast of the Damping of Winter Grain Crops) METODICHESKIYE UKAZANIYA (Methodological Instructions), Moscow, Gidrometeoizdat, 1971.

8. Moiseychik, V. A., SOSTAVLENIYE DOLGOSROCHNYKH AGROMETEOROLOGICHESKIKH PROGNOZOV PEREZIMOVKI OZIMYKH KUL'TUR NA TERRITORII OBLASTEY, RESPUBLIK I V TSELOM PO SSSR: METODICHESKOYE UKAZANIYE (Preparation of Long-Range Agrometeorological Forecasts of the Wintering of Winter Crops in the Territory of Oblasts, Republics and the USSR as a Whole: Systematic Instructions), Leningrad, Gidrometeoizdat, 1978.

9. Tiunov, A. N., Glukhikh, K. A., Khor'kova, O. A., OZIMAYA ROZH' (Winter Rye), Moscow, Kolos, 1969.

UDC 551.46.08

OPTIMUM CALIBRATION OF REMOTE INSTRUMENTS USING THE RESULTS OF DIRECT MEASUREMENTS IN THE OCEAN

Moscow METEOROLOGIYA I GIDROLOGIYA in Russian No 4, Apr 80 pp 107-112

[Article by Candidate of Physical and Mathematical Sciences S. V. Dotsenko and L. G. Salivon, Marine Hydrophysical Institute, submitted for publication 24 April 1979]

Abstract: A study was made of the possibilities of calibrating remote instruments on the basis of direct measurement instruments for the case of a "nonfrozen-in" field and models of fields and instrument functions close to real fields and instrument functions. It is shown that the relative calibration error is considerably reduced if the direct measurements are subjected to time averaging with some optimum weight.

[Text] Instrumentation for remote noncontact sounding is coming into increasingly broader use in the practice of physical measurements at sea. Remote instruments, in comparison with direct contact measurement instruments, have a number of advantages. One of the most important is the possibility of measuring the physical characteristics of the ocean at points situated at a great distance from them. This makes it possible to install remote sounding instruments both on ships and on aircraft, affording new possibilities for studying the ocean at the most different spatial and temporal scales.

The use of remote instruments can be adequately effective only when they ensure the required measurement accuracy. The differences between the readings of a remote instrument and the readings of a direct contact measurement instrument, intended for measuring the same physical parameter and situated at the center of a resolution element of a remote instrument sensor, are due to the following factors:

1. Characteristic noise of the remote instrument. This is reduced by employing special sensing elements and measurement circuits.

2. The influence of hydrometeorological factors for whose measurement the particular instrument is intended (influence of physical parameters of the atmosphere on the results of measurement of all the physical characteristics of the ocean, influence of the state of the sea surface on the results of temperature measurement, etc.). A decrease in these factors is achieved by the proper choice of the spectral windows of remote instruments, appropriate processing of the output signals of the latter and calibration of remote instruments on the basis of measurements of the physical characteristics of definite regions of the ocean (polygons) made by direct direct methods.

3. Differences in the averaging scales of the measured field of the compared instruments. Any direct-measurement contact instrument used under sea conditions in measurements both from a ship and from autonomous craft or buoy has an incomparably lesser field averaging scale than a remote instrument. A remote instrument carries out spatial averaging of the measured field with some instrument function $h(\vec{r})$, describing the contribution of each volume of the measured field to the total instrument output signal.

The instrument function $h(\vec{r})$ is determined by the directional diagram of the measuring instrument sensor, the orientation of this diagram relative to the sea surface and the height at which the instrument is positioned above sea level. The broader the instrument directional diagram and the higher it is situated above sea level, the larger is the resolution element of the remote instrument used in field averaging. For example, the noncontact devices used in measuring temperature which are carried aboard artificial earth satellites can have radii of the resolution elements of several kilometers [1]. Accordingly, on the basis of signals from direct measurement signals containing a very broad spectrum of high-frequency field fluctuations it is impossible directly and with the required accuracy to evaluate the behavior of the low-frequency signal at the output of the remote instrument, considerably smoothed by its instrument function. In order to increase calibration accuracy it is necessary to carry out preliminary averaging (smoothing) of the signals of polygon instruments. It is evident that the closer the scale and the weighting function in averaging of signals of direct measuring detectors to the scale and instrument function of the sensors of remote instruments, the higher will be the calibration accuracy, and accordingly, the greater will be the accuracy of remote measurements as a whole.

We will find methods for the optimum averaging of signals of direct measurement contact instruments intended for calibration of remote instruments and we will evaluate the calibration errors observed in such cases. The parameters of the field obtained by some optimum averaging of the signal of a direct-measurement contact instrument will be used as the standard (Y_{st}).

There are three possible methods for such averaging: spatial, temporal and spatial-temporal. The authors of [4] investigated a method for the optimum spatial averaging of the signals of a set of different numbers of direct

measurement instruments and it is demonstrated that a high accuracy in finding the standard field parameters for comparison of the results of remote measurement with it, even with an optimum configuration of the network of direct measurement instruments relative to a resolution element of the remote instrument sensor, requires the simultaneous use of a great number of direct measurement instruments distributed over a considerable area of the polygon. Such an organization of an experiment for determining the standard field parameters can be technically difficult to implement. Spatial-temporal averaging is accomplished by temporal averaging of the signals of several direct measurement instruments and also requires considerable technical means.

We will investigate the temporal averaging of the signal of a contact instrument, requiring the use of only one instrument, and we will find the optimum method for such averaging ensuring the best calibration accuracy. We will assume that the following conditions are satisfied:

1. The measured field is centered, uniform, isotropic and "nonfrozen-in." The model of anisotropic "nonfrozen-in" fields was examined in detail in studies [3,5,6]. In describing them it is sufficient to know the multidimensional spectra $G_n(\vec{\alpha})$; the spectra with $n>1$ can be found from the known one-dimensional spectrum $G_1(\alpha)$. Under isotropicity conditions these fields are characterized by the following values: spatial correlation interval r_x, correlation time interval τ_c and mean velocity $\vec{v}_0$ of field movement relative to the contact instrument sensor. The degree of "freezing-in" of the field is characterized by the dimensionless parameter $\eta = v_0\tau_c/r_x$, and it is the greater the greater the η value.

2. The instruments for both direct and remote measurement are inertialess. The contact instruments have point sensors.

Now we will examine the following scheme for obtaining the standard value of a field by a direct measurement instrument intended for calibration of a remote instrument. Assume that a direct measurement instrument registers field values $X(\vec{r}, t)$ at some point in a polygon used as the origin of coordinates $\vec{r} = 0$. It is evident that the changes in these values are related to both the movement of the field relative to the fixed instrument and its temporal evolution, determined by the "nonfrozen-in" properties [19]. Accordingly, applicable to a direct measurement instrument it is necessary to take into account both the velocity of field movement $\vec{v}_0$ and its "nonfrozen-in" properties. Using some weighting function $U(\tau)$, whose optimum form will be determined below, at each moment in time t it is possible to obtain a mean weighted signal at the output of the direct measurement instrument

[пр = direct]
$$Y_{np}(t) = \int_{-\infty}^{\infty} X[\vec{v}_0 \times (t-\tau);\ t-\tau]\, U(\tau)\, d\tau. \qquad (1)$$

We will assume that at the time t = 0 it is necessary, using the transform (1), to obtain the best evaluation of that signal value at the output of the remote instrument which the latter would have in the absence of

distorting factors (for example, the atmosphere). Since the remote instrument is usually mounted on rapidly moving carriers, the field for it can be considered "frozen-in" and the strength of the undistorted signal at its output at the time t = 0 is

[Д = remote]
$$Y_д = \int X(-\vec{\rho}; 0)\, h(\vec{\rho})\, d\vec{\rho}. \qquad (2)$$

Thus, optimum calibration of a remote instrument essentially involves obtaining the mean weighted value of the signal at the output of the direct measurement instrument

[Пр = direct]
$$Y_{пр}(0) = \int_{-\infty}^{\infty} X(-\vec{v}_0\tau; -\tau)\, U(\tau)\, d\tau, \qquad (3)$$

differing least from the Y_{remote} value determined by formula (2) and its use for comparison with the real signal value at the output of the remote instrument at the time t = 0.

The mean square error in comparison of the Y_{remote} and $Y_{direct}(0)$ values is

[Пр = direct; Д = remote]
$$\varepsilon^2 = \overline{[Y_{пр}(0) - Y_д]^2}.$$

It was demonstrated in [7] that the optimum weighting function $U(\tau)$, ensuring the minimum of the ε^2 value, should have the spectrum

[ОПТ = opt]
$$\tilde{U}_{опт}(\omega) = \frac{\sqrt{1+\gamma_l^2}}{G_1\left(\frac{1}{\sqrt{1+\gamma_l^2}}\frac{\omega\tau_c}{r_x}\right)} \int G_3\left[\sqrt{|\vec{\beta}|^2 + \left(\frac{\tau_c}{r_x}\right)^2 (\omega - \vec{\beta}\vec{v}_0)^2}\right] \tilde{h}^*(\vec{\beta})\, d\vec{\beta}, \qquad (4)$$

where $\tilde{h}(\vec{\beta})$ is the spectrum of the instrument function h(r). The square of the absolute error in optimum calibration is

$$\varepsilon^2_{мин} = \frac{\tau_c}{r_x} \int G_3\left[\sqrt{|\vec{\alpha}|^2 + \left(\frac{\tau_c\omega}{r_x}\right)^2}\right] |\tilde{U}_{опт}(\omega + \vec{\alpha}\vec{v}_0) - \tilde{h}(\vec{\alpha})|^2\, d\vec{\alpha}\, d\omega. \qquad (5)$$

However, if the calibration is accomplished on the basis of one instantaneous reading of the output signal of a direct measurement point instrument without averaging of the registered data, then the square of the absolute calibration error is

$$\varepsilon^2 = \int G_2(|\vec{\alpha}|)\, |1 - \tilde{h}(\vec{\alpha})|^2\, d\vec{\alpha}$$

and is not dependent on the degree to which the field is "frozen-in."

The gain in accuracy of optimum calibration in comparison with calibration on the basis of a single point measurement has the value

[ОПТ = opt]
$$\mu = \frac{\varepsilon^2}{\varepsilon^2_{опт}}.$$

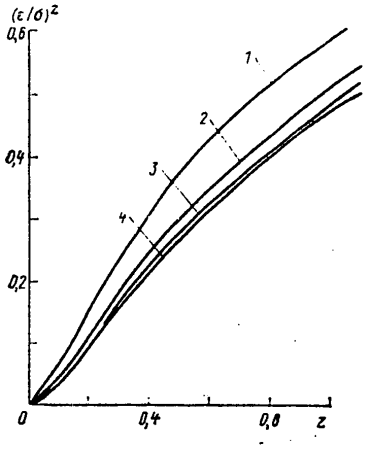

Fig. 1. Error in measuring a field with a remote instrument with p = 0.5. 1) ν = 1.0; 2) ν = 2.0; 3) ν = 3.0; 4) ν = 4.0

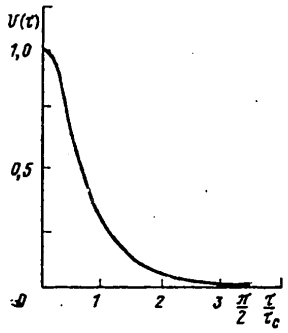

Fig. 2. Optimum weighting function for p = 0.5; 2) 0.5; η = 4; ν = 1.5

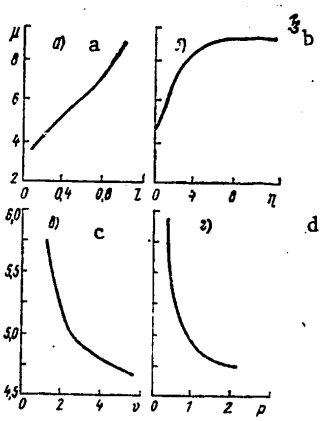

Fig. 3. Dependence of gain in accuracy in optimum calibration on different field parameters and instrument sensor with p = 0.5. a) on relative radius of instrument resolution element z with ν = 1.5; η = 1; b) on "frozen-in" parameter η with z = 0.5; ν = 1.5; c) on sensor parameter ν with z = 0.5; η = 1; d) on field parameter p with ν = 1.5; η = 1.

The authors of [7], on the basis of the derived expressions, investigated the calibration of a remote instrument with a sensor having an axially symmetric bell-shaped instrument function, using a field whose spectrum also has a bell shape. Such models of the field and sensor made it possible to carry out computations in analytical form to a full extent and confirm the high effectiveness of the considered method.

The field and instrument models considered in this study reflect the adequately broad classes encountered in practical work. Thus, it is postulated that one-dimensional field spectra have the form

$$G_1(\alpha) = \frac{\sigma^2 r_x}{\pi}\left[1 + \left(\frac{\alpha r_x}{\varkappa_p}\right)^2\right]^{-(p+1/2)}, \qquad (6)$$

where σ^2 is field dispersion, p is a parameter characterizing the degree of dropoff of its spectrum, $\Gamma(x)$ is the gamma function and the $\varkappa_p$ coefficient has the form

$$\varkappa_p = \sqrt{\pi}\,\frac{\Gamma\left(p+\frac{1}{2}\right)}{\Gamma(p)}.$$

A change in the p parameter makes it possible to examine a broad class of fields. With $p = 1/2$ an exponential autocorrelation field function corresponds to the spectrum (6), that is, the field in this case is not differentiable. An increase in the p parameter leads to an increase in field smoothness. With $p \to \infty$ the spectrum (6) acquires a bell-shaped form, that is, the field has all the derivatives.

The instrument functions of the sensors of remote instruments are described by the expressions

$$h(r) = \frac{\varkappa^2_{\nu-1/2}}{2\pi(2\nu-1)R_x^2}\,\frac{2}{\Gamma\left(\nu-\frac{1}{2}\right)}\left(\frac{\varkappa_{\nu-1/2} r}{2R_x}\right)^{\nu-1/2} K_{\nu-1/2}\left(\varkappa_{\nu-1/2}\frac{r}{R_x}\right) \qquad (7)$$

where $\nu > 1/2$, $K_\lambda(x)$ is a Macdonald function, and R_x is the characteristic radius of a sensor resolution element. Using them, with an appropriate choice of R_x and ν, it is possible to approximate many real monotonically decreasing instrument functions. In particular, with $\nu \to \infty$ the function h(r) acquires a bell shape. The spectra of the functions (7)

$$\tilde{h}(\alpha) = \left[1 + \left(\frac{R_x \alpha}{\varkappa_{\nu-1/2}}\right)^2\right]^{-(\nu+1/2)}$$

with large α decrease as $\alpha^{-(2\nu+1)}$, that is the ν parameter characterizes the degree of their decrease.

No analytical solution of the formulated problem is possible under the condition that the field spectrum is given by formula (6) and the instrument function is given by expression (7). Accordingly, we prepared a program for computing the above-mentioned parameters on an electronic computer. The

program was difficult to develop due to the necessity for computing the triple integrals with infinite limits and the presence in formula (5) of the spectrum of the weighting function $\tilde{U}(\omega)$ with a biased argument. The required computation accuracy was ensured by replacement of the variables in the integrals, leading to the possibility of integration in finite limits, and by use of the Gauss quadrature formulas.

As already mentioned, the simplest method for calibrating a remote instrument is calibration on the basis of one instantaneous reading of a point contact measurement instrument. The dependence of the square of the error arising in this case on the ratio $z = R_x/r_x$ of the characteristic radius of a resolution element to the characteristic scale of the field for $p = 1/2$ and different ν is represented in Fig. 1. The $(\varepsilon/\sigma)^2$ value increases monotonically with an increase in z, assuming lesser values with larger ν, that is, with a greater degree of smoothing of the field by the sensor. If the calibration accuracy is considered acceptable with $\varepsilon/\sigma = 0.3$, the simplest calibration is accomplished with $z = 0.15$. An increase in the necessary calibration accuracy still further reduces this value. Accordingly, using one point reading it is possible to calibrate instruments the radius of whose resolution element is small in comparison with the characteristic scale of the measured field.

Now we will turn to optimum calibration with temporal averaging. A typical optimum weighting function $U(\tau)$, whose spectrum was computed using formula (4), and then subjected to a Fourier transform, is shown in Fig. 2 for $\tau \geqslant 0$. This function is symmetric relative to the point $\tau = 0$ and decreases with an increase in τ. Thus, in accordance with the procedure (3) in the optimum calibration process there is an averaging of data from measurement of the field by a point instrument with the weight $U(\tau)$, which has considerable importance in some finite region, which corresponds to low-frequency filtering of direct measurement data. Accordingly, in order to bring the values of the data from direct contact measurements closer to the values of remote measurements, spatially averaged due to the presence of a finite spatial resolution element, the data from the contact measurements, obtained at one field point, were subjected to temporal averaging. Such a procedure is optimum if the spectrum of the weighting function has the form (4). It cannot lead to a complete exclusion of calibration error because in remote sounding there is two-dimensional spatial averaging of the field, whereas in contact measurements -- one-dimensional averaging in time. As a result of the different number of measurements of the averaging functions the signals of the remote instrument and the smoothed signal of the contact instrument on the average will always have some differences from one another.

The effectiveness of use of the optimum smoothing procedure in calibration can be evaluated from Fig. 3, which represents the dependence of the gain in the accuracy of this calibration on different field and instrument parameters.

Figure 3a indicates that optimum calibration is the more effective the greater is the radius of a resolution element of the remote instrument in comparison with the characteristic field scale, that is, specifically in the region where calibration on the basis of a single reading gives a high error. This, for example, makes it possible, with $\eta = 1$, to carry out calibration with the above-mentioned accuracy to z = 1. Accordingly, in this case there can be calibration of remote instruments having a large resolution element on the basis of physical fields in the ocean. However, it gives an appreciable accuracy gain also with small resolution elements.

With an increase in the degree to which the field is "frozen-in" the accuracy gain increases. This increase occurs particularly sharply with $\eta < 4$; as can be seen from Fig. 3b, saturation sets in from the time $\eta = 0$. Accordingly, it is best to carry out calibration using "frozen-in" fields, that is, those fields which experience weak evolution with time.

The gain increases with a decrease in the parameter ν characterizing the shape of the instrument function for the remote instrument sensor (Fig. 3c). For instruments with instrument functions of an exponential shape the gain is greater than for instruments having a bell-shaped instrument function.

With an increase in the coefficient p, determining the degree of field smoothness, the gain decreases, but remains quite high. Therefore, the effect of use of optimum calibration is higher when it is carried out using a field with an exponential autocorrelation function than when using a field with a bell-shaped autocorrelation function.

Now we will illustrate the possibility of increasing calibration accuracy when measurements are made by remote instruments with the assistance of the described optimum calibration method, employing the instrument functions of wide-angle and five-channel radiometers aboard the TIROS II and the radiometer aboard the Cosmos-149 satellite. When these instruments are installed on artificial earth satellites with an orbital altitude h = 500 km the radii of the resolution elements R_x of their sensors [8] are 240, 27.8 and 12.8 km respectively.

Taking into account that the characteristic spatial correlation radius of surface temperatures in the Black Sea [2] is r_x = 130 km and that for the enumerated radiometers the z parameter has values 1.85, 0.214 and 0.0985, we find that the calibration errors for these instruments based on a single instantaneous reading have values 84, 33 and 27%. As indicated in Fig. 3, the use of optimum calibration gives a gain μ in measurement accuracy which is equal to 12, 3.25 and 3 respectively (with η = 1), which reduces the calibration error to values 24.3, 18.3 and 15.6%.

Thus, the optimum processing of signals at the output of direct measurement instruments considerably increases the accuracy in calibrating remote instruments. The greatest gain is noted for wide-angle instruments, whereas

the greatest calibration accuracy is for instruments with a narrow angle. Optimum calibration gives a considerable accuracy gain in comparison with calibration on the basis of a single reading and is the more feasible the greater the ratio z of the radius of a resolution element of the instrument sensor to the characteristic field scale.

Similar computations made for an altitude of lifting of the sensor h = 10 km (which occurs when the remote instruments are carried aboard an aircraft) will make it possible to reduce the measurement error from 6 to 4.3%, from 7 to 5% and from 1.7 to 1% respectively. The gain for low altitudes is considerably lower, but as indicated by the comparison, the absolute calibration error for these altitudes is relatively small.

BIBLIOGRAPHY

1. Astkheymer, R., Vaard, De R., Dzhekson, Ye., "IR Radiometers on the TIROS II Satellite," RAKETY I ISKUSSTVENNYYE SPUTNIKI V METEOROLOGII (Rockets and Artificial Satellites in Meteorology), Moscow, IL, 1963.

2. Belyayev, V. I., OBRABOTKA I TEORETICHESKIY ANALIZ OKEANOGRAFICHESKIKH NABLYUDENIY (Processing and Theoretical Analysis of Oceanographic Observations), Kiev, Naukova Dumka, 1973.

3. Gusev, V. D., "Correlation Method for Investigating Large Ionospheric Inhomogeneities," VESTNIK MGU. SERIYA MATEMATIKI, MEKHANIKI, ASTRONOMII, FIZIKI, KHIMII (Herald of Moscow State University. Series on Mathematics, Mechanics, Astronomy, Physics and Chemistry), No 6, 1959.

4. Dotsenko, S. V., Ryzhenko, V. A., "Optimum Calibration of Remote Instruments from Readings of Direct Measurement Instruments," MORSKIYE GIDROFIZICHESKIYE ISSLEDOVANIYA (Sea Hydrophysical Investigations), No 4(71), 1975.

5. Dotsenko, S. V., "On Mathematical Description of Random Scalar Anisotropic Fields," MORSKIYE GIDROFIZICHESKIYE ISSLEDOVANIYA, No 1(51), 1971.

6. Dotsenko, S. V., "Spectra of Random Scalar Anisotropic Hydrophysical Fields," MORSKIYE GIDROFIZICHESKIYE ISSLEDOVANIYA, No 3(53), 1971.

7. Dotsenko, S. V., Salivon, L. G., "Optimum Calibration of Remote Instruments Using Time Averaging," MORSKIYE GIDROFIZICHESKIYE ISSLEDOVANIYA, No 4(75), 1976.

8. Dotsenko, S. V., Nedovesov, A. N., Poplavskaya, M. G., Ryzhenko, V. A., "Spatial-Spectral Characteristics of Remote Sensors," MORSKIYE GIDROFIZICHESKIYE ISSLEDOVANIYA, No 2(65), 1974.

9. Monin, A. S., Yaglom, A. M., STATISTICHESKAYA GIDROMEKHANIKA (Statistical Hydromechanics), Part 2, Moscow, Nauka, 1967.

UDC 551.509.314

EMPIRICAL ORTHOGONAL FUNCTIONS METHOD AND ITS APPLICATION IN METEOROLOGY

Moscow METEOROLOGIYA I GIDROLOGIYA in Russian No 4, Apr 80 pp 113-119

[Article by Candidate of Physical and Mathematical Sciences M. I. Fortus, Institute of Atmospheric Physics, submitted for publication 26 June 1979]

Abstract: This is a brief review of studies carried out for the most part after 1970 in which the empirical orthogonal functions method is used for the purpose of an analysis or prediction of meteorological fields and also studies in which there is a discussion of the methods for evaluating empirical orthogonal functions on the basis of empirical data. Particular attention is devoted to some theoretical problems related to the specifics of application of the empirical orthogonal functions method in meteorology.

[Text] Since the time of the studies of Lorenz, Bagrov and Obukhov (see [1]) the empirical orthogonal functions method has become popular in meteorology; hundreds of studies have appeared in which this method is used as one of the principal methods for drawing statistical conclusions from meteorological information. A monograph [5] appearing in 1970 presented and analyzed the results of the investigations made up to that time in which the EOF method was used for studying the statistical structure of meteorological fields and also in forecasting problems, the interpretation of data from indirect measurements, etc. [A quite detailed bibliography is also cited there.] During the time which has elapsed since 1970 the number of studies in which the EOF method is used has increased still more. In this connection it seems to us that the time has come to examine some of these studies in detail, devoting particular attention to some theoretical problems related to the specifics of use of the EOF method in meteorology which have either not been discussed at all or which were not covered sufficiently completely in monograph [5]. We will discuss for the most part studies published after 1970; this review article can be considered a supplement to the book [5].

Assume that the field of some element F(x, t), dependent on the space coordinates x and the time t, at the time t is described by a set of numbers $\{F(x_i, t), i = 1,\ldots, m\} = \{F_i(t)\}$. Most frequently the empirical orthogonal functions are determined as the normalized base of m-dimensional vectors $\varphi^j = \{\varphi_i^j, i = 1,\ldots,m\}$, being the eigenvectors of the matrix of covariations

$$B_{ik} = B(x_i, x_k) = \overline{F_i'(t)\, F_k'(t)}, \quad i, k = 1, \ldots, m, \tag{1}$$

where the line at top denotes time averaging (in actuality -- on the basis of the available sample) and the prime denotes deviation of the $F_i(t)$ value from its mean value $\overline{F_i}(t)$. It is important that these eigenvectors are numbered in decreasing order of the corresponding eigenvalues λ_j (which are non-negative because the B matrix is always non-negatively determined). The vector $\{F_i(t)\}$ can be represented precisely in the form of an expansion of m vectors of a base of natural orthogonal functions (as for any other orthonormalized base in m-dimensional space). The advantage of an expansion in empirical orthogonal functions is that if we limit ourselves to a number of terms $p < m$ less than m:

$$F_i'(t) \approx \sum_{j=1}^{p} a_j(t)\, \varphi_i^j, \quad i = 1, \ldots, m, \tag{2}$$

the mean square error $\sigma(p)$ in the approximation of (2) will be minimum for a base consisting of empirical orthogonal functions (if we discard terms corresponding to empirical orthogonal functions with maximum numbers). The square of the error $\sigma(p)$ is determined using the formula

$$\overline{\sigma^2}(p) = \overline{\sum_{i=1}^{m} \left[F_i'(t) - \sum_{j=1}^{p} a_j(t)\, \varphi_i^j \right]^2}. \tag{3}$$

For most meteorological fields the $\sigma(p)$ value for p values small in comparison with m is already quite small (precisely this circumstance also determines the desirability of expansion in empirical orthogonal functions). Therefore, expansion in empirical orthogonal functions makes it possible to represent the most important information on the F'(x,t) field by means of a small number of terms in the series, and specifically, the F'(x,t) field considered at m points x_i, $i = 1,\ldots,m$ at each moment in time can be precisely described by p values $a_1(t),\ldots, a_p(t)$, (where $p < m$), by the mentioned main components. Their mean values are equal to zero:

$$\overline{a_j(t)} = 0, \quad j = 1, \ldots, p,$$

The sample correlations between them are also equal to zero and the dispersions coincide with the corresponding eigenvalues of the B matrix:

$$\overline{a_j(t)\, a_k(t)} = \lambda_j \delta_{jk}, \quad \delta_{jk} = \begin{cases} 1 \text{ with } j = k \\ 0 \text{ with } j \neq k \end{cases}. \tag{4}$$

In this sense expansion in empirical orthogonal functions can be called an expansion into uncorrelated components. In the particular case when the field is dependent on one variable the main components are the uncorrelated numerical coefficients. Most frequently the sole argument will be time. Then the empirical orthogonal functions are called time functions.

First we will examine one important class of fields -- statistically homogeneous fields, when the space coordinates x are the argument, and statistically stationary processes when the argument is time t. In this case the covariation matrix is dependent only on the difference of its arguments. This condition is satisfied for several time series (see below) for the cloud cover field (or the brightness field), which are measured from satellites and are functions of the horizontal coordinate directed along a parallel and time, in the case of not very great spatial scales, and also for the geopotential field in the middle latitudes with distances along the horizontal not greater than 2,000-3,000 km.

Now it is convenient to proceed from a description of a field by a set of its values at a finite number of points x_i, $i = 1, \ldots, m$ to its description by means of functions of the continuous argument x. Proceeding in this way exerts little influence on the large-scale empirical orthogonal functions of interest to us, and on the other hand makes it possible to use their more convenient analytical description. In place of the covariation matrix $B(x_i, x_k)$ we will consider the covariation function of the continuous argument

$$B(x, y) = B(y - x), \tag{5}$$

and in place of the vectors $\varphi^j = \{\varphi^j(x_i)\}$ -- the functions $\varphi^j(x)$. These functions, which as before we will call empirical orthogonal functions, are eigenfunctions of the integral operator

$$\int_G B(x - y)\, \varphi^j(y)\, dy = \lambda_j \varphi^j(x), \quad x \in G. \tag{6}$$

Here g is the region in which the F(x) field is considered. We will assume that the G region is limited; then the eigenfunctions will be used in the calculations. In the case of a process dependent on time, the argument in (6) is time t, and G is a segment [-T/2, T/2] (the corresponding eigenvalues will be denoted ν_j).

For statistically homogeneous fields (stationary processes), together with the covariation function it is useful to introduce into consideration the spectral density f(k) (accordingly, $f(\omega)$), unambiguously determined from from the covariation function by the formula

$$f(k) = 1/(2\pi)^r \int B(x) \exp(-ikx)\, dx, \tag{7}$$

where r is the dimensionality of space, and accordingly

$$f(\omega) = 1/2\pi \int_{-\infty}^{\infty} B(t) \exp(-i\omega t)\, dt. \tag{8}$$

In [10-11] a study was made of the properties of solutions of equation (6) and an algorithm for their computation was described. It was found that with unlimited expansion of the G region the greatest eigenvalue $\lambda_1 = \lambda_{max}$ of equation (6) is related to the spectrum f(k) by the asymptotic expression

$$\lambda_1 = (2\pi)^r f(k_{max}), \tag{9}$$

where k_{max} is the point of the absolute maximum of the f function.

In [10] equation (6) was solved for the case of a stationary process stipulated in a time segment with the length T when the covariation function is a linear combination of functions in the form

$$\exp\{-\alpha t\};\ \cos\beta t \exp\{-\alpha t\};\ \sin\beta t \exp\{-\alpha t\}$$

(that is, spectral density is a fractional-rational function of ω). It is shown that with sufficiently great T (for example, by an order of magnitude exceeding the correlation attenuation time), the $\varphi^j(t)$ functions are close to the trigonometric functions:

$$\varphi^j(t) \approx \cos\omega_j t\ (\sin\omega_j t). \tag{10}$$

An algorithm is given for computing ω_j, from which it is possible to determine the eigenvalues ν_j from the expression

$$2\pi f(\omega_j) = \nu_j. \tag{11}$$

On the basis of (10) and (11), and making use of the spectral density form it is possible to judge the sequence of "eigenfrequencies" ω_j. We will examine the two most typical cases.

1. The spectral density has one absolute maximum with $\omega = 0$, that is, $\omega_1 = \omega_{max} = 0$ and decreases monotonically. It can be shown that the first eigenfunction is even and does not become equal to zero in the segment [-T/2, T/2]; the second eigenvector is odd and passes through zero once; the third eigenvector is again even and has two zeroes, etc. With sufficiently large T, for the j-th eigenfunction

$$\omega_j \sim (\pi/T)(j-1), \tag{12}$$

so that with sufficiently large T for all the spectra relating to the case considered here, the system of empirical orthogonal functions is universal.

2. Now assume that $f(\omega)$ has one absolute maximum with $\omega_{max} > 0$. Then the first eigenfunction is odd and with large T is close to $\sin\omega_{max}t$; the second eigenfunction is close to a cosine, then even and odd functions

as before alternate, but in contrast to case 1, the first function, at least, changes sign once, is odd, and its behavior, in any case, with large T, is determined by the ω_{max} value.

Evidently, the properties of the φ^j functions enumerated above, dependent on the spectral maximum, are observed for a broader class of processes than considered above.

The results are applicable, in particular, for those real fields which can be considered statistically homogeneous. For such fields it makes sense, in place of unwieldy computation of the eigenvectors of the matrices, to approximate the covariation functions by simple formulas, and if $\omega_{max} = 0$, use the conclusions obtained for case I (if the length of the T segment appreciably exceeds the correlation attenuation interval, (12) is used). However, if $\omega_{max} \neq 0$, it is necessary to evaluate ω_{max} and use results relating to case 2, and in the case of large T -- the formula $\varphi^1 \approx \sin \omega_{max} t$.

In [11] the results in [10] were generalized for the case of homogeneous fields of two variables.

The condition of statistical homogeneity is frequently not satisfied for real fields, but sometimes it can be assumed that it is satisfied for fields normalized to the root of the dispersion (for example, for fields on a plane it is necessary to normalize to $[B(x,y)]^{1/2}$).

As indicated in [5], for most real fields there is a situation when the first empirical orthogonal function does not change sign; the second changes sign once, etc. This means that the greatest intensity falls in the large-scale fluctuations, and then with a decrease in the characteristic scale the intensity decreases monotonically (similar to the monotonically decreasing spectral density in case 1). Accordingly, for real fields an analysis of empirical orthogonal functions is similar to spectral analysis. It can also be called scale analysis.

There are cases when the "natural" sequence of empirical orthogonal functions is disrupted. Most frequently the first function changes places with the second (similar to case 2). Most frequently this happens when the considered field is the field of first differences (compare with the derivative of a stationary standard process for which $f(\omega)$ is always equal to zero when $\omega = 0$, and $\omega_{max} > 0$). Proceeding to the first differences for the most part filters out the largest-scale components, which leads to a decrease in the characteristic scale. It is desirable, even necessary, that in all cases when such an inversion of the first empirical orthogonal functions arises as a result of the computations that there be a physical justification for this similar to that cited above. When this justification is not found, especially in the case of a small sample, the conclusion that an inversion is present is usually not statistically significant.

Using the empirical orthogonal functions method in general it is possible to detect any field component in which the predominant fraction of energy falls. In [14] the authors computed the empirical orthogonal functions of the H_{500} geopotential field over the northern hemisphere. The covariation matrix was determined by averaging in time, but without prior subtraction of the mean field $\overline{H(x, y)}$. As a result, as might be expected, the first empirical orthogonal function was very similar to the mean field $\overline{H(x,y)}$. The first main component $a_1(t)$ of the temperature field obtained in a series of studies virtually coincides with a sine curve whose period is equal to one year due to the fact that the correlation matrices were computed for deviations from values averaged for all seasons. A considerable fraction of the energy (80-90%) falls on such components. However, it is scarcely feasible to discriminate this sort of component by such an unwieldy procedure as computation of empirical orthogonal functions. It is better that this be done prior to computations of covariations using linear operations.

The stability of empirical orthogonal functions is noted in many studies [7]. On this basis it sometimes makes sense to use one and the same system of empirical orthogonal functions for different seasons and observation points, for several first main components of one and the same field and even for different meteorological elements.

In many cases for the description of meteorological structure it is feasible to use data on several meteorological elements. In this case the state of the atmosphere will be described by a vector with the dimensionality s·m, consisting of s m-dimensional vectors, where s is the number of elements and m, as before, is the number of observation points. The empirical orthogonal functions method can also be applied to the totality of such composite vectors, but first the components of the vectors must be made dimensionless, for example, by dividing by the corresponding standard deviations. In constructing the empirical orthogonal functions the cross correlations between the considered elements will also be taken into account.

Until now reference has been to the eigenfunctions of the empirical covariation matrices. It is natural to raise the question: is it possible to find empirical orthogonal functions on the basis of equations describing general circulation of the atmosphere? The problem is formulated as follows: for the random field $F(x, t)$ satisfying the system of equations in hydrothermodynamics on a sphere or a part of a sphere, find the spatial covariation function $B(x,y)$ corresponding to a stationary distribution of probabilities and construct an "eigenbase" for this covariation function. It is well known how complex this problem is in such a general formulation. However, it makes sense to examine it at least in simple special cases. In a study by Monin and Obukhov [6] use was made of a very simple model of the following type:

$$\partial F/\partial t = LF, \tag{13}$$

where L is a linearized "dynamic" operator dependent only on space coordinates. It is shown that under the energy conservation condition ($L^* = -L$) the eigenfunctions (analogues of empirical orthogonal functions) of the synchronous spatial covariation matrix of the F field, corresponding to a stationary probabilistic distribution, coincide with the eigenfunctions of the L operator. It can therefore be understood why empirical orthogonal functions are far more stable characteristics than the dispersions λj; the empirical orthogonal functions are related to the dynamic operator, whereas the dispersions are established as a result of nonlinear interactions [6].

Without being able to discuss in detail the results obtained during recent years for the empirical orthogonal functions of real meteorological fields, we will enumerate the principal directions in which the empirical orthogonal functions method has been used in meteorological investigations. We note that the extensive use of this method in the USSR began earlier than abroad.

Most investigations have been devoted to an analysis of the fields of surface pressure, H_{500} and H_{700}, air temperature at sea level, temperature of the ocean surface and precipitation both for the entire northern hemisphere and for its individual parts. In particular, special attention is being devoted to processes transpiring over the Atlantic and Pacific Oceans and attempts are being made to establish correlations between them. Study of the vertical structure of meteorological fields is continuing [8].

Many attempts have been made to apply the empirical orthogonal functions method for forecasts both for intermediate times and long-range forecasts. In such cases as the predictors it is customary to use the first main components of the principal meteorological fields carrying the most important information concerning the course of long-period processes. Then, using linear regression equations, an evaluation is made of the values of the main components of the predicted field and these are used in restoring the field in the future [5]. We note [3], in which the predictor for a five-day forecast of precipitation over the western half of the USSR was the H_{500} field obtained as a result of a hydrodynamic forecast. The type of circulation is taken into account. In [13], for the purpose of predicting the mean seasonal temperature over North America, information on the totality of mean seasonal H_{700} and OT_{1000}^{700} fields and the fields of surface temperature, temperature of the ocean surface and the precipitation field was represented in the form of a 12-dimensional "climatic" vector close to the vector of the main components and then in place of the regression equations use was made of the analogues method. In [4] the breakdown of the geopotential fields in the northern hemisphere in seven levels was used for constructing a hydrodynamic model of the atmosphere with few parameters which was used in making a forecast for six days.

It can be seen from what has been set forth above that the use of the empirical orthogonal functions method in meteorology leads to the necessity for computing empirical orthogonal functions for matrices of very great

dimensionalities. This gives rise to a number of problems, both purely computational and those related to the complexity of rigorous validation of statistical conclusions relative to empirical orthogonal functions evaluated using small samples. With respect to computation algorithms, in addition to [5] it is possible, for example, to mention [15], which proposes an economical iteration method, and also a number of others, citations to which can be found in reviews and monographs, some of which are given in the bibliography.

A procedure used for the first time in the meteorological literature in [16] was very useful in 1969 for computing empirical orthogonal functions in cases when the dimensionality m of the covariation matrix is greater than the volume n of the sample. This procedure is based on the fact that the nonzero eigenvalues of a matrix of the m-th order $Z = \| Z_{ij} \|$, determined from some rectangular matrix $F = \| F_{iq} \|$, $i = 1,\ldots,m$, $q = 1,\ldots, n$; $n < m$:

$$Z_{ij} = \sum_{q=1}^{n} F_{iq} F_{jq} = FF^*, \quad i, j = 1, \ldots, m, \tag{14}$$

coincide with the eigenvalues of a matrix of the n-th order $Y = \| Y_{qs} \|$:

$$Y_{qs} = \sum_{i=1}^{m} F_{iq} F_{is} = F^* F, \quad q, s = 1, \ldots, n, \tag{15}$$

and the eigenvectors of the matrices Z and Y, z and y respectively, corresponding to one and the same eigenvalue, are expressed through one another:

$$y = F^* z \tag{16}$$

(the asterisk is the transposition symbol). In general, the y and z vectors do not have to be normalized simultaneously to unity. The remaining (m - n) eigenvalues of the Z matrix are equal to zero.

As F_{iq} we take the values $F'(x_i, t_q)$. It is easy to see that the spatial covariation matrix B is related to Z by the expression

$$B_{ij} = (1/n)\, FF^* = (1/n)\, Z_{ij} \tag{17}$$

(compare with (1)). We will show that with the additional condition of statistical spatial homogeneity the Y matrix is proportional to the time covariation matrix R of the F(x, t) field:

$$R_{qs} = R(t_q, t_s) = \langle F_{iq} F_{is} \rangle = \frac{1}{m} F^* F = \frac{1}{m} Y_{qs}; \; s, q = 1, \ldots, n. \tag{18}$$

Here the "$\langle\ \rangle$" symbol denotes averaging for m points x_j. In (18) it would be necessary, strictly speaking, to take the deviations from the means, which for each moment t_q can be evaluated by averaging for m points x_i. Here we will assume that for the field of deviations from the means in time F' the spatial deviations from the means are close to zero, which is probable under the conditions of statistical homogeneity with respect to

t and x. We will denote the coinciding nonzero eigenvalues of the matrices Y and Z by μ_j, j = 1,...,n. It follows from (17) and (18) that the eigenvalues of the matrices B and R are related to μ_j by the expressions

$$\lambda_j = \mu_j/n, \quad \nu_j = \mu_j/m, \tag{19}$$

respectively, and the eigenvectors -- by a formula similar to (16).

Now we will turn to the representation (2), which with $t = t_q$, q = 1,...,n and p = min (m, n) is transformed to equality. Instead of $a_j(t_q)$ we introduce the normalized vectors

$$\alpha_j(t_q) = a_j(t_q)/(n\lambda_j)^{1/2}; \quad (1/n)\sum_{q=1}^{n} \alpha_j^2(t_q) = 1 \tag{20}$$

(compare with (4)). Using (19), we rewrite (2) in a form symmetric relative to x and t:

$$F_{lq} = \sum_{j=1}^{\min(m,\,n)} \mu_j^{1/2}\,\varphi^j(x_l)\,\alpha_j(t_q). \tag{21}$$

Using the orthonormality of the spatial eigenvectors $\varphi^j(x_i)$ and equation (18) it is easy to show that $\alpha_j(t_q)$ is the "eigenbase" of the time covariation matrix R. The question as to what in (21) should be considered the main components and what should be considered the empirical orthogonal functions must be answered in dependepence on the relationship between m and n.

In actuality, if, for example, $n \ll m$, and the field values are weakly correlated spatially, it can be hoped that the time covariation matrix R, its first eigenvalues $\nu_j = \mu_j/m$ and the α_j vectors are evaluated using formula (18) quite reliably. This means that it is possible to use the considerations which led us to the formulas (10)-(12), from which we conclude that with sufficiently large $m \gg n$ the ν_j (and μ_j) values and the α_j vectors describe the energy distribution in the time spectrum. In actuality, in many cases the main components $a_j(t)$, evaluated using real data, are not similar to the realizations of the random functions, but instead are close to the trigonometric functions (and the first main component is close to a constant or to a cosine with a large period), which corresponds to formula (10) for empirical orthogonal functions $\alpha_j(t)$. It is therefore understandable why the spectra of "random" functions $a_j(t)$ in these cases have sharp peaks in the neighborhood of one or two frequencies. On the other hand, when $m \gg n$ the dispersions of the evaluations of the spatial covariation matrix B and its eigenvectors can be great and comparable to the dispersions of evaluations of the initial field.

Taking into account everything which has been said above, it is natural to call the α_j vectors (time) empirical orthogonal functions and call the $\mu_j^{1/2}\varphi^j$, being functions of space coordinates, the main components. Thus, the α_j vectors (and this also means the $a_j(t)$ functions) can be considered

determined (that is, nonrandom), and the $\varphi^j(x)$ functions -- random, whose fluctuations for each x reflect the individual peculiarity of the time realization of the field at the point x. Therefore, the $\varphi^j(x)$ functions cannot be regarded as reliable characteristics of the spatial statistical structure. With respect to the eigenvalues λ_j of the B matrix, they are proportional to the eigenvalues of the R matrix:

$$\lambda_j = (m/n)\,\nu_j, \tag{22}$$

and therefore have no relationship to the spatial structure.

If $m \ll n$, the spatial and temporal eigenfunctions change roles and the λ_j eigenvalues characterize the spatial spectrum. In each of the considered cases, when one of the numbers m or n is very large and the other small, it is possible to use the known theorems concerning the asymptotic normality of the evaluations of interest to us [15]. However, for meteorology a more timely case is when m and n are large (of the order of tens or 100-200) and are comparable in order of magnitude. Accordingly, the question of which functions -- $\varphi(x)$ or a(t) -- are reliable evaluations of the statistical structure and how precise these evaluations are is very complex because the question is tied in to the problem, still unsolved in mathematical statistics, of finding the distribution of probabilities of the eigenfunctions and the eigenvalues of the empirical covariation matrices with the above-mentioned relationships between m and n. Since the observations are correlated in both time and space, this problem is still more complicated.

In actuality, it is necessary to take into account not only the m and n values, but also an equivalent number of independent observations of both variables [15]. Additional difficulties also arise because the real fields are not statistically uniform with respect to time or (as is still more important) space. Together with analytical examinations, it is fitting to use the Monte Carlo method here [1]. [For meteorological applications it is important that the spatial statistical characteristics of the modeled fields be close to the similar characteristics determined on the basis of observational data. Such work is now being carried out at the Institute of Physics of the Atmosphere USSR Academy of Sciences. Corresponding results will be published later.]

The question of which empirical orthogonal functions can be considered statistically significant is discussed in [1, 5, 15] and a number of other studies. We note in conclusion that the empirical orthogonal functions method is also finding use in other geophysical problems [2, 9, 12].

BIBLIOGRAPHY

1. Bagrov, N. A., "Natural Components of Small Samples in the Case of a Great Number of Parameters," METEOROLOGIYA I GIDROLOGIYA (Meteorology and Hydrology), No 12, 1978.

2. Gorchakov, G. I., Sviridenkov, M. A., "Statistical Analysis of Light Scattering Matrices," IZVESTIYA AN SSSR, FIZIKA ATMOSFERY I OKEANA (News of the USSR Academy of Sciences, Physics of the Atmosphere and Ocean), Vol 12, No 9, 1976.

3. Kats, A. L., Fedulova, M. N., Shendakova, V. A., "Results of Routine Testing and Application of an Improved Method for Predicting Precipitation for Five Days," TRUDY GIDROMETTSENTRA SSSR (Transactions of the USSR Hydrometeorological Center), No 205, 1978.

4. Marchuk, G. I., Penenko, V. V., Protasov, A. V., "Model of Atmospheric Dynamics of the Spectral-Difference Type With Few Parameters," METEOROLOGIYA I GIDROLOGIYA, No 11, 1978.

5. Meshcherskaya, A. V., Rukhovets, L. V., Yudin, M. I., Yakovleva, N. I., YESTESTVENNYYE SOSTAVLYAYUSHCHIYE METEOROLOGICHESKIKH POLEY (Natural Components of Meteorological Fields), Leningrad, Gidrometeoizdat, 1970.

6. Monin, A. S., Obukhov, A. M., "Statistical Investigations of Large-Scale Atmospheric Processes," DINAMIKA KRUPNOMASSHTABNYKH ATMOSFERNYKH PROTSESSOV (Dynamics of Large-Scale Atmospheric Processes), Moscow, Nauka, 1965.

7. Rukhovets, L. V., "On the Problem of the Stability of Empirical Orthogonal Functions," METEOROLOGIYA I GIDROLOGIYA, No 2, 1976.

8. Tatarskaya, M. S., "Orthogonal Expansions of the Temperature and Humidity Fields in the Lower Troposphere," IZVESTIYA AN SSSR, FIZIKA ATMOSFERY I OKEANA, Vol 10, No 3, 1974.

9. Tatarskiy, V. I., Kharitonova, T. N., "Application of Orthogonal Statistical Expansions in the Theory of Atmospheric Refraction," IZVESTIYA AN SSSR, FIZIKA ATMOSFERY I OKEANA, Vol 10, No 9, 1974.

10. Fortus, M. I., "Statistical Orthogonal Functions for Finite Segments of a Random Process," IZVESTIYA AN SSSR, FIZIKA ATMOSFERY I OKEANA, Vol 9, No 1, 1973.

11. Fortus, M. I., "Statistical Orthogonal Functions for a Random Field Stipulated in a Finite Region of a Plane," IZVESTIYA AN SSSR, FIZIKA ATMOSFERY I OKEANA, Vol 11, No 11, 1975.

12. Yakovlev, A. A. "Structure of Information on the Spectrum of Sizes of Scattering Particles Obtained from Measurements of the Scattering and Polarization Indicatrices," IZVESTIYA AN SSSR, FIZIKA ATMOSFERY I OKEANA, Vol 15, No 1, 1979.

13. Barnett, T. P., Preisendorfer, R. W., "Multifield Analog Prediction of Short-Term Climate Fluctuations Using a Climate State Vector," J. ATMOS. SCI., Vol 35, No 10, 1978.

14. Craddock, J. M., Flintoff, S., "Eigenvector Representations of Northern Hemispheric Fields," QUART. J. ROY. METEOROL. SOC., Vol 96, No 407, 1970.

15. Fukunaga, K., Koontz, W. L. G., "Prepresentation of Random Processes Using the Finite Kahrunen-Loéve Expansion," INFORM. AND CONTROL., Vol 16, No 1, 1970.

16. Hirose, M., Kutzbach, J. E., "An Alternative Method for Eigenvector Computation," J. APPL. METEOROL., Vol 8, No 4, 1969.

SEVENTIETH BIRTHDAY OF YEVGENIY KONSTANTINOVICH FEDOROV

Moscow METEOROLOGIYA I GIDROLOGIYA in Russian No 4, Apr 80 pp 120-123

[Article by Yu. A. Izrael']

[Text] Academician Yevgeniy Konstantinovich Fedorov marked his 70th birthday on 10 April 1980.

Yevgeniy Konstantinovich Fedorov is an outstanding professional geophysicist, a leading organizer of Soviet science and an outstanding public and political worker.

The scientific activity of Ye. K. Fedorov began after his graduation from Leningrad State University. During the years 1932-1939 Ye. K. Fedorov carried out unique geophysical investigations of the Arctic at a number of polar stations.

Study of the magnetic anomalies in Franz Josef Land, determination of variations of the magnetic field on Taymyr and meteorological and oceanological investigations in many regions of the Arctic -- such was the main direction of scientific activity of Yevgeniy Konstantinovich during those years. The results of these studies assisted in an understanding of the course of geophysical processes in this virtually unstudied region, which facilitated beginning of operation of the Northern Sea Route and the mastery of the Arctic as a whole. Observations and investigations on the "Severnyy Polyus" drifting station were of particular importance. In particular, they refuted the earlier widely held idea that over the Central Arctic Basin there is constantly an extensive anticyclone with a maximum in the region of the pole.

Data on ice drift in this region were exceptionally important, in turn important for long-range ice forecasts. The observational data served as a basis for new concepts concerning the long-term movement of ice in the Central Arctic.

During the 1930's Ye. K. Fedorov advanced from a rank-and-file polar worker to Director of the Arctic Institute. For his brilliant geophysical investigations he was awarded the academic degree of Doctor of Geographical Sciences (1938). He was elected Corresponding Member of the USSR Academy of Sciences and later, because of these investigations, Yevgeniy Konstantinovich was awarded the State Prize. He was awarded the title of Hero of the Soviet Union for his heroic work on the "Severnyy Polyus-1" drifting station.

He will always be remembered by everyone as a member of the Papanin group; the great work of the four at the pole was always regarded highly and will always he honored by the Soviet people.

In 1939 an event occurred which for many years determined the fate of Ye. K. Fedorov: he became head of the Hydrometeorological Service of the Soviet Union, which he headed for almost 20 years (1939-1947, 1963-1974). During this period Yevgeniy Konstantinovich invested enormous efforts for its development and reconstruction and achieved important practical results along these lines. This led to a great growth in the authority of the Service in the country and abroad.

Before the war Ye. K. Fedorov emphasized the strengthening of the scientific and technical base of the Service, the creation of a unified national reference network of hydrometeorological stations and posts, the combining of all types of forecasting organizations into a unified system.

During the time of the Great Fatherland War Yevgeniy Konstantinovich, becoming Chief of the Main Administration of the Hydrometeorological Service of the Red Army, reorganized the Service for the best supply of hydrometeorological information to the organizations and units of the Red Army.

During the post-war period Ye. K. Fedorov devoted much effort in improving the hydrometeorological support of the national economy, strengthening and developing the scientific institutions of the Service.

During 1947 Yevgeniy Konstantinovich proceeded to scientific work. During this time he devoted his greatest attention to study of weather and climate, water resources, investigation of the seas and oceans, ionosphere, earth's magnetic and radiation fields, and theoretical and experimental studies for the purpose of artificial modification of hydrometeorological processes; he was engaged in the creation of scientific and methodological principles for monitoring and evaluating the state of contamination of the environment and problems involved in the interaction between human society and nature.

His studies in the field of artificial modification of meteorological processes are of particular importance. In these studies he emphasizes the importance of use of unstable states during such modification when insignificant expenditures of energy are needed for the changing of processes.

An important scientific event was the organization of the Institute of Applied Geophysics in 1956. This institute, founded by Ye. K. Fedorov, was headed by him from 1956 through 1968. In 1974 he again became director of the Institute of Applied Geophysics. This became the leading institute for a number of geophysical investigations in the country, including in the field of thorough study of the state of the environment.

During the period 1959-1962 Ye. K. Fedorov, in the post of Chief Scientific Secretary of the Presidium USSR Academy of Sciences, made a great contribution to improving the planning and organization of scientific investigations in the USSR Academy of Sciences.

In 1960 Yevgeniy Konstantinovich was elected a full member of the USSR Academy of Sciences.

After 1962 Ye. K. Fedorov, as chief of the Main Administration of the Hydrometeorological Service of the USSR Council of Ministers, carried out work for the general technical reconstruction of the Service on the basis of use of the latest technical means -- meteorological earth satellites, meteorological radars and rockets, automatic hydrometeorological stations and equipment for the automatic collection, processing and dissemination of hydrometeorological information. He established a permanently operating system for monitoring radioactive contamination, radiation conditions, and the degree of contamination of the environment; he organized new major

central and regional scientific institutions (Institute of Experimental Meteorology, All-Union Scientific Research Institute of Hydrometeorological Information, State Scientific Research Center for Study of the Environment, Central Asiatic and West Siberian Scientific Research Hydrometeorological Institute, Central Design Bureau).

His was the initiative in creating new methods for the prediction of the yield of agricultural crops and the introduction of these forecasts into the practical work of servicing key agencies. He organized work on the formulation of requirements on the make-up, accuracy and discreteness of information for prediction work and the servicing of different branches of the national economy. This work is important for increasing the effectiveness of use of hydrometeorological information.

He developed investigations in the field of cloud microphysics and aerosols and for this purpose under his direction there was creation of unique apparatus in the aerosol building at the Institute of Experimental Meteorology.

His attention to the development of work on study of the propagation of different impurities in the atmosphere is well known; for this he organized and carried out large-scale expriments and created a high meteorological mast with a height of more than 300 m at Obninsk.

We should also mention the initiative of Ye. K. Fedorov in the development and introduction of methods for a gamma survey of the snow cover and an aerophotometric method for determining the state of pasture vegetation.

Work in the field of artificial modification of local atmospheric processes, initiated under the direction of Ye. K. Fedorov, received extensive development.

Yevgeniy Konstantinovich, spending all his life in the study of different natural processes, devoted more and more attention to the need for a careful, meticulous and concerned attitude toward nature, man's environment. He proceeded from a study of natural processes to the active protection of nature, the struggle for its preservation, the search for ways to optimize interaction between human society and nature, as he himself writes: "from the description to the planning of nature."

Yevgeniy Konstantinovich did this energetically, with deep conviction and without fail with practical conclusions and recommendations.

He concerned himself with the developing of a forecast of anthropogenic loads on the environment, the search for practical measures for lessening these loads.

Ye. K. Fedorov was especially excited by the social aspects of preservation of the environment and he had a zealous attitude toward natural resources. In this field he carried out a number of scientific studies, the

most important of which was the brochure VZAIMODEYSTVIYE OBSHCHESTVA I PRIRODA (Interaction Between Society and Nature) (1972) and the book EKOLOGICHESKIY KRIZIS I SOTSIAL'NYY PROGRESS (Ecological Crisis and Social Progress) (1977).

It is known that under the conditions of ever-increasing effect of man on the environment many scientists are discussing the possible effects of such modification and ways to prevent negative consequences. The scientific literature contains different forecasts -- including pessimistic -- concerning the impending ecological crisis. In essence, the following question arises: "until when, how and under what conditions can mankind grow and develop on a limited planet," writes Ye. K. Fedorov. He also devotes his book, in which he describes ways to overcome the possible ecological crisis and attain social progress, to this interesting and important problem.

In evaluating the "earth's capacity" Yevgeniy Konstantinovich devotes particular attention to the broadening and enlargement of this capacity, that is, the productivity of nature, its reserves, "by means of intentional calculation, planning and its many-sided transformation."

In an era of vigorous industrial development, contradictory social systems, and the development of centers of international stress he insists not only on the need for making an objective evaluation of the existing and future situation in nature, regarding it as inadequate to formulate recommendations for the stabilization and improving of this situation, but that there is a need for actively attacking the problem.

Ye. K. Fedorov feels that the struggle for peace is of particular importance under these circumstances because war and preparations for it absorb enormous resources and are capable of inflicting irreparable losses on the environment.

Accordingly, Yevgeniy Konstantinovich, participating in the World Conference, "Climate and Mankind" (1979), insisted that the conference emphasize the importance of the relaxation of tensions and the importance of preserving a solid peace on the earth for ensuring optimum conditions for the preservation of nature and climate. And the editorial group, with his participation, wrote in the Declaration (then adopted by the conference):

"The countries of the world must act together so as to preserve soil fertility, avoid the incorrect use of world resources,..., decrease contamination of the air and oceans. These actions will require great resoluteness on the part of different countries...and will be effective only under conditions of peace on earth."

The public and political activity of Yevgeniy Konstantinovich Fedorov is widely known and enjoys great recognition in the USSR and abroad.

During the years of the Great Fatherland War he was Chairman of the Antifascist Committee of Soviet Youth. Beginning in 1962 he actively participated in the Work of the Soviet Committee for the Defense of Peace;

beginning in 1965 he was deputy chairman, and in March 1979 he became chairman of this committee.

The diversfied and enterprising activity of Ye. K. Fedorov in the World Peace Council (member of the Peace Council since 1961; vice president of the Peace Council since 1977) is of great social and political importance.

Ye. K. Fedorov has repeatedly participated in the work of international conferences and meetings, as well as in the international work of groups of experts. The work of the group of Soviet technical experts in 1957-1958 in Geneva, which he headed, was an important step in preparations for the Moscow agreement on the banning of nuclear tests in the atmosphere, space and underwater.

During 1963-1971 Ye. K. Fedorov was Vice President of the World Meteorological Organization and in 1977 he was awarded the WMO gold medal for his major contribution to the activity of that organization.

Ye. K. Fedorov was elected deputy of the USSR Supreme Soviet for the first and ninth convocations; in 1979 he was again elected deputy of the USSR Supreme Soviet, tenth convocation.

Since 1977 Ye. K. Fedorov has been a member of the Presidium USSR Supreme Soviet.

At the 25th Congress CPSU Ye. K. Fedorov was elected a candidate for membership in the Central Committee CPSU.

In presenting this brief biographical sketch of Yevgeniy Konstantinovich Fedorov, we should particularly emphasize his most important human characteristics -- humanity, dedication to principle and exceptional energy, not yielding to the influence of the years. Because of this energy his life has been filled with several times more events and deeds than the life of almost any other man.

In addition to his scientific works and publicity articles, Ye. K. Fedorov recently has been writing his recollections, the memoirs of his life and his work in the Arctic. In the very recently published book POLYARNYYE DNEVNIKI (Polar Diaries) we writes with enormous warmth concerning his friends and polar colleagues. He enthusiastically describes their day-to-day life. With respect to its emotional content this book can be assigned to the category of polar lyrics and because of its purposefulness and mood it can be a book of instruction and serve as an education for the present-day generation of youth.

In conclusion, in the name of all who know Yevgeniy Konstantinovich, I would like to congratulate him on his anniversary and wish him excellent health and new major successes in creativity and tireless social-political activity.

SOVIET AWARDS TO WORKERS IN FIELD OF HYDROMETEOROLOGY

Moscow METEOROLOGIYA I GIDROLOGIYA in Russian No 4, Apr 80 pp 123-124

[Unsigned article]

[Text] For their services in the development of hydrometeorological science and support of the national economy of the country with hydrometeorological information the Presidium of the USSR Supreme Soviet has presented awards to the following workers at the USSR Hydrometeorological Center:

Order of the October Revolution

Mikhail Aramaisovich Petrosyants -- Director of the USSR Hydrometeorological Center

Order of the Red Banner of Labor

Vladlena Aleksandrovna Seregina -- group leader

Yevgeniya Stanislavovna Ulanova -- division head

Order of Friendship of Peoples

Yekaterina Nikitichna Blinova -- division head

Konstantin Petrovich Vasil'yev -- division head

Order "Emblem of Honor"

Valentin Dmitriyevich Komarov -- senior scientific specialist

Dmitriy Antonovich Ped' -- laboratory head

Yuriy Vladimirovich Rybushkin -- deputy chief of the computation center

Vladimir Dmitriyevich Spirin -- mechanic

Boris Dmitriyevich Uspenskiy -- laboratory head

Medal "For Illustrious Work"

Galina Grigor'yevna Gromova -- division head

Yekaterina Arkad'yevna Chistyakova -- senior scientific specialist

Anna Danilovna Shamenkova -- engineer

Medal "For Distinction in Work"

Yevgeniya Nikonorovna Arabey -- group leader

Aleksey Pavlovich Zhidikov -- laboratory head

Vera Aleksandrovna Moiseychik -- senior scientific specialist

Lidiya Vasil'yevna Nagreshnikov -- engineer

Nadezhda Vasil'yevna Olisova -- engineer

Genadiy Pavlovich Ugol'kov -- modeler-instrument maker

The following workers of the State Committee on Hydrometeorology were presented awards for active participation in the development of methods for investigating natural resources and supplying information to interested organizations:

Order of the Red Banner of Labor

Sergey Ivanovich Avdyushin -- First Deputy Director of the Institute of Applied Geophysics

Anatoliy Ivanovich Burtsev -- Deputy Director for Scientific Work of the State Scientific Research Center for Study of Natural Resources

Andrey Vasil'yevich Bushuyev -- Laboratory Director at the Arctic and Antarctic Scientific Research Institute

Vladimir Vasil'yevich Shevchenko -- Head of the Far Eastern Administration of the Hydrometeorological Service

Order "Emblem of Honor"

Sergey Viktorovich Vinogradov -- Head of the Experimental Workshops at the Main Geophysical Observatory

Dombkovskaya, Yekaterina Petrovna -- laboratory head at the State Scientific Research Center for the Study of Natural Resources

Popova, Tat'yana Pavlovna -- senior scientific specialist at the USSR Hydrometeorological Center

Rachkulik, Viktor Ivanovich -- laboratory head at the All-Union Scientific Research Institute of Agricultural Meteorology

Sitnikova, Margarita Valer'yanovna -- division head at the Central Asiatic Regional Scientific Research Hydrometeorological Institute

Timofeyeva, Vera Sergeyevna -- deputy division chief at the West Siberian Regional Scientific Research Hydrometeorological Institute

Tishchenko, Aleksandr Pavlovich -- division chief at the State Scientific Research Center for the Study of Natural Resources

Order of Work Glory (Third Degree)

Bessonova, Anna Ivanovna -- printer at the printing plant at the USSR Hydrometeorological Center

Popov, Vladimir Il'ich -- laboratory mechanic at the State Scientific Research Center for the Study of Natural Resources

Romanishina, Valentina Vasil'yevich -- telegraph operator of the ASPD service of the Far Eastern Administration of the Hydrometeorological Service

Usachev, Gennadiy Petrovich -- metal worker in the experimental workshops of the Institute of Applied Geophysics

Medal "For Illustrious Work"

Andreyev, Boris Mikhaylovich -- senior scientific specialist in the Leningrad Division of the State Oceanographic Institute

Formotov, Boris Mikhaylovich -- expert in the Administration of Space Systems of the State Committee on Hydrometeorology and Environmental Monitoring

Bel'tishchev, Nikolay Fedorovich -- laboratory head at the USSR Hydrometeorological Center

Gusev, Vladimir Nikolayevich -- division head at the State Scientific Research Center for Study of Natural Resources

Yegorikhin, Yevgeniy Dmitriyevich -- senior engineer of the Baykal-Amur Expedition of the State Hydrological Institute

Loshchilov, Viktor Sergeyevich -- senior scientific specialist at the Arctic and Antarctic Scientific Research Institute

Malygin, Aleksandr Ivanovich -- group leader in the Obninsk Division of the State Scientific Research Center for the Study of Natural Resources

Minina, Lyudmila Sil'vesterovna -- senior scientific specialist at the USSR Hydrometeorological Center

Prokacheva, Valeriya Grigor'yevna -- senior scientific specialist at the State Hydrological Institute

Solov'yev, Valeriy Ivanovich -- division head at the State Scientific Research Center for Study of Natural Resources

Formozov, Boris Aleksandrovich -- engineer of the same institute

Chepelev, Viktor Andreyevich -- senior radio engineer of the Far Eastern Administration of the Hydrometeorological Service

Medal "For Distinction in Work"

Barkova, Nina Kuz'minichna -- senior technician at the State Scientific Research Center for Study of Natural Resources

Zhigarkova, Larisa Aleksandrovna -- senior technician of the West Siberian Regional Scientific Research Hydrometeorological Institute

Kabanov, Boris Iosifovich -- chief engineer at the same institute

Kozhevnikov, Boris Kuz'mich -- division head at the same institute

Kruzhkova, Tat'yana Sergeyevna -- laboratory head at the USSR Hydrometeorological Center

Kulagin, Yuriy Mikhaylovich -- division head at the Institute of Applied Geophysics

Nazirov, Magomedgadzhi, senior scientific specialist at the State Scientific Research Center for Study of Natural Resources

Popov, Yevgeniy Petrovich -- engineer at the same institute

Rabinovich, Yuriy Izrailevich -- senior scientific specialist at the Main Geophysical Observatory

Khristich, Polina Petrovna -- laboratory head at the Far Eastern Administration of the Hydrometeorological Service

AT THE USSR STATE COMMITTEE ON HYDROMETEOROLOGY AND ENVIRONMENTAL MONITORING

Moscow METEOROLOGIYA I GIDROLOGIYA in Russian No 4, Apr 80 pp 124-126

[Article by A. V. Kolokol'chikov]

[Text] A session of the Presidium of the Scientific and Technical Council of the State Committee on Hydrometeorology and Environmental Monitoring was held on 25 December 1979. The Presidium examined studies presented for award of the departmental prizes of the State Committee on Hydrometeorology and Environmental Monitoring for 1979.

The "Yu. M. Shokal'skiy" Prize in the amount of 1,500 rubles was awarded to B. A. Birman, O. G. Kornyushin, Yu. A. Krayushkin, T. A. Parmuzina and L. A. Petrova (All-Union Scientific Research Institute of Hydrometeorological Information-World Data Center), K. P. Vasil'yev, V. A. Volzhenkov (USSR Hydrometeorological Center), B. A. Kogan (Murmansk Affiliate Arctic and Antarctic Scientific Research Institute) for the ATLAS OPASNYKH I OSOBO OPASNYKH DLYA MOREPLAVANIYA I RYBOLOVSTVA GIDROMETEOROLOGICHESKIKH YAVLENIY. SEVERNAYA CHAST' ATLANTICHESKOGO OKEANA (Atlas of Hydrometeorological Phenomena Dangerous and Especially Dangerous for Navigation and Fishing. Northern Part of the Atlantic Ocean).

This atlas, published in 1978 by the Main Administration of Navigation and Oceanography, is the world's first practical statistical-climatic manual which gives an evaluation of the probability, intensity and duration of meteorological conditions constituting a danger for navigation and fishing in the open part of the ocean at different seasons of the year. It gives information on the frequency of recurrence, mean and maximum continuous duration of wind velocity $\geqslant 15$, $\geqslant 17$, $\geqslant 25$, $\geqslant 33$ m/sec, on wave heights $\geqslant 4$, $\geqslant 6$, $\geqslant 8$ m, on visibility $\leqslant 2$, $\leqslant 1$, $\leqslant 0.5$ miles, $\leqslant 1$, $\leqslant 0.5$ cable lengths; data on wind velocity and wave heights with a 1% guaranteed probability, on the maximum registered wind velocities, on the prevailing direction and stability of the storm wind. The atlas also contains data on the mean and extremal positions of the ice edge and the mean boundary of icebergs, on the frequency of recurrence and intensity of icing, on the extent of the wind storm field caused by the passage of a tropical storm, on its lifetime and standard synoptic situations under which severe storms and hurricanes arise.

The atlas is used extensively for ensuring the safety of navigation and fishing.

The "Yu. M. Shokal'skiy" Prize in the sum of 300 rubles was awarded to Ye. P. Borisenkov, N. Z. Ariyel', R. S. Bortkovskiy, E. K. Byutner, M. A. Kuznetsov (Main Geophysical Observatory) for a series of studies on parameterization of the ocean and atmosphere.

The first part of the mentioned series includes investigations on the creation of a physical model of the turbulent exchange between the atmosphere and the sea surface and the development of a method for computing turbulent flows on the basis of data from standard hydrometeorological measurements on ships. The developed method takes into account the influence exerted on turbulent exchange in the near-water layer by wind velocity, temperature stratification, air humidity and the stage of wave development. The comparison of turbulent flows carried out at the Institute of Experimental Meteorology, computed by the Main Geophysical Observatory method and measured with fluctuation sensors, confirmed the merits of the developed method. This method is included in the new edition of the OKEANOGRAFICHESKIYE TABLITSY (Oceanographic Tables) and has also been given in an edition of the REGISTR SSSR. VETER I VOLNY V OKEANAKH I MORYAKH. SPRAVOCHNYYE DANNYYE (USSR Register. Wind and Waves in the Oceans and Seas. Reference Data).

In the second part of the series there is an investigation of the effect of the specific mechanism of interaction between the ocean and the atmosphere during a storm. Theoretical models, based on field data, including data obtained by the authors of the study, made it possible to obtain realistic evaluations of the drag coefficient, coefficients of heat exchange and evaporation from the sea surface during a storm. A study was made of the state of the sea surface -- the area occupied by foam and whitecaps -- determining the intensity of generation of spray at the surface. Evaluations of the role of storms in global heat and mass exchange between the ocean and the atmosphere were obtained and means were formulated for taking into account the investigated mechanism in models of general circulation of the atmosphere.

The principal results were published in the study PROTSESSY PERENOSA VBLIZI SVERKHNOSTI RAZDELA OKEAN-ATMOSFERA (Transfer Processes Near the Ocean-Atmosphere Interface), Gidrometeoizdat, Leningrad, 1974, in the TRUDY GGO (Transactions of the Main Geophysical Observatory), No 282, 398, in the TRUDY AANII (Transactions of the Arctic and Antarctic Scientific Research Institute), Vol 312, in METEOROLOGIYA I GIDROLOGIYA (Meteorology and Hydrology), No 5, 1973, No 11, 1975, No 5, 1976 and in a number of other publications.

The "B. P. Mul'tanovskiy" Prize in the sum of 1,000 rubles was awarded to B. D. Uspenskiy, A. N. Mertsalov, Ye. M. Orlova, I. A. Petrichenko, T. A. Galakhova (USSR Hydrometeorological Center) for the work "Numerical Synoptic-Hydrodynamic Model for Short-Range Prediction of Continuous and Shower Precipitation."

In comparison with the known numerical forecasting models the numerical operational synoptic-hydrodynamic model for the forecasting of continuous and shower precipitation for a period up to 36 hours is characterized by completeness of allowance for precipitation-forming factors. For the first time the model provides for separate forecasting of the quantity of liquid precipitation. According to the test materials, the accuracy in predicting precipitation somewhat exceeds the accuracy of synoptic forecasts for an identical advance time.

In conformity to a resolution of the Central Methodological Committee of the State Committee on Hydrometeorology and Environmental Monitoring dated 3 October 1978, the daily transmission of a prognostic map of precipitation by facsimile began in March 1979. This facsimile map gives the quantity of continuous and shower precipitation for 0900-2100, 2100-0900 and 0900-2100 hours for the current and subsequent days.

The principal results of the study have been published in the TRUDY GIDROMETTSENTRA SSSR (Transactions of the USSR Hydrometeorological Center), Nos 157 and 176.

The V. G. Glushkov-V. A. Uryvayev Prize, in the sum of 1,000 rubles, was awarded to A. V. Karaushev, K. V. Kazumikhina, K. N. Lisitsyna, I. V. Bogolyubova, A. Ya. Shvartsman, G. A. Petukhova, V. V. Romanovskiy and N. N. Bobrovitskaya (State Hydrological Institute) for the monograph TEORIYA I METODY RASCHETA RECHNYKH NANOSOV (Theory and Methods for Computing River Alluvium) and the monograph STOK NANOSOV, YEGO IZUCHENIYE I GEOGRAFICHESKOYE RASPROSTRANENIYE (Runoff of Alluvium, its Study and Geographical Distribution) (Gidrometeoizdat, Leningrad, 1977).

The basis for these monographs was the results of long-term investigations of laboratory alluvium at the State Hydrological Institute and also a number of major Soviet and foreign scientists. Both monographs constitute a unified whole, taking in all the principal aspects of the problem of river alluvium and are related by a unified scientific concept. The science of river alluvium formulated in these monographs, interpreted as one of the branches of hydrology, includes the theory of transport of alluvium, the processes of formation of their runoff, methods for computing their movement, the method for field investigations on slopes, in rivers and reservoirs, problems involved in the territorial distribution of the parameters of runoff and makeup of the alluvium.

Many of the findings examined in the monographs constituted the basis of norm-setting documents of interdepartmental and all-union importance (UKAZANIYA PO RASCHETU ZAILENIYA PRI STROITEL'NOM PROYEKTIROVANII (Instructions on Computation of Silting in Construction Planning), Leningrad, Gidrometeoizdat, 1973; UKAZANIYA PO RASCHETU STOKA NANOSOV VSN-01-73 (Instructions on Computing the Runoff of Alluvium VSN-01-73), Leningrad, Gidrometeoizdat, 1974; INSTRUKTSIYA PO OPREDELENIYU RASCHETNYKH GIDROLOGICHESKIKH KHARAKTERISTIK PRI PROYEKTIROVANII PROTIVOEROZIONNYKH

MEROPRIYATIY NA YEVROPEYSKOY TERRITORII SSSR, VSN-04-77 (Instructions on Determining the Computed Hydrological Characteristics in the Planning of Antierosion Measures in the European Territory of the USSR, VSN-04-77), Leningrad, Gidrometeoizdat, 1979, and others.)

The two monographs constitute a fundamental treatise on river alluvium. With respect to theoretical level, depth of analysis of processes and breadth of coverage of the subject, as well as with respect to practical importance these publications have no equals in the hydrological literature.

Two prizes for the best scientific research studies, in the sum of 500 rubles each, were awarded to V. I. Sapozhnikov, Z. I. Rubtsova and V. T. Kurbatova (USSR Hydrometeorological Center) for the study "Method of Long-Range Forecasting of the Hydrograph of Water Inflow into Reservoirs of the Volga-Kama Cascade During the High-Water Period" and Ye. S. Ulanova, N. V. Gulinova, T. A. Maksimenkova, V. A. Moiseychik, A. N. Derevyanko, S. L. Pluchik, M. G. Lubnin, L. V. Komotskaya, N. L. Sakharova, T. A. Pobetova (USSR Hydrometeorological Center), and also former workers of the All-Union Scientific Research Institute of Agricultural Meteorology M. S. Kulik and the USSR Hydrometeorological Center N. Z. Ivanova-Zubkova for the study "Agrometeorological Conditions and Productivity of Agriculture in the Nonchernozem Zone of the RSFSR."

The first study was devoted to the timely problem of long-range forecasting of the hydrograph of water inflow into reservoirs and is of great practical importance. These models make it possible to predict the distribution of unregulated water inflow by 10-day periods and months with an advance time up to two months. The study is the final stage in long-term investigations. The method is extensively used in routine practice; forecasts based on this method have a high probable success. The principal results of the study have been published in the TRUDY GIDROMETTSENTRA SSSR (Transactions of the USSR Hydrometeorological Center), No 138, 163, 197 and in the journal METEOROLOGIYA I GIDROLOGIYA (Meteorology and Hydrology), No 12, 1975.

The monograph AGROMETEOROLOGICHESKIYE USLOVIYA I PRODUKTIVNOST' SEL'SKOGO KHOZYAYSTVA NECHERNOZEMNOY ZONY RSFSR (Agrometeorological Conditions and Productivity of Agriculture in the Nonchernozem Zone of the RSFSR), Leningrad, Gidrometeoizdat, 1978, generalizes methodological work during recent years in the Nonchernozem zone of the RSFSR devoted to agrometeorological conditions for carrying out spring field work and formation of the yield of spring grains, industrial and vegetable crops, meadow and hay grasses. It gives an evaluation of weather conditions during harvesting.

CONFERENCES, MEETINGS AND SEMINARS

Moscow METEOROLOGIYA I GIDROLOGIYA in Russian No 4, Apr 80 pp 126-127

[Article by A. A. Vasil'yev and M. V. Rubinshteyn]

[Text] A scientific and practical conference on timely problems in aviation meteorology was held at the All-Union Exhibition of Achievements in the National Economy during the period 24-26 October 1979.

The conference was attended by more than 100 specialists from institutions of the State Committee on Hydrometeorology and Environmental Monitoring, the Ministry of Civil Aviation, the Ministry of the Aviation Industry, the Ministry of Higher and Intermediate Special Education USSR and others. The participants included workers from a number of republic and local administrations of the State Committee on Hydrometeorology and Environmental Monitoring and representatives of operational subdivisions: Moscow Civil Aviation Air Weather Center, Air Weather Centers and Air Weather Stations, and also territorial administrations of the Ministry of Civil Aviation.

The conference was opened by the chairman of the organizing committee V. M. Kosenko, who mentioned the importance of timely implementation of a number of complex interdepartmental plans for studying the influence of meteorological phenomena on the activity of aviation and the development of methods for predicting meteorological phenomena important for aviation. In speaking of the tasks of the conference, V. M. Kosenko noted the timeliness of the discussion of the status of research and scientific-practical studies in the field of aviation meteorology. He emphasized the necessity for further definition of the principal directions in future research for developing more reliable methods for predicting weather phenomena important for aviation for the purpose of increasing the safety and regularity of civil aviation aircraft flights.

In the course of the conference there were 33 reports and communications devoted to the most timely problems in aviation meteorology.

The problems involved in meteorological support of the safety and regularity of civil aviation flights and the possibility of a quantitative evaluation of the influence of meteorological conditions on the safety and regularity

of flights were covered in reports by I. M. Ivanov and A. S. Rasputikov, representatives of the Ministry of Civil Aviation.

A report on the requirements on prognostic meteorological information necessary for supporting civil aviation was presented by A. M. Baranov, a representative of the Civil Aviation subdivision OLAGA [expansion unknown].

A considerable part of the report was devoted to the meteorological conditions for the appearance of a wind shear in the lower part of the boundary layer and its influence on the takeoff and landing of aircraft.

Reports on this subject were presented by L. R. Orlenko (Main Geophysical Observatory), B. G. Vager (Leningrad Institute of Civil Engineers), V. G. Glazunov (USSR Hydrometeorological Center), V. V. Lomovskiy (State Scientific Research Institute of Civil Aviation), N. L. Byzova and Z. I. Volkovitskaya (Institute of Experimental Meteorology), A. I. Voskresenskiy and I. I. Tsigel'nitskiy (Arctic and Antarctic Scientific Research Institute), S. N. Lapina (Saratov State University), I. G. Guterman and F. F. Bryukhan' (All-Union Scientific Research Institute of Hydrometeorological Information-World Data Center).

A number of reports were devoted to weather phenomena exerting an influence on the activity of aviation and prediction of these phenomena. In particular, reports were presented on the meteorological conditions for landing and prediction of these conditions. These reports were presented by V. Ye. Minervin (Central Aerological Observatory), N. V. Petrenko, M. V. Rubinshteyn and N. N. Gusevoy (USSR Hydrometeorological Center), I. V. Koshelenko (Ukrainian Scientific Research Hydrometeorological Institute). A report on the influence of a built-up urban area on low-altitude flight conditions was presented by S. M. Shmeter (Central Aerological Observatory). Investigations of aircraft flight conditions along flight routes and prediction of these conditions were the subjects of reports by Z. M. Makhover and S. N. Rapot (Moscow Division All-Union Scientific Research Institute of Hydrometeorological Information), A. A. Bubnova (State Scientific Research Institute of Civil Aviation), S. A. Bortnikov (USSR Hydrometeorological Center), K. G. Abramovich and I. A. Gorlach (USSR Hydrometeorological Center), V. D. Yenikeyeva (Leningrad Hydrometeorological Institute) and S. I. Mazover (Leningrad Hydrometeorological Institute).

Three reports were devoted to the problems involved in the electrification of aircraft by atmospheric electricity, their damage by electric discharges outside a convective cloud and the synoptic conditions under which these phenomena are observed. Reports on these subjects were presented by V. F. Yevteyev (State Scientific Research Institute of Civil Aviation), Ye. V. Nesterov (State Scientific Research Institute of Civil Aviation) and G. D. Reshetov (USSR Hydrometeorological Center).

The results of regional investigations of weather phenomena dangerous for aviation were discussed in reports by T. P. Kovalevskaya and I. Ya. Alikina (Perm State University), L. I. Barovskaya (Tomsk State University),

O. A. Lyapina and Ye. I. Sofiyev (Central Asian Regional Scientific Research Hydrometeorological Institute), and Yu. V. Petrov (Tashkent State University).

The problems involved in the organization and automation of meteorological observations and the use of observational data in the operational meteorological support of civil aviation flights were the subject of reports by G. N. Shur (Central Aerological Observatory), S. M. Persin (Main Geophysical Observatory), Yu. F. Moyseyev (Main Geophysical Observatory), G. B. Brylev (Main Geophysical Observatory), G. M. Kruchenitskiy (Central Aerological Observatory) and G. N. Kostyanyy (Central Aerological Observatory).

After the discussion the conference adopted an expanded resolution in which, in particular, it was noted that the results of investigations carried out in the scientific research institutes of the State Committee on Hydrometeorology and Environmental Monitoring, the Ministry of Civil Aviation, a number of universities and institutes and scientific research institutes of other departments are finding practical application in the operational practice of meteorological support of civil aviation. At the same time, it was noted in the resolution that with the development of aviation, the increase in the intensity of flights and an increase in the number of routes and the flight range there are increasing requirements on the accuracy of meteorological observations and reliability of forecasts of weather conditions and the list of meteorological phenomena which must be predicted is expanding.

The conference deemed that for the purpose of more effective support of the activity of aviation there must be an increase in the quality of the research and the concentration of efforts on study of the most important problems in aviation meteorology.

Among these problems are the following:
-- prediction of the altitude of the lower cloud boundary and visibility in combinations close to the minima in ICAO categories I, II and III;
-- mesostructure, conditions of formation and the prediction of wind shear, turbulence, squalls and thunderstorms;
-- influence of microrelief and built-up areas in the neighborhood of the airports on the formation and intensity of weather phenomena dangerous for aviation;
-- optimization of the distribution of weather observation points in the neighborhood of the airports;
-- development of new technical means for meteorological observations and automation of these observations;
-- conditions for the formation and prediction of zones of clear-sky turbulence, icing and active convection;
-- peculiarities of development of weather phenomena over mountainous terrain;
-- meteorological conditions for flights of aircraft in the lower layer of the troposphere, especially the conditions for flights of special-purpose aircraft;

-- meteorological conditions for the electrification of aircraft and the development of means for protecting ships against electric discharges.

For the successful solution of the enumerated problems the conference deemed it necessary to broaden scientific and scientific-methodological studies at the regional scientific research institutes of the State Committee on Hydrometeorology and in other departments with the simultaneous strengthening of scientific direction and coordination by the key scientific research institutes.

The following, in particular, are necessary:
-- development of numerical models for predicting the fields of meteorological elements to an altitude of 18-20 km;
-- development of mesoscale numerical models for predicting the fields of meteorological elements;
-- automation of processing of meteorological information, creation of operational data banks and automation of preparation of weather forecasts for aviation;
-- automation of auxiliary studies in carrying out research, creation of archives of data from meteorological observations on technical carriers.

In the course of the discussion of practical directions of scientific research studies carried out at the scientific research institutes of the State Committee on Hydrometeorology and Environmental Monitoring the conference deemed it desirable to broaden the publications of methodological aids, letters and other scientific-methodological instructions for weathermen in operational subdivisions.

Publication of the RUKOVODSTVO PO AVIATSIONNYM PROGNOZAM POGODY (Manual on Aviation Weather Forecasts) was recommended.

NOTES FROM ABROAD

Moscow METEOROLOGIYA I GIDROLOGIYA in Russian No 4, Apr 80 pp 127-128

[Article by B. I. Silkin]

[Text] As reported in SCIENCE NEWS, Vol 115, No 11, 1979, the quantity of water vapor present in the atmosphere is important for the interpretation of data from astronomical observations. Accordingly, at the request of astronomical institutes, a group of specialists at NOAA in the United States, headed by Peter Coon, has carried out a number of observations aboard an aircraft laboratory outfitted with IR radiometric equipment.

An earlier unknown phenomenon was unexpectedly discovered: in every case after the next water vapor concentration had appeared on the radiometer screen, within three or four minutes the aircraft experienced turbulence obviously associated with turbulent flows in the atmosphere.

In checking this effect the experimenters directed the radiometer ray forward along the aircraft flight path, which led to an increase in the correlation between the radiometer readings and the appearance of turbulence.

Specialists drew the conclusion that the earlier known "destruction waves," associated with turbulent flows in the atmosphere, are accompanied by traveling "blobs." These "blobs" with a high degree of reliability and with an advance time of 3-4 minutes can be recorded by means of existing radiometric apparatus, which requires only insignificant modification for this purpose. Practical tests of the new method are being made by civil aircraft in the United States.

*****

Investigation of atmospheric electricity in general and lightning discharges, in particular, is necessary not only for an understanding of the physics of the earth's air envelope and geomagnetic phenomena, but also for the practical purposes of carrying out radio communication.

It is reported in SCIENCE NEWS, Vol 115, No 24, 1979 that the results of study of lightning by means of two meteorological satellites were covered in a report by scientific specialists of the University of the State of

New York at Albany R. E. Orville and D. W. Spencer, which they presented at the annual conference of the American Geophysical Union held in Washington in June 1979.

According to the data obtained using the instrumentation carried aboard these satellites, the number of lightning flashes over the land is 8-20 times greater than the number over ocean areas (such a great spread is dependent on where one assigns the discharges observed in coastal regions).

By midnight the mean number of lightning flashes decreases by a factor of approximately 4-8. Their total number attains a maximum in the region falling between 10 and 20°N in summer in the northern hemisphere and between 0 and 10°N in summer in the earth's southern hemisphere. During the course of the entire year the lightning occurring near midnight is concentrated for the most part between 10°S and 10°N, but in the southern summer the region of the maximum takes in a broader region, as far as 10°S.

Both at twilight and near midnight the frequency of lightning discharges over the entire planet in general is approximately 1.4 times greater during the period when it is summer in the northern hemisphere than when it is winter there. Satellite investigations of lightning are continuing.

*****

As reported in NEW SCIENTIST, Vol 81, No 1139, 1979, according to the theory which is now widely accepted, the electric currents flowing in the space between the earth's surface and the atmosphere are usually balanced by lightning discharges and weak electric currents flowing between the earth and its air envelope during good weather.

In studying these processes, during the south polar summer (November 1978) American meteorologists launched pilot balloons in the neighborhood of Amundsen-Scott scientific station, situated at the South Geographic Pole.

In processing the data from these observations, work done by specialists at the Environmental Studies Laboratory, Boulder, Colorado, there was found to be an unusually high saturation of air which coincided in time with a powerful solar flare. A region characterized by this quality was situated at an altitude 25-30 km above the underlying surface of the Antarctic glacier. Changes in weak currents connecting this surface with the atmosphere, postulated by theory, in this case were not registered.

The conclusion can therefore be drawn that atmospheric electricity is in direct dependence on solar activity, but the role of lightning discharges in the discharging of this voltage evidently until now has been exaggerated.

LETTER TO THE EDITOR

Moscow METEOROLOGIYA I GIDROLOGIYA in Russian No 4, Apr 80 p 128

[Communication from B. I. Silkin]

[Text] In a reference to a study by American scientists, printed in NATURE, Vol 277, No 5692, p 121, 1979 and devoted to a study of the change in concentration of atmospheric carbon dioxide (METEOROLOGIYA I GIDROLOGIYA, No 1, p 127, 1980), for reasons for which I have no responsibility, there were several errors. In particular, the authors of the study drew the conclusion that there has been an increase in the CO_2 concentration during recent decades, not a decrease in this concentration, as was incorrectly mentioned in the reference.

[8-5303]

5303 -END-
CSO: 1864